Probabilistic analysis of immersed tunnel settlement using CPT and MASW

Bob van Amsterdam

January 16, 2019
Version: Final report

TU Delft

Probabilistic analysis of immersed tunnel settlement using CPT and MASW

Bob van Amsterdam

Thesis committee:

Prof. Dr. ir. K.G. Gavin	*Geo-engineering*	*TU Delft*
Assoc. prof. Dr. ir. W. Broere	*Geo-engineering*	*TU Delft*
Ir. K.J. Reinders	*Hydraulic engineering*	*TU Delft*
Dr. ir. C. Reale	*Geo-engineering*	*TU Delft*

January 16, 2019

Abstract

Settlement data of the Kiltunnel and the Heinenoordtunnel show that immersed tunnels in the Netherlands have been experiencing much larger settlement than expected when designing the tunnels causing cracks in the concrete and leakages in the joints. Settlements of 8 - 70 mm have been measured at the Kiltunnel and of 7 - 30 mm at the Heinenoordtunnel while settlements in the range of 0 - 1 mm were expected. Both sites are investigated through non-invasive geophysical site investigation method MASW (Multichannel Analysis of Surface Waves) for each 2.5 meter along the length of the tunnel and invasive site characterisation method CPT's (Cone Penetration Tests).

The settlement of immersed tunnels is similar to that of a shallow foundation. It can be modelled using the Mayne equation which uses the small strain shear stiffness and the degradation of secant stiffness based on the load compared to the ultimate bearing resistance.

A way of characterising the site is determining the small strain stiffness directly from the shear wave velocity using the uncertainties in the relationship between shear wave velocity and cone penetration resistance and correlating the cone penetration resistance to this value. The correlation between the cone penetration resistance and shear wave velocity or small strain shear stiffness at the Heinenoord site is, however, so weak that it practically means that all possible q_c values should be considered.

Another way is to use both the shear wave velocity and the cone penetration resistance separately to characterise the site. The cone penetration resistance profiles are modelled stochastically based on the statistical data and the scales of fluctuations from the CPT's. The vertical scale of fluctuation at the Heinenoord site ranges from 0.06 - 1.44 meter for sands and 0.19 - 1.37 meter for clays. The horizontal scale of fluctuation of the cone penetration test could not be determined accurately enough to use in a model due to lack of data within the correlation length. The horizontal scale of fluctuation of the shear wave velocity is a different quantity than

the horizontal scale of fluctuation of the cone penetration resistance because it has been shown that it is at least a factor 10 larger for the Heinenoord site.

The 5% and 95% boundaries of the initial settlement at the middle element of the Heinenoordtunnel are 4.04 - 4.68 mm, this settlement can not be compared to the measured settlement because it has occurred before the start of the measurements. The 5% and 95% boundaries of the creep settlements that are calculated for the middle element of the Heinenoordtunnel are 0.39 - 0.80 mm in 1996. This is much smaller than the measured settlement of around 7 mm.

The 5% and 95% boundaries of the initial settlement at the middle element of the Kiltunnel are 1.82 - 2.27 mm. The creep settlements that are calculated for the middle element of the Kiltunnel are in the order magnitude of 1.98 - 3.19 mm in 2018. This is much smaller than the measured settlement of around 7.5 - 18.1 mm in 2018.

To see if cyclic loading has an effect on the settlement of the middle section the effect of thermal expansion and contraction of the elements and the cyclic loading of the tides is examined.

The thermal expansion and contraction of the elements at an angle loaded the middle element. The expansion of the Gina Gaskets between the flat element and the elements at an angle is between -3 and 3 mm. This expansion and contraction of the Gina Gasket causes a vertical load on each of the edges of the middle element of 268 kN. This causes a settlement of 0.47 - 0.58 mm in 1996 at the edges of the middle element of the Heinenoordtunnel and a settlement of 0.42 - 0.55 mm in 2018 of the edges of the middle element of the Kiltunnel. This means that it does have a small influence on the settlement of both tunnels measured at these joints but does not explain all occurred settlement.

The tide loads both tunnels because there is a layer of sludge on the bottom of the rivers that could cause a decay and a lag in the fluctuation of the pore pressures in the deeper sand layers. This means that the effective stress in the deeper sand layers can increase and decrease due to the tides. No accurate measurements are available for the fluctuations of these pore pressures in the deeper sand layers.

For an indication of the settlement of the Heinenoordtunnel and the Kiltunnel under the loading of the tides a few calculations have been performed using an assumed lower bound of 40% and an upper bound of 90% of loading of the tides.

At the Heinenoord the lower bound scenario gave results between 4.99 - 7.51 mm, which means that the measured values of around 7 mm are within the range of the

results, while the upper bound scenario gave results between 10.05 and 15.57 mm which is larger than the measured values.

At the Kiltunnel there is no real trend of which bound is more accurate compared to the measured settlements. At location 21 and 23 the lower bound is more accurate, at location 19, 25 and 27 the upper bound is more accurate while for location 29 the measured settlement is somewhere in between the two bounds.

At location 19 even the 95 % of the upper bound (21.34 mm) is much smaller than the measured settlement (around 34 mm). The difference in shear wave velocity is not that large and can not explain the large difference in settlement while the information from the CPT's is so limited that it is not possible to determine if there is a difference between location 19 and the other locations.

These calculations show that there is a possibility that the settlements have occurred through a combination of the creep, the temperature effects and the loading of the tides but it does not conclude that all settlements occur because of these loading conditions.

Contents

List of Figures

List of Tables

List of symbols

A	Cyclic settlement parameter
A_c	Area of the concrete in the cross-section
A_s	Total area of the cross-section
A_w	Area of the soil on top of the tunnel
B	Width of foundation
c'	Cohesion
$^{\circ}C$	Degrees Celsius
d	Average distance between two intersections of the cone penetration resistance and the trend line
D_{50}	Median grain size
E'	Drained elastic soil modulus
E_0	Small strain modulus
f_s	Cone friction
G_0	Small strain shear modulus
I	Elastic displacement influence factor
I_c	Soil type indication
I_{hrv}	Shape factor of the footing
K	Kelvin
k	Number of observations
L_0	Initial length of the two segments at an angle
m	Creep settlement factor
n	Factor based on soil type
P_a	Atmospheric pressure
R^2	Coefficient of determination
R_f	Friction ratio
s	Settlement
s_c	Creep settlement
s_e	Elastic part of settlement of cyclic settlement

s_N	Cyclic settlement after N cycles
T_1	Temperature at onset of thermal expansion
T_2	Temperature at end of thermal expansion
t	Time
t_{ref}	Time corresponding with the onset of creep
V_s	Shear wave velocity
V_{s1}	Normalised shear wave velocity
Q_{app}	Applied force
Q_{ult}	Ultimate bearing resistance
q_{app}	Applied stress
$q_{b0,1}$	Applied stress at 10% normalised settlement
q_c	Cone penetration resistance
q_{c1}	Normalised cone penetration resistance
$q_{c,net}$	Cone penetration resistance corrected for pore pressure and total vertical stress
Z_i	Zone of influence
α	Factor between q_c and $q_{b0,1}$
α_c	Linear coefficient of thermal expansion
α_E	Empirical elastic soil modulus factor
γ	Unit weight soil
ΔL	Difference in lenght after thermal expansion
η	Psuedo strain (Normalised settlement)
θ	Scale of fluctuation
μ	Mean
$\hat{\mu}$	Estimated mean
ν	Poisson's ratio
ρ_s	Unit weight of soil on top of tunnel
ρ_w	Wet unit weight
ρ_{water}	Unit weight displaced water
$\rho(\tau)$	Theoretical correlation at distance τ
$\hat{\rho}(\tau)$	Estimated correlation at distance τ
σ	Standard deviation
$\hat{\sigma}$	Estimated standard deviation
$\sigma_{v,0}$	In situ total vertical stress
σ'_v	Effective vertical stress
$\sigma'_{v,0}$	In situ effective vertical stress
τ	Correlation distance

List of abbreviations

MASW	Multichannel analysis of surface waves
CPT	Cone penetration test
ULS	Ultimate limit state
SLS	Service limit stat
TBM	Tunnel boring machine
UB	Upper bound
LB	Lower bound
FEM	Finite element method

1 Introduction

1.1 Problem statement

An immersed tunnel is a tunnel used to cross a waterway and is built according to the immersion construction method. In short this means that the elements are prefabricated on the dry in a dry dock, shipyard or a factory, floated to the site, immersed and connected with immersion joints.

In the 1960's and 1970's eight immersed tunnels are built in the Netherlands. During the lifetime of an immersed tunnel it experiences settlement. Commissioned by Rijkswaterstaat these deformations are measured in immersed tunnels to be able to study the behaviour and act if necessary. Two examples are the Kiltunnel and the Heinenoordtunnel. In these two tunnels the settlements were larger than predicted in the design of the tunnels. The design predicted settlement was in the order of 0-1 mm. The settlements that were measured are in the range of 10-70 mm for the Kiltunnel and 10-30 mm for the Heinenoordtunnel. A problem occurs when this settlement is differential settlement. This can cause leakage and cracks in the concrete which has already occurred in both tunnels.

The settlement of an immersed tunnel is similar to the settlement of a shallow foundation. The only real difference between a typical shallow foundation and the typical immersed tunnel is the size of the footing.

1.1.1 Kiltunnel

The Kiltunnel tunnel is an immersed tunnel that crosses the Dordtse Kil. Before the Kiltunnel tunnel the only connection between Dordrecht and the Hoekse Waard were some ferries. The Kiltunnel construction started in 1974 and was finished in 1977. At the moment around 10,000 to 15,000 vehicles use the Kiltunnel every day [Weg18b].

The three tunnel elements were constructed in the Barendrecht dry dock and are 31.0 meter wide, 8.75 meter high and 111.5 meter long. The design was based on and almost identical to the design of the Heinenoordtunnel. The lowest point of the

tunnel is at 17.09 meter below NAP. The tunnel has 2x2 lanes and has a separate shielded lane for slow traffic such as agricultural vehicles, cyclists and pedestrians.

The tunnel settlements have been monitored from 1978 up till now. The settlements are shown below in figure 1.1 and the locations of the measurements are shown in figure 1.2.

Fig. 1.1.: Settlement of the Kiltunnel in mm at the immersions joints and dilation joints (x-axis indicates the number of the measurement point)

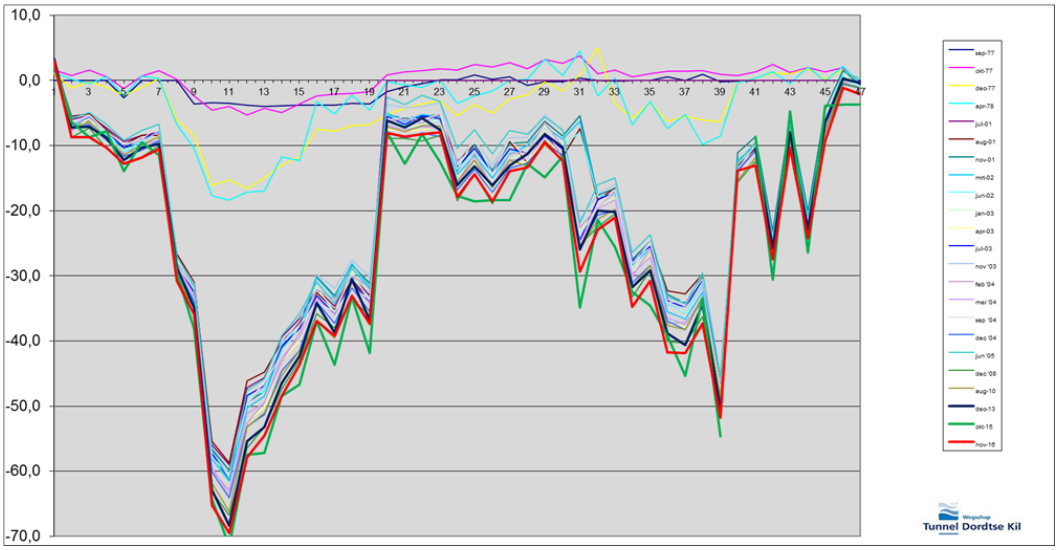

Fig. 1.2.: Locations and depth in m NAP of the settlement measurements points at the Kiltunnel

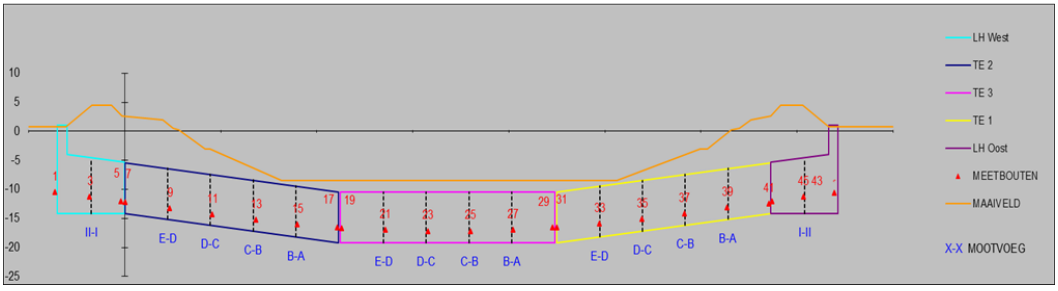

The Kiltunnel experiences much larger settlements during this period than initially estimated 0-1 mm when designing the tunnel causing cracks and leakages in the tunnel.

1.1.2 Heinenoordtunnel

The Heinenoordtunnel is an immersed tunnel that crosses the Oude Maas. Before the Heinenoordtunnel the only connection between Rotterdam and the Hoekse Waard

and Goeree-Overflakkee, apart from some ferry's was the Barendrechtse bridge, which was a pivot bridge. The increasing traffic loads in the 1960's on this bridge caused traffic jams every day. The Heinenoordtunnel was built to overcome this problem. The Heinenoordtunnel construction started 1966 and was finished in 1969. By 2015 92,100 vehicles used the Heinenoordtunnel every day [Weg18a].

For the construction a dry dock was built in Barendrecht, which was used later for building numerous dutch tunnel segments including the Kiltunnel. In this dry dock the tunnel 5 elements of each 8.8 meters high, 30.7 meters wide and 115.0 meters long were constructed of 5 segments each.

The tunnel settlements have been monitored from 1978 up till now. The settlements from 1978 up till 1996 are shown below in figure 1.3. In this figure the settlement at the abutment is set at 0. In figure 1.4 below, the tunnel profile of the Heinenoordtunnel is shown.

Fig. 1.3.: Settlement of the Heinenoordtunnel at the immersions joints relative to the abutments

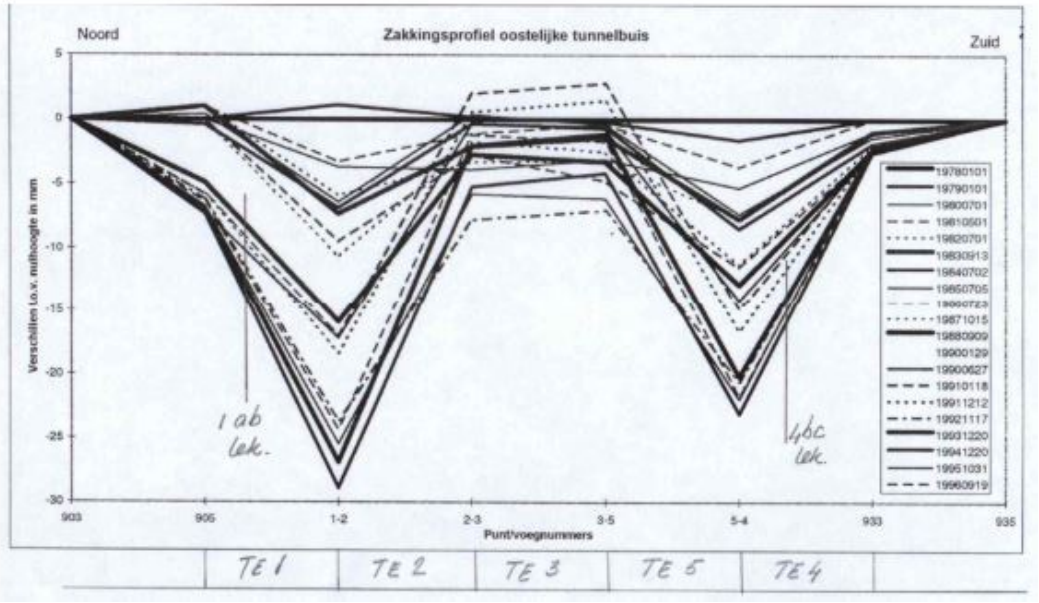

Fig. 1.4.: Heinenoordtunnel profile

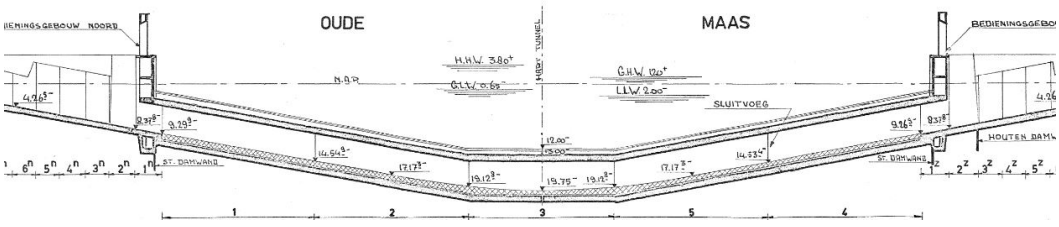

The relative settlement of the Heinenoordtunnel is only measured at the immersion joints. Because the settlement is relative to the abutment, and the abutment is also settling, the absolute settlement are larger than is shown in this figure, but it is unknown how much larger. The two locations that are indicated in the figure are locations where leakage has occurred, most likely due to differential settlement at dilation joints. Just as the Kiltunnel the tunnel experiences much larger settlements during this period than the initially estimated 0-1 mm when designing the tunnel.

1.2 Scope of the project and research questions

The goal of the project is to find out what drives the settlement and to model the prediction of the initial and long-term settlement of immersed tunnel by using the site investigation data from the non-invasive geophysical site investigation method MASW (Multichannel Analysis of Surface Waves) for each 2.5 meter along the length of the tunnel and invasive site characterisation method CPT's (Cone Penetration Tests) while taking into account the uncertainty in soil parameters.

The research is going to be put into practice by applying it to two case studies. The case studies will be about the Kiltunnel and the Heinenoordtunnel in the Netherlands.

The main research question is: What drives the settlement of the Heinenoord and the Kiltunnel and how to model it? The research consist of four parts:

1. Characterising the site taking into account the uncertainty in soil parameters across the sites.

2. Determining the loading conditions on the tunnel.

3. Modelling the load-settlement response of the tunnel.

4. Compare the results of the model to the results from the measurements.

1.3 Reading guide

Chapter 2 contains the literature study that is performed. In chapter 3 the site investigation that is performed on both sites are shown. Chapter 4 and 5 contain 2 ways of approaching the characterisation of the sites and calculating the settlement using this approach. Chapter 4 looked into the possibility of using the MASW as an input and correlating the CPT's to those measurement, while chapter 5 uses the information of both the CPT and the MASW as an input for the model. Chapter 5 also contains the calculated initial settlement and creep settlement for both tunnels. Chapter 6 describes the calculated settlement including cyclic loading of both temperature and loading from the tidal fluctuation of the estuaries. Chapter 7 concludes with the conclusions and the recommendations from this report.

2 Literature study

Two site investigation techniques were used on both the Kiltunnel and the Heinenoordtunnel: MASW and CPT's. The advantage of CPT's with respect to MASW is the proven accuracy of settlement predictions based on cone penetration resistance at a given location and the much smaller distance between two measurement in depth direction. The advantage of MASW measurements with respect to CPT's is the much smaller distance between two measurements in x-direction and the accurate determination of the initial stiffness of the soil. Theoretically CPT's could be just as closely spaced, but this would less economically feasible.

The combination of the presence of both site characterisation data of the CPT's and the MASW and the settlement data in time at both the Kiltunnel and the Heinenoordtunnel makes it good sites to test the settlement model.

2.1 Multichannel analysis of surface wave (MASW)

The MASW (Multichannel Analysis of Surface Waves) is a non-invasive in situ soil investigation method. The method differs from conventional seismic methods by using frequencies of 3-30 Hz and using surface waves, so called Rayleigh waves, while conventional methods uses frequencies higher than 50 Hz and is based on high resolution reflection or refraction. The MASW method measures the shear wave velocity V_s of the soil a few to a few tens of meters the surface at intervals of around 0.5 – 4.0 m, depending on how deep the measurement is to the surface. Park et al. (1999) and Park et al. (2007).

The method deals with the wave dispersion caused by a seismic source, for example a sledgehammer, by measuring using a multichannel recording system, with over 24 channels, and a receiver deployed over a certain length with intervals of a few meters. The main advantage of MASW over conventional methods is the ability to compensate for noise such as traffic waves, body waves and higher modes of surface waves. A schematic of the method is shown in figure 2.1.

Fig. 2.1.: Schematic of the active MASW field survey [Cho18].

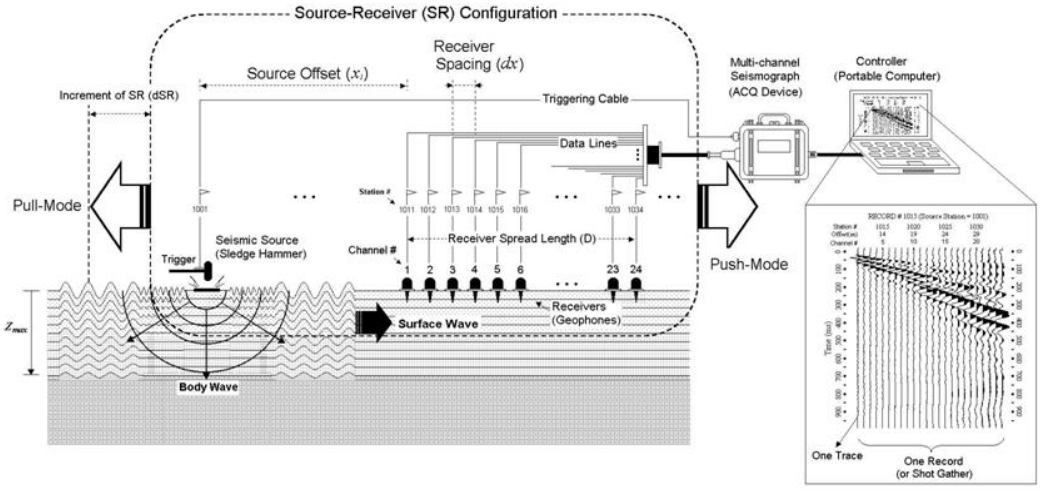

The shear wave velocity profile in 1D is obtained by acquiring multichannel records, estimating the fundamental mode dispersion curves (one curve from each record) from the multichannel raw field data and inverting these curves to obtain 1D (depth) Vs profiles (one profile from one curve). This process is shown in a diagram in figure 2.2. If these 1D profiles are in one line, as is the case in the immersed tunnel, the values can be linearly interpolated horizontally to obtain semi-continuous 2D profiles of the soil beneath the tunnel.

Fig. 2.2.: Diagram of the MASW method from Xia et al. (2002).

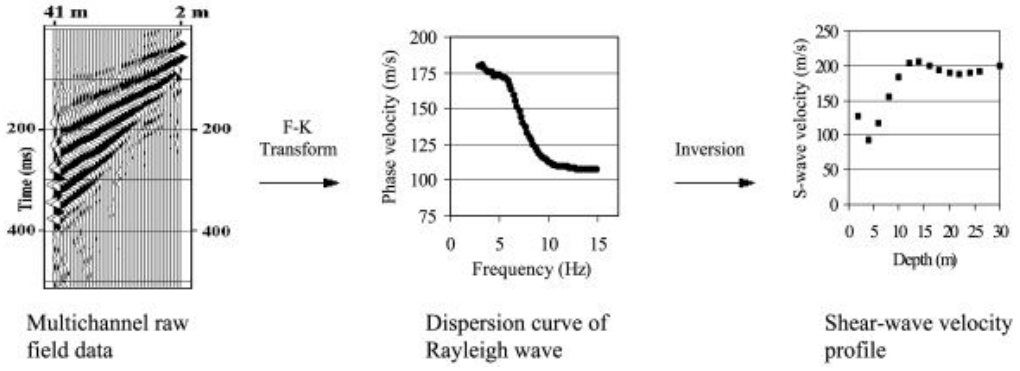

MASW is an interesting tool in geotechnical engineering because of the strong relation of shear wave velocity, which can be derived from MASW measurements, with the small strain shear stiffness. This is an important parameter in geotechnical problems, especially in settlement related issues such as shallow foundation settlement. This relation is discussed in more detail in chapter 2.1.1.

The shear wave velocity obtained from MASW is actually not a measurement. It is a best-fit solution on the curve inversion mentioned before. This means that there is

an uncertainty in the shear wave velocity, even after the MASW measurement. Xia et al. (2002) investigated the difference between shear wave velocities obtained from MASW measurements and shear wave velocities obtained from direct borehole measurements. The results showed that the difference was random and approximately 15% or less.

2.1.1 Parameter selection from MASW

The shear wave velocity is often normalised for vertical stress to be able to compare shear wave velocity values from different depths while minimising the influence of the vertical stress on the values. The normalised shear wave velocity can be calculated using the following equation according to Youd et al. (2001, cited by Hussien and Karray, 2016):

$$V_{s1} = V_s * (\frac{P_a}{\sigma'_v})^{0.25} \tag{2.1}$$

Where V_{s1} is the normalised shear wave velocity, $V_s$is the shear wave velocity, P_a is the atmospheric pressure and σ'_v is the vertical effective stress. First the effective vertical stress on top of the soil is assumed to be 25 kPa (10 kPa for 1 m of soil on top of the tunnel and 15 kPa from the buoyant weight of the immersed tunnel) and then the effective vertical stress is calculated at the centre of each shear wave velocity measurement.

Anbazhagan et al. determined a correlation between the wet unit weight of the soil ρ_w and the shear wave velocity V_s. The correlation was in the shape of:

$$\rho_w = a * (V_s)^b \tag{2.2}$$

Where ρ_w is in kN/m^3 and $V_s$in m/s and a and b are fit parameters of the correlation and have a mean and a standard deviation. Parameter a and b are described by mean $\mu_a = 4.12$ with a standard deviation of $\sigma_a = 0.021$ and mean $\mu_b = 0.262$ with a standard deviation of $\sigma_b = 0.0087$ for coarse-grained soil. The coefficient of determination R^2 was 0.781.

The shear modulus is an important parameter when calculating the settlement. The most likely shear modulus at very small strain G_0 can be calculated directly from the

measured shear wave velocity using equation 2.2 together with equation 2.3 from Hussien and Karray (2016).

$$G_0 = \rho_w * (V_s)^2 \tag{2.3}$$

Where the small strain shear stiffness G_0 is in kPa, the wet unit weight ρ_w is in kN/m^3 and the shear wave velocity $V_s$is in m/s. The theory behind this formula is that the shear wave propagates through the soil and causes a very small shear deformation of a soil element as shown in figure 2.3.

Fig. 2.3.: Deformation of the soil through shear waves from Hussien and Karray (2016).

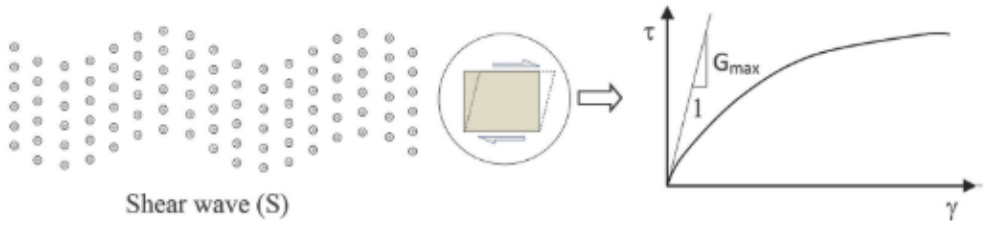

The small strain modulus can be determined from the small strain shear using equation 2.4.

$$E_0 = G_0 * 2 * (1 + \nu) \tag{2.4}$$

Where E_0 is the small strain modulus. For small strains ν can be approximated as 0.1. Which means that E_0 = 2.2 * G_0.

2.2 Cone penetration test (CPT)

The Cone penetration test (CPT) is most used geotechnical site investigation method in the Netherlands, and one of the most used worldwide. The test consists of a cone at the end of a rod that is being pushed into the soil. The cone penetration resistance of the cone q_c and friction on the sleeve of the cone f_s are measured continuously. CPT's can be performed to depths over 100 m in soft soils and large capacity equipment. The interval of between two measurements in depth has a constant value of 2 cm. The cone is shown in figure 2.4.

Fig. 2.4.: Cone penetrometer from Robertson (2015).

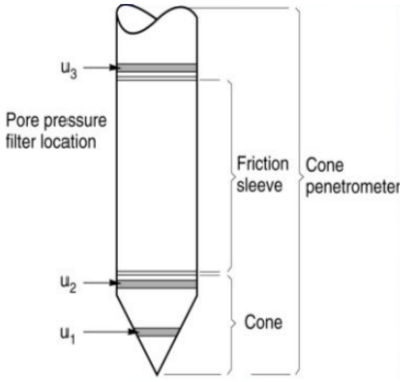

This cone is pushed into the soil using pushing equipment. This pushing equipment is usually a truck which can exert it's own weight on the rod connecting the truck to the cone.

The cone penetration resistance q_c is the force that is needed to push the cone into the soil divided by the area of the cone. The skin friction is the force of the friction on the sleeve divided by the area of the sleeve. Distinctive for different types of soils is the ratio between the cone penetration resistance and the skin friction. This ratio is called the friction ratio R_f and can defined as:

$$R_f = \frac{f_s}{q_c - \sigma_{v0}} * 100 \tag{2.5}$$

Where R_f is the friction ratio, f_s is the cone friction, q_c is the cone penetration resistance and σ_{v0} is total effective stress.

Apart from strength parameters, CPT's can be used to classify the soil type that is present at a certain depth at that location. Robertson (1990) created a widely accepted method to classify soils based on the normalised cone penetration resistance and the friction ratio. The classification is shown in figure 2.5.

To use figure 2.5 the cone penetration resistance must be normalised for vertical stress first. The normalised cone penetration resistance can be calculated using the following equation 2.6 from Robertson (1990):

$$Q = q_{c1} = \frac{q_t - \sigma_{v0}}{P_a} * (\frac{P_a}{\sigma'_{v0}})^n \tag{2.6}$$

Where q_{c1} is the normalised cone penetration resistance, q_t is the cone resistance corrected for water effects, σ_{v0} is the current in situ total vertical stress, P_a is the atmospheric pressure, σ'_{v0} is the vertical effective stress and n is a factor based on the soil type. The effective vertical stress is calculated with the assumption that the effective unit weight of all the soil above is 8 kPa/m. n is 1.0 for an I_c value, which is an indicator parameter of the soil type, larger than 2.6 and 0.5 for an I_c value smaller than 2.6. This means that $n = 0.5$ for sandy mixtures up to dense sands and $n = 1.0$ for silt mixtures clays and organic soils.

Fig. 2.5.: Soil classification by Robertson (1990) using the cone penetration test.

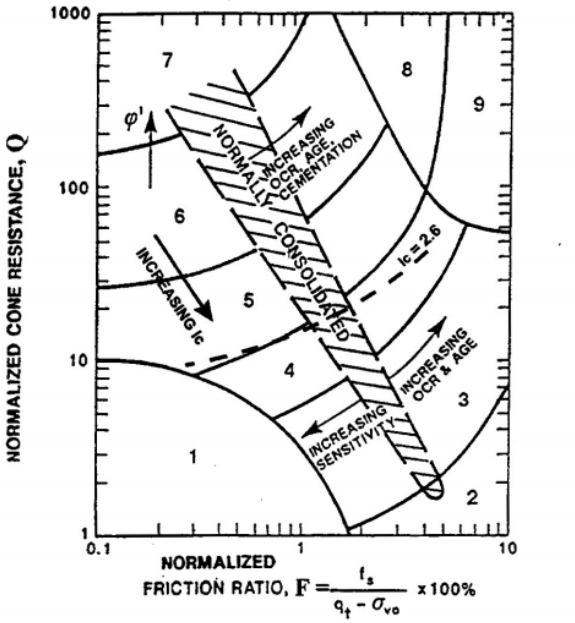

1. Sensitive, fine grained
2. Organic soils - peats
3. Clays - silty clay to clay
4. Silt Mixtures - clayey silt to silty clay
5. Sand Mixtures - silty sand to sandy silt
6. Sands - clean sand to silty sand
7. Gravelly sand to dense sand
8. Very stiff sand to clayey sand*
9. Very stiff, fine grained*

* *Heavily overconsolidated or cemented*

Using the normalised cone penetration resistance and friction ratio the I_c value can be calculated with the following equation from Robertson (1990):

$$I_c = ((3.47 - log_{10}(q_{c1}))^2 + (1.22 + log_{10}(f_r))^2)^{0.5} \tag{2.7}$$

The I_c indicates the type of soil that is present at that location. It matches the soil types from figure 2.5 closely. The soil type and the corresponding number in the Roberson graph for each interval of I_c is shown in table 2.1.

Ic [-]	Soil Type	Number in Robertson graph
1.31 - 2.05	Sands	6
2.05 - 2.60	Sandy mixtures	5
2.60 - 2.95	Silt mix	4
2.95 - 3.60	Clays	3
> 3.60	Organic soils	2

Tab. 2.1.: Soil type with corresponding I_c-value.

2.3 Settlement and bearing capacity calculations for shallow foundations

A shallow foundation is a type of foundation that transfers load to the subsurface at, or very near at, surface level instead of transferring it to a deeper layer as for example a pile foundation would do.

Both immersed tunnels rest on the riverbed. The mechanism of the settlement of an immersed tunnel is similar to the settlement of a shallow foundation. The difference that causes different behaviour between a typical shallow foundation and the typical immersed tunnel is the size of the footing. The footing size of an immersed tunnel is much larger.

There are many methods of calculating settlement for shallow foundations. In this chapter only the conventional approach and a CPT-based approach, the Mayne model, are considered.

2.3.1 Conventional calculations

The conventional bearing capacity equations were formulated by Terzaghi (1943). The method calculates bearing capacity as:

$$q_{ult} = s_c * c' * N_c + s_q * \sigma'_v * N_q + 0.5 * s_\gamma * \gamma * B * N_\gamma \tag{2.8}$$

Where: s_c, s_q and s_γ are shape correction factors, N_c, N_q and N_γ are bearing capacity factors based on the cohesion and the friction angle, c' is the cohesion at the base of the footing, σ'_v is the effective stress at the base of the footing, γ is unit weight of the soil and B is the width of the shallow foundation.

Briaud (2007) states that the equations are only valid when soil strength profile has a linear increase in depth due to hypotheses of a constant unit weight of the soil and a constant friction angle made by Terzaghi. This means the equation can not be used in over-consolidated soils which typically have a constant value in depth.

According to the Canadian Foundation Engineering Manual (1992), cited by Fellenius (2017), the bearing capacity factors are:

$$N_q = e^{\pi tan(\phi')} * (\frac{1 + sin(\phi')}{1 - sin(\phi')}) \tag{2.9a}$$

$$N_c = (N_q - 1) * cot(\phi') \tag{2.9b}$$

$$N_\gamma = 1.5 * (N_q - 1) * tan(\phi') \tag{2.9c}$$

N_c, N_q and N_γ are strongly dependant of the friction angle of the soil, especially in the range higher than 30 degrees, which is the range where sands usually are. The friction angle of the soil is hard to determine accurately. In small project usually only correlations with CPT or SPT measurements are used. Lab tests can also be used to determine the friction angle, but difficulties with sampling and testing the sand undisturbed causes lab tests to be inaccurate as well. This causes a high uncertainty in the calculation of the ultimate bearing resistance using this method, even if one assumes the method to be highly accurate.

Ultimate limit state design (ULS) can be interesting, serviceability limit state design (SLS) is usually more significant because even though the shallow foundation might not fail, the building on top can fail due to extensive (differential) settlements. Related to the conventional approach is the linear settlement model from Uzielli and Mayne (2012). This model calculates the initial settlement of shallow foundation according to an elastic model:

$$s = \frac{q_{app} * B * I * (1 - \nu^2)}{E'} \tag{2.10}$$

Where s is the initial settlement, q_{app} is the applied pressure by the foundation, B is the width of the foundation, ν is the Poisson's ratio and E' is the drained elastic soil modulus which can be calculated using equation 2.11. I is the elastic displacement influence factor, which is, among other things, depending on the foundation shape, soil homogeneity, layer depth, foundation roughness, Poisson's ratio and foundation stiffness. The elastic displacement influence factor I can be determined for different

situations using the graphs from a study from Mayne and Poulos (1999) on the influence of the earlier mentioned parameters on the elastic displacement influence factor.

The drained elastic soil modulus E' can be determined based on CPT data and an empirical factor using equation 2.11.

$$E' = \alpha_E * q_{c,net} \tag{2.11}$$

Where α_E is an empirical factor based on the soil type, relative density and loading conditions and $q_{c,net}$ is the cone penetration resistance corrected for the pore pressure and the total vertical stress.

2.3.2 CPT-based approaches

Lately, research tends towards approaching the shallow foundation problem through in situ testing (Briaud (2007), Gavin, Adekunte and O'kelly (2009) and Gavin (2018)). When the applied load is plotted against settlement the size of the footing has a huge impact on the load-settlement curve. However, when the applied load is normalised to the applied stress, and this is plotted against the pseudo strain η (normalised settlement s/B), the effect of the footing width is filtered out and a close to unique relation for that specific site is shown. An example is shown in figure 2.6 (from Uzielli and Mayne (2012)) of the applied load and applied stress versus the settlement and pseudo strain on three footings with different dimensions on a site in Fittja, Sweden.

Fig. 2.6.: Plate load tests of three different sized shallow footings in Fittja, Sweden from Uzielli and Mayne (2012)

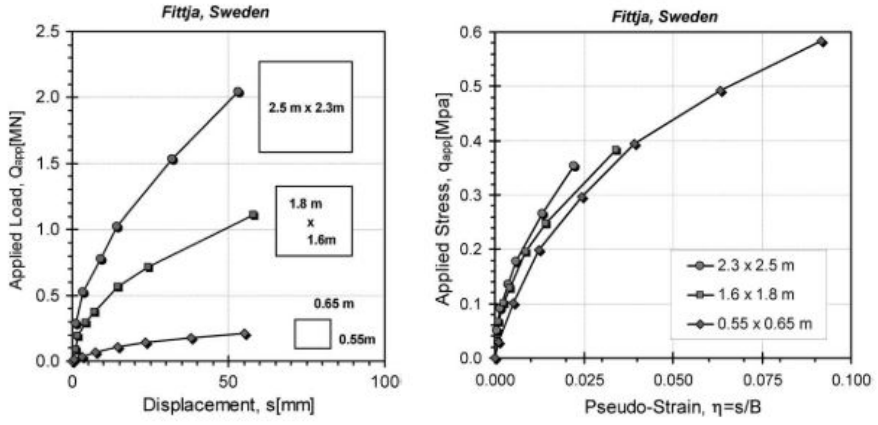

(a) Applied load versus settlement **(b)** Applied stress versus psuedo strain

To overcome the fact that this curve is site specific, the applied stress should be divided by the average cone penetration resistance q_c in the zone of influence.

Gavin, Adekunte and O'kelly (2009) gathered data from 5 different sites with different footing widths and compared the normalised resistance q/qc (-) to the normalised settlement s/B (%) and concluded from figure 2.8 that at larger normalised settlements ($>$ 5%) the settlement curves tend to converge but have unique relations at lower normalised settlements (<4%).

Fig. 2.8.: Normalised resistance versus normalised settlement from Gavin, Adekunte and O'kelly (2009)

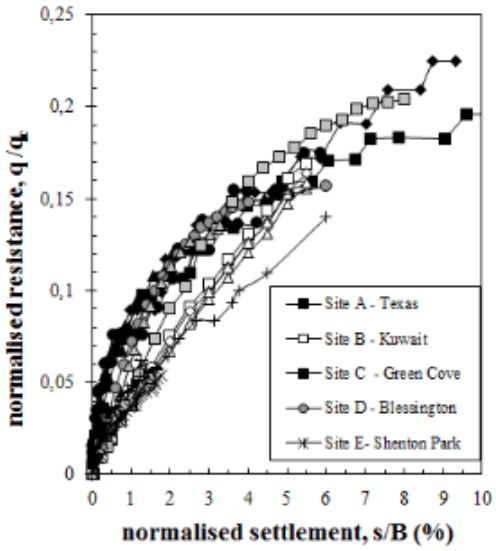

A definition of failure that can be used is when the settlement exceeds a normalised settlement of 10%. The applied stress at this settlement can be described as a constant times the cone penetration resistance

$$q_{b0.1} = \alpha * q_c \tag{2.12}$$

Where $q_{b0,1}$ is the applied stress causing a normalised settlement of 10%, α is the factor of $q_{b0,1}$ compared to q_c. A range of α-values of 0.13 to 0.21 is reported by Randolph et al. (2004, cited by Gavin, 2018).

2.3.3 Mayne model

A model that is well suited to model the settlement given the available site investigation data is the Mayne model from Uzielli and Mayne (2011) because the it requires

input parameters E_0, which can be obtained from MASW, and Q_ult, which can be obtained from CPT's. The model is shown in equation 2.13.

$$s = \frac{Q_{app} * I_{hrv}}{B * E_0 * [1 - (\frac{Q_{app}}{Q_{ult}})^{0.3}]} \tag{2.13}$$

Where s is the intial settlement in m, Q_{app} is the applied force in kN, I_{hrv} is the shape factor of the footing, which is 0.85 for a rigid rectangular footing, B is the width of the foundation in m, E_0 is the small strain stiffness of the soil and Q_{ult} is the ultimate bearing resistance of the soil. The model is similar to the linear settlement model of equation 2.10. However, it takes the degradation of the secant linear stiffness at higher loading into account.

At a normalised settlement s/B of 10% the applied load can be written as $\alpha * q_c$ as is shown in equation 2.12. If equation 2.13 is divided by B and $s/B = 0.1$ and $Q_{app} = \alpha * q_c * B * L$ is filled into equation 2.13, the ultimate bearing resistance can be calculated with equation 2.14.

$$Q_{ult} = \frac{\alpha}{(1 - \frac{10 * \alpha * q_c * I_{hrv} * L}{E_0 * B})^{1/0.3}} * (q_c * B * L) \tag{2.14}$$

The rewritten of the equation that results into equation 2.14 is shown in appendix .

2.3.4 Zone of influence

The zone of influence is the zone of soil which is influenced by stress caused by the shallow foundation causing it to settle. The parameters for the Mayne equation are averaged over this zone of influence to determine the mean values to use as input parameters for the probabilistic analysis.

Eurocode 7 states that for design purposes the zone of influence can be assumed to be the depth to which the increase in stress due to the load is larger than 25% of the previous in situ effective stress. The zone of influence can be determined by calculating the increase of the stress in the subsurface due to the load of the tunnel and using the limit of the zone of influence as defined in the Eurocode.

Boussinesq solution

The most widely used method of determining the increase of stress in a soil under a load is using the Boussinesq' set of equations. The Boussinesq set of equations solve the Boussinesq' problem which is the problem of the influence of stress fields and displacement under the loading of a point load in a linearly elastic, isotropic, homogeneous half space. Boussinesq's theory formula is based on following assumptions stated by Nwoji et al. (2017) :

1. The soil mass is semi-infinite, homogeneous and isotropic. The soil is more or less semi-infinite, but the sites of the Kiltunnel and the Heinenoordtunnel are not homogeneous or isotropic, so this is an important assumptions.

2. The soil has a linear stress-strain relationship. This is not actually the case but is a very good approximation because of the very low normalised stress levels induced by the immersed tunnels.

3. The soil is weightless. This means that only the stress increase due to the point load is considered.

Using these assumptions the stress increase in the soil due to a point load can be calculated using equation 2.15 from Murphy (2003):

$$q_v = \frac{3Q}{2\pi z^2} * \frac{1}{(1 + (r/z)^2)^{\frac{5}{2}}} \tag{2.15}$$

Where q_v is the vertical stress increase at the location chosen in the subsurface, Q is the force of the point load in kN, z is the depth below the point load, r is the horizontal distance from the point load to the location chosen in the subsurface which means that $r = (x^2 + y^2)^{0.5}$. The axis and definition of r is shown in figure 2.9.

Equation 2.15 can be rewritten as:

$$q_v = \frac{Q}{z^2} A_b \tag{2.16}$$

Fig. 2.9.: Axis for the defined equation 2.15 for the solution to the Boussinesq problem from Murphy (2003)

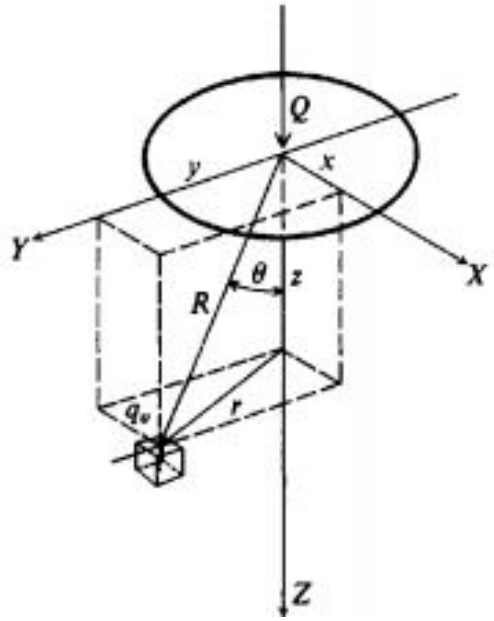

Where A_b is a parameter that is a function of r/z that is defined as:

$$q_v = \frac{3}{2\pi * (1 + (r/z)^2)^{\frac{5}{2}}} \tag{2.17}$$

Boussinesq solution for shallow foundations

The Boussinesq solution mentioned is for point loads while the whole purpose of shallow foundations is to spread the load to the soil to avoid large concentrations of stresses in the subsurface.

The easiest way to solve this problem is to divide the immersed tunnel into very small pieces (for example 0.1 x 0.1 meter), model the load of the small area as a point load and calculate the increase of stress at all locations in the subsurface due to this point load. Repeat this procedure for every area and sum the stresses of all these loads for the given location in the subsurface.

2.3.5 Creep settlement

Creep is the increase of strain (settlement) of the soil under a constant effective stress over time. This means that it is not a part of the elasto-plastic behaviour of the soil, but it is part of the viscoelastic properties of the soil.

Lehane et al. (2008, cited by Gavin, Adekunte and O'Kelly., 2009) conducted four plate load tests of different sizes. Each load step was followed by 10 minutes of constant loading. Significant creep settlement occurred, even at low stress levels. This means that it may have a significant effect on the settlement of the immersed tunnel as well. Lehane et al. (2008) reported that creep settlement increased with the natural logarithm of the elapsed time. They proposed the following relationships:

$$s_c/B = m * ln(\frac{t}{t_ref}) \tag{2.18}$$

Where s_c is the creep settlement, B is the width of the foundation, m is the creep coefficient, t is the elapsed time and t_{ref} is the reference time that corresponds with the onset of the creep settlement. This t_{ref} is an arbitrary value that is chosen to be 1 day that needs to be consistent over all calculations. The creep coefficient can be calculated using equation 2.19.

$$m = 0.02 * (\frac{q}{q_{ult}})^2 \tag{2.19}$$

Where q is the applied stress on the foundation and q_{ult} is the ultimate bearing resistance of the foundation. q_{ult} is assumed to be $\alpha * q_c$ with an α value of 0.20.

2.3.6 Cyclic loading model for sand

Cyclic loading is the repeatedly loading and unloading of the soil. This will cause the soil to change in stress and strain over time. Cyclic loading can cause a much larger settlement than if the same load is static. This is because the increase in strain at loading is larger than the decrease in strain at unloading. This difference in increase and decrease in strain becomes smaller at each loading causing a high rate of settlement at the first loading cycles and a lower rate of settlement after many loading cycles.

The cyclic loading is modelled using a simplified settlement model for cyclic loading from Garnier (2013). The equation that is being used is:

$$s_N = s_e * A^{ln(N)} \tag{2.20}$$

Where s_N is the settlement after N loading cycles, s_e is the elastic settlement from one loading cycle, A is a constant based on the material properties of the sand and N is the number of loading cycles that have occurred.

2.4 Scales of fluctuation

Describing the spatial variation of the soil is of great importance in the stochastic analysis of a geotechnical problem. An important parameter for describing this spatial variation is the scale of fluctuation. The scale of fluctuation is a measure of the distance between adjacent strong or weak zones relative to the depth trend. It is the distance beyond which there is negligible correlation between properties relative to the depth trend. This distance is shown in figure 2.10.

A database of the ranges of possible scales of fluctuations is missing but a scale of fluctuation of a few decimetres can be seen as a small scale of fluctuation and a scale of fluctuation of over a meter can be seen as a large scale of fluctuation.

Fig. 2.10.: Distance between adjacent strong zones (Prendergast, Reale and Gavin (2018))

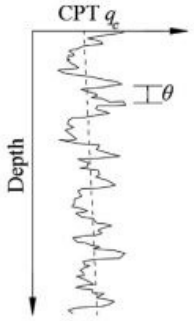

An approximate method created by Vanmarcke (1977) is that the scale of fluctuation can be calculated using the following equation:

$$\theta_v = 0.8 * d \tag{2.21}$$

Where θ_v is the scale of fluctuation, in this example vertical, and d is the average distance between two intersections of the cone penetration value and the trend line.

The scale of fluctuation differs in the different directions. The scale of fluctuation in vertical direction is smaller than in horizontal direction due to the layered deposition process. A more accurate way of determining the scale of fluctuation is using best fitting on one of these theoretical correlation model from equations 2.22-2.25 from Lloret Cabot, Fenton and Hicks (2014):

$$Markov : \rho(\tau) = exp(\frac{-2 * |\tau|}{\theta}) \tag{2.22}$$

$$Gaussian : \rho(\tau) = exp(-\pi * (\frac{|\tau|}{\theta})^2) \tag{2.23}$$

$$Triangular : \rho(\tau) = 1 - \frac{|\tau|}{\theta} \text{ if } |\tau| \leqslant \theta \quad 0 \text{ if } |\tau| > \theta \tag{2.24}$$

$$Spherical : \rho(\tau) = 1 - 1.5 * \frac{|\tau|}{\theta} + 0.5 * (\frac{|\tau|}{\theta})^3 \text{ if } |\tau| \leqslant \theta \quad 0 \text{ if } |\tau| > \theta \tag{2.25}$$

Where $\rho(\tau)$ is the theoretical correlation at a distance τ with a value between 1 and -1 with 1 being a fully positive correlation, -1 a fully negative correlation and 0 being no correlation and θ is the scale of fluctuation.

These models should be fitted to the estimated correlation function from Lloret Cabot, Fenton and Hicks (2014):

$$\hat{\rho}(\tau) = \frac{1}{\hat{\sigma}^2_{res} * (k - j)} * \sum_{i=1}^{k-j} (X_i - \hat{\mu}) * (X_j - \hat{\mu}) \tag{2.26}$$

Where $\hat{\rho}(\tau_j)$ is the estimated correlation based on the data at a distance of τ_j, $\hat{\mu}$ is the estimated mean, $\hat{\sigma}$ is the estimated standard deviation, X is the property that is correlated and $\tau = j * \delta\tau$. Where $j = 0, 1, 2, ..., k - 1$ where k is the number of

observations. For the way that equation 2.26 is defined it is necessary that the data points are equally-spaced in distance.

The error measure of each of the correlation models 2.22-2.25 compared to the estimated correlation functions can be calculated using equation 2.27.

$$E = \sum_{j=1}^{k} (\hat{\rho}(\tau) - (\rho(\tau))^2 \tag{2.27}$$

Where E is the summed squared error of the difference between the estimated correlation and the theoretical correlation. The best approximation for the scale of fluctuation is the value with the lowest error measure calculated in with equation 2.27.

2.4.1 Vertical scale of fluctuation

Numerous studies have examined the vertical variation of in situ soil properties and attempted to model them as accurate as possible based on the estimated correlation functions created by Vanmarcke (1977) using CPT data. These studies include (Degroot (1993), Jaksa et al. (1997), Baecher (2003), Giasi et al. (2003), Lloret-cabot, Fenton and Hicks (2014)), Firouzianbandpey et al. (2015) and Prendergast, Reale and Gavin (2018).

Results of these studies include for example 0.20 - 0.77 meter and 0.09 - 0.45 meter for sand layers at two different sites in Denmark from Firouzianbandpey et al. (2015), 0.42 - 0.44 meter for a sand layer in a sand fill for an artificial island in the Canadian Beauford Sea from Lloret Cabot, Fenton and Hicks (2014), 1.40 - 1.45 meter and 1.73 - 1.81 meter for two sand layers in the Rotterdam harbour from Prendergast, Reale and Gavin (2018) and 0.062 - 0.245 meter and 0.142 meter for clay layers at two different sites in Australia from Jaksa, Brooker and Kaggwa (1997).

A database of all possible ranges for different soil types is missing, but from these examples it can be concluded that the vertical scales of fluctuation are in the range 0.0 up to 2.0 meter or more and that it varies a lot from different sites and even at one site in one layer.

The vertical scale of fluctuation can only be determined using the CPT data because the measurement interval in z-direction for the MASW is in the range of 0.8 - 4.5

meter which means that there are not enough data point to determine the vertical correlation.

2.4.2 Horizontal scale of fluctuation

Some research have examined the horizontal scale of fluctuation as well. However, it is not as well examined as the vertical scale of fluctuation. This is due to the fact that to determine the horizontal scale of fluctuation the CPT's should be at least within the scale of fluctuation and preferably much closer, which is not the case for most sites. This is because if the spacing between 2 CPT's is larger than the scale of fluctuation, the correlation is close to 0, at which it can not be determined if the correlation is random or due to actual correlation.

For the same example studies as in chapter 2.4.1 the results are 1.2 meter and 2.0 meter for sand layers at two different sites in Denmark from Firouzianbandpey et al. (2015), 1.82 - 15.86 meter for a sand layer in a sand fill for an artificial island in the Canadian Beauford Sea from Lloret Cabot, Fenton and Hicks (2014) and 1.0 - 1.8 meter for clay layers at two different sites in Australia from Jaksa, Brooker and Kaggwa (1997).

MASW measurement are typically much closer spaced than CPT measurement in x-direction. This would make it seem that this is a perfect in situ measurement technique to determine the horizontal scale of fluctuation. Determining the horizontal scale of fluctuation using MASW measurements has not been done before in literature. This means that to actually use the scale of fluctuation from MASW it should be verified by comparing it to the horizontal scale of fluctuation determined by CPT at the same site, which has been shown before that it is a possible way to determine the horizontal scale of fluctuation.

2.5 Correlations CPT's and MASW in literature

The relationship between CPT data and shear wave velocity, and small strain shear stiffness, can be a powerful tool to describe a site for all relevant parameters based on one measurement technique. In this case, ideally all relevant parameters are described by the shear wave velocity parameter as this measurement technique is available for each interval of 2.5 m in x-direction. This relationship has been examined since Robertson and Companella (1983) to date.

2.5.1 Correlation shear wave velocity and cone penetration resistance

Andrus et al. (2007) performed a database study after these studies and concluded that the relationship is influenced by the cone penetration resistance, cone sleeve friction, confining stress, depth, soil type and the geological age. All relationships established before this study are for a certain soil type, either sands or clays, and for relatively young deposits. The study of Andrus et al. (2007) focuses on the relationship for all soil types and geological ages.

Figure 2.11 shows the database of the above mentioned study where the data is separated based on geological age.

Fig. 2.11.: Database Andrus et al. (2007)

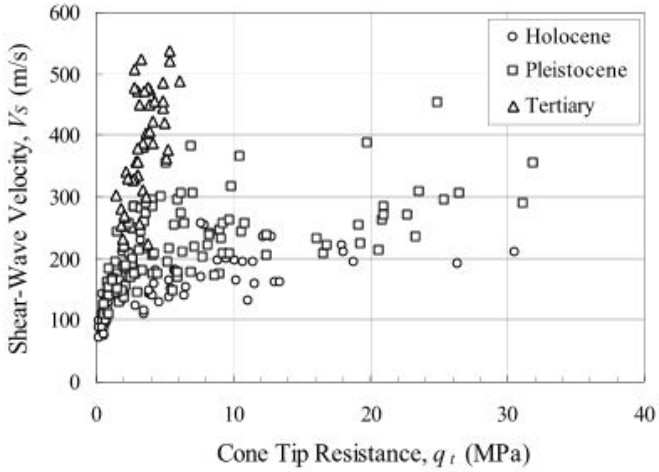

The measurements are from thick uniform layers, the CPT's are within a distance of 5 m of the shear wave velocity measurement, at least 2 full shear wave velocity measurements are within one layer and it should be possible to estimate the vertical stress reasonably accurate. The I_c value of the Holocene and Pleistocene data ranges from around 1-4 and the Tertiary data ranges from around 2-3. Figure 2.11 indicates that the geological age has an influence on the relationship between shear wave velocity and cone penetration resistance. But it still shows a large spread in data within a geological age, which could be due to the soil type.

Andrus et al. (2007) normalised both parameters according to equations 2.1 and 2.6. The study predicts normalised shear wave velocity based on the normalised cone penetration resistance, the soil type index I_c and an age scaling factor. The results of the fit for data that fitted best, $R^2 = 0.758$, is shown in figure 2.12. The data of the Pleistocene age had a coefficient of determination of 0.430 and the Tertiary age had a coefficient of determination of 0.397.

Fig. 2.12.: Prediction of normalised shear wave velocity versus the measured normalised shear wave velocity from Andrus et al. (2007)

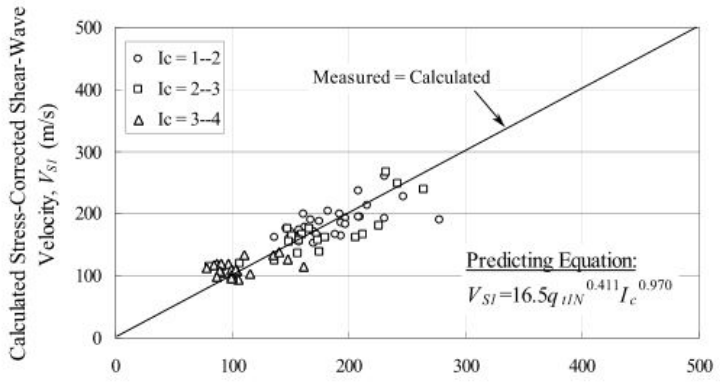

According to Karray et al. (2011) the above study did not mention one soil characteristic that influences the relationship between shear wave velocity and cone penetration as well, the grain size (even though it is implicitly taken into account using the I_c value). The database used and the fit made based on the grain size is shown in figure 2.13.

Fig. 2.13.: Influence of D_{50} on the V_{s1}-q_{c1N} relationship Karray et al. (2011)

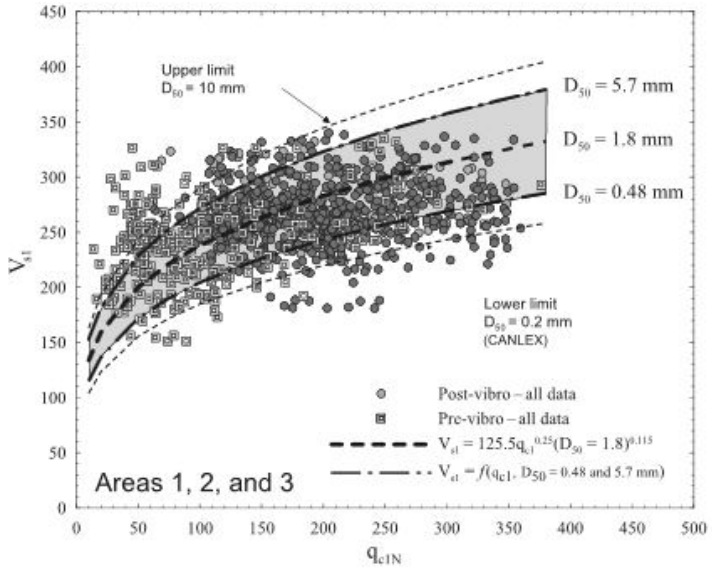

The average relationship according to Karray et al. (2011) can be described using equation 2.28. The equation is valid for median particle sizes D_{50} ranging from 0.2 to 10 mm.

$$V_{s1} = 125.5 * q_{c1}^{0.25} * D_{50}^{0.115} \tag{2.28}$$

Where V_{s1} is the normalised shear wave velocity, q_{c1} is the normalised cone penetration resistance, D_{50} is the median particle size. The median particle size D_{50} can be estimated with the normalised cone penetration resistance using equation 2.29. This equation is valid for I_c values lower than 2.6.

$$D_{50} = (\frac{4.6 - I_c}{2.944})^{\frac{1}{0.26}} \tag{2.29}$$

2.5.2 Correlation small strain shear stiffness and cone penetration resistance

In stead of correlating the results of both measurement techniques it is also possible to correlate the small strain shear stiffness and the cone penetration resistance directly, as these are the two parameters that are interesting for a load settlement response of a structure. Anagnostopoulos et al. (2003) performed a study of this correlation in Greek soils with q_c values ranging from 0.5 to 10 MPa. Figure 2.14 shows the fit made through the point for the different types of cones and all the data points.

Fig. 2.14.: Relationship small strain shear stiffness and cone penetration resistance from Anagnostopoulos et al. (2003)

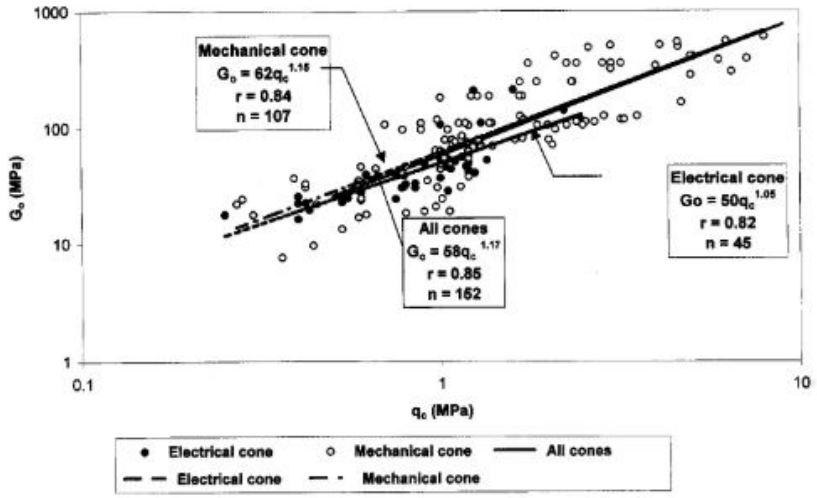

From this figure can be concluded that even though there is some kind of trend in the relationship between the small strain shear stiffness and the cone penetration resistance the uncertainty is high. For example at a q_c value of 1 MPa the G_0 ranges from at least 20 - 200 MPa, which is a factor 10, while for G_0 of 100 MPa the q_c ranges from at least 0.8 - 5 MPa, which is a factor of over 5.

2.6 Concluding remarks literature study

A logical way of modelling the foundation of an immersed is as a shallow foundation, given the similarities between the two. With the data available from the site investigation at both sites the best way to model it would be using a CPT-based model. The input parameters, apart from the loading, that need to be determined are the cone penetration resistance and the small strain stiffness. The first few tenths of percents of normalised settlement, which is the range which immersed tunnels will be in due to the low stress levels exerted on the soil, is dominated by the small strain stiffness of the soil.

Describing the spatial variation of the soil is of great importance in the stochastic analysis of a geotechnical problem. The vertical and horizontal scale of fluctuation differ for all different types of soils and locations. The horizontal scale of fluctuation is a factor larger than the vertical scale of fluctuation due to the horizontal deposition process of soils. Vertical scales of fluctuation of 0.09 up to 2.0 meter or more can be possible while horizontal scale of fluctuation of 1.0 up to 20 meters or more are possible. Vertical scale of fluctuation can be determined with CPT measurements, but not with shear wave velocity measurement due to the large interval between MASW measurements in vertical direction. Horizontal scale of fluctuation is in theory best done in with MASW due to the much smaller interval than the CPT's. However, this has never been done before in literature, which means it has to verified with horizontal scale of fluctuation calculate with CPT's as this has been done before and verified.

The correlations between the cone penetration resistance and the shear wave velocity or the small strain shear stiffness has quite some uncertainty, even in ideal circumstances. The relationship is influenced by cone penetration resistance, cone sleeve friction, confining stress, depth, soil type, median grain size and the geological age. Uncertainty in these factors contribute to the uncertainty in the relationship.

A fundamental problem mentioned by Andrus et al. (2007) with these relations, whether it is between cone penetration resistance and shear wave velocity or small strain shear stiffness, is that these are two totally different soil parameters. The cone penetration resistance is the strength at large strains while the small strain shear stiffness is a stiffness parameter at very small strain. This could be one of the reasons why the relationship between the two is not as strong.

3 Site investigation

3.1 Site investigation Kiltunnel

The Kiltunnel site contains a MASW profile over the full length of the tunnel, 6 CPT's and settlement data, shown earlier in figure 1.1, of the tunnel of a few decades. The locations of the CPT's and the MASW profile of the Kiltunnel site is shown figure 3.1. The MASW profile is shown with a red dashed line, it contains a measurement every 2.5 meter in x-direction.

Fig. 3.1.: Location MASW profile and CPT's Kiltunnel

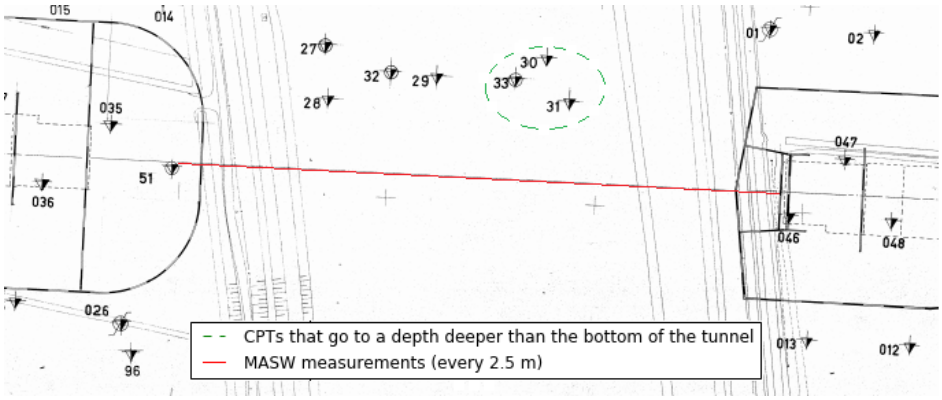

Figure 3.1 shows more than 6 CPT's. However, only CPT 27 and 29-33 are still available and CPT 30,31 and 33 are the only CPT's that are to a depth deeper than the bottom of the tunnel. These three CPT's are within a small area compared to the length of the tunnel as is shown in figure 3.1.

3.1.1 MASW Kiltunnel

The horizontal distance between two 1D shear wave profiles from MASW is 2.5 m. If all the 1D profiles of the Kiltunnel are linearly interpolated a 2D map of the shear wave velocity can be made. This map is shown in figure 3.2 for the Kiltunnel site.

Fig. 3.2.: 2D map of shear wave velocity profiles of the Kiltunnel

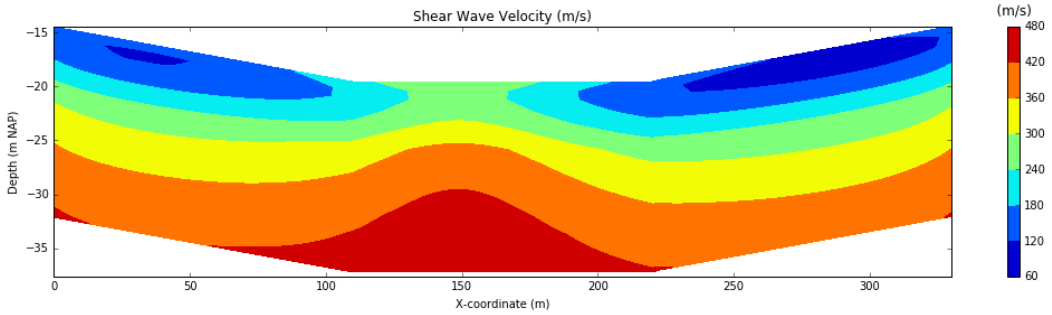

If the most likely wet unit weight is calculated with equation 2.2 using the mean values of fit parameters a and b, and the small strain shear stiffness is calculated with equation 2.3, it gives figure 3.3.

Fig. 3.3.: Small strain shear modulus (G0) profile of the Kiltunnel site.

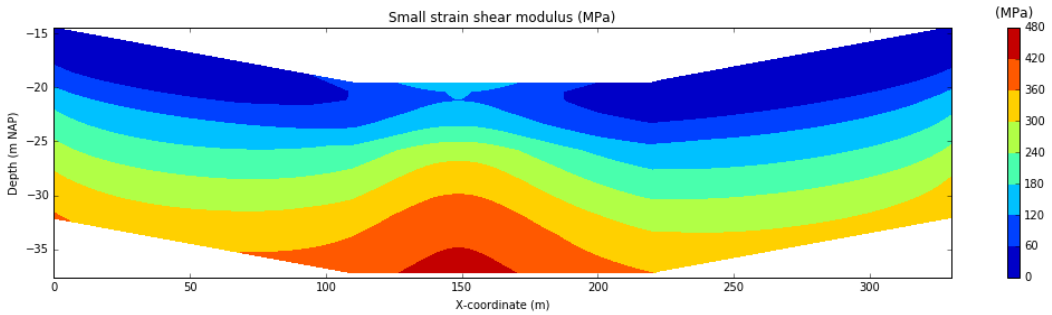

The lower G_0 values in the small strain shear stiffness profile of the Kiltunnel match the higher settlement in the settlement profile of figure 1.1. This indicates that the lower stiffness at the elements on the side might be one the reasons why the settlement is larger at those areas.

3.1.2 CPT's Kiltunnel

At the Kiltunnel site there are only the three earlier mentioned CPT's that go deeper than the bottom of the tunnel. At the Kiltunnel only the cone penetration resistance is known and not the sleeve friction and it is not known on which scale it is plotted. However, the soil type at the location of CPT 30 is known, which can be used to get a rough indication of the q_c value. The three CPT's and the bottom of the tunnel are shown in figure 3.4.

Fig. 3.4.: CPT's Kiltunnel

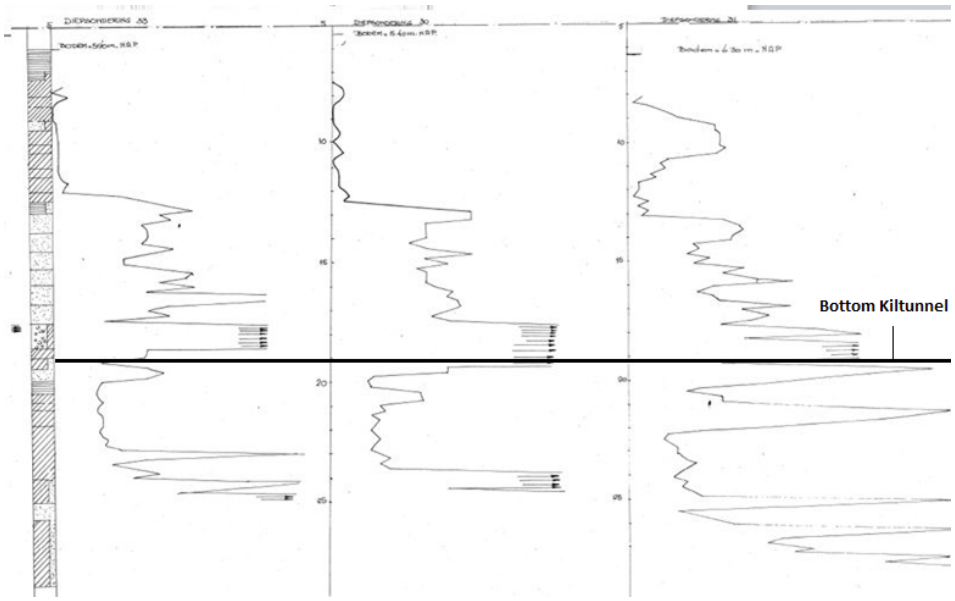

The three CPT measurements that are shown in figure 3.4 are performed before the installation of the Kiltunnel. Before the Kiltunnel was built the soil beneath the Kiltunnel was dredged to an unknown depth and backfilled with sand. This means that these three CPT's do not give an indication of the q_c values of the backfilled soil beneath the Kiltunnel.

3.2 Site investigation Heinenoordtunnel

The Heinenoordtunnel site contains a MASW profile over the full length of the tunnel, 65 CPT's and settlement data, shown earlier in figure 1.3, of the tunnel of a few decades. The locations of the CPT's and the MASW profile at the Heinenoord site is shown in figure 3.5

Fig. 3.5.: Location MASW profile and CPT's Heinenoord

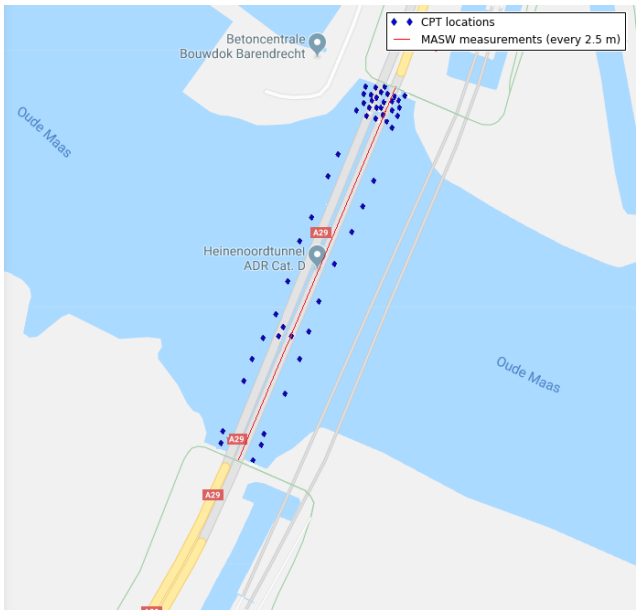

3.2.1 MASW Heinenoordtunnel

The maps for the Heinenoord site made from MASW are from data with a constant interval of 2.5 m in x-direction for a length of 600 m. In z-direction the intervals are irregular because the accuracy of the measurements decline with depth. The intervals range from 0.8 m at surface to 5.0 m at the lowest measured point. The map of the shear wave velocity of the Heinenoord site is shown in figure 3.6.

Fig. 3.6.: Shear wave velocity profile of the Heinenoord site.

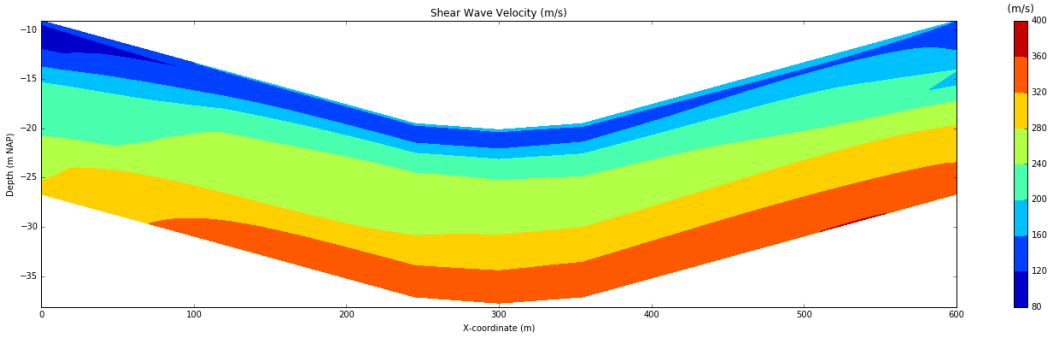

Equation 2.2, including an approximation of the top load of 25 kPa (15 kPa from the buoyant weight of the tunnel and 10 kPa from the soil on top of the tunnel), can be used to calculated the effective vertical stress. This can be used to calculate the most likely normalised shear wave velocity with equation 2.1. The result is shown in figure 3.7.

Fig. 3.7.: Normalised shear wave velocity profile of the Heinenoord site.

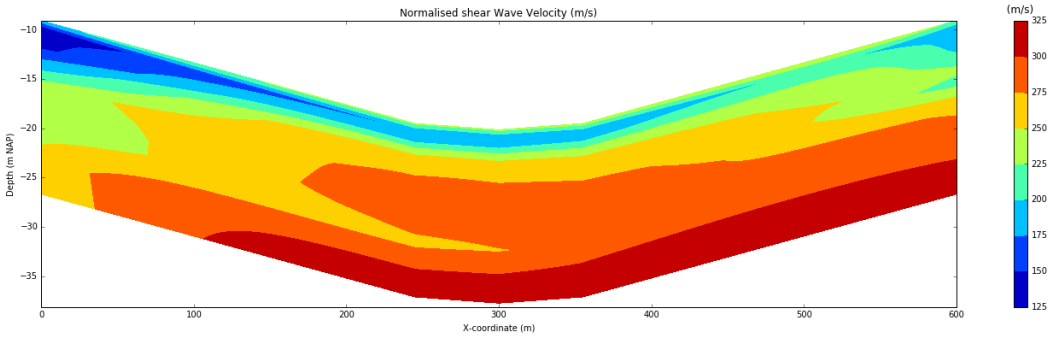

Using equation 2.2 to calculate the most likely wet unit weight of the soil, the most likely small strain shear stiffness can be calculated using equation 2.3. The resulting map is shown in figure 3.8

Fig. 3.8.: Small strain shear modulus (G0) profile of the Heinenoord site.

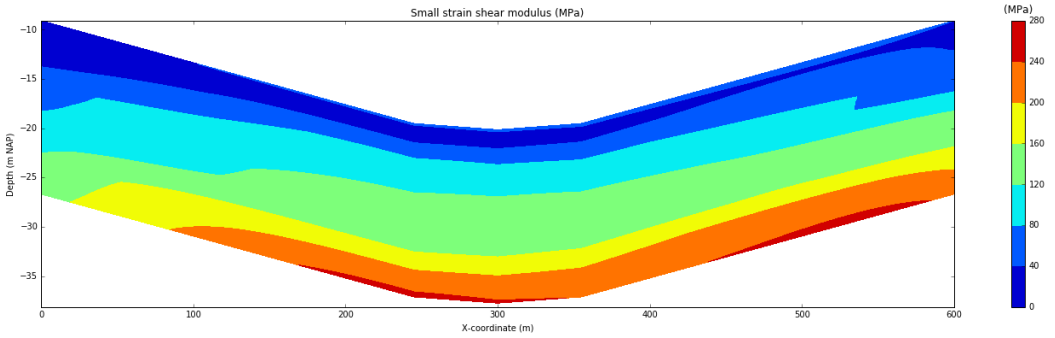

Combining equation 2.2 and 2.3 and the uncertainties of equation 2.2 the small strain shear modulus G_0 can be used in an probabilistic model, taking the uncertainties into account.

3.2.2 CPT's Heinenoord

13 of the 65 CPT's are used characterise the soil of the Heinenoord site. The 13 CPT's that are used are more or less in one line and about 15 – 20 m from the MASW profile. The locations of the CPT's are shown in figure 3.9.

Three typical CPT profiles of the Heinenoordtunnel are shown in figure 3.10. The first being typical for the Southwest section, the second for the middle section and the last for the Northeast section.

Fig. 3.9.: Location MASW profile and CPT's Heinenoord

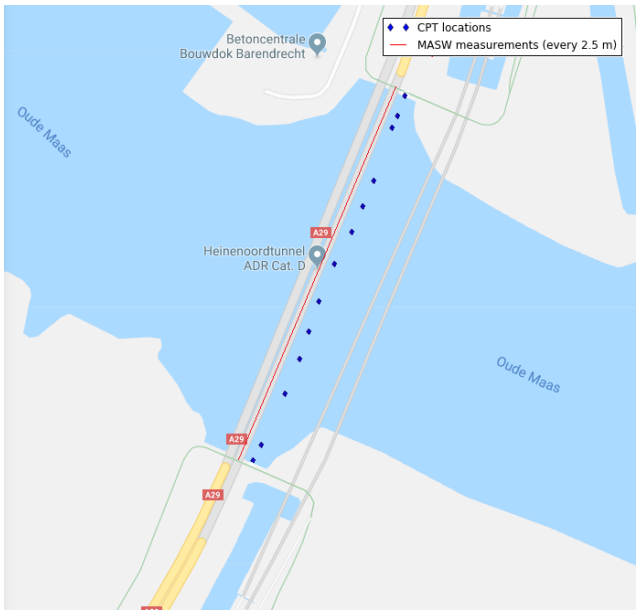

Fig. 3.10.: Typical CPT profiles for the Heinenoordtunnel

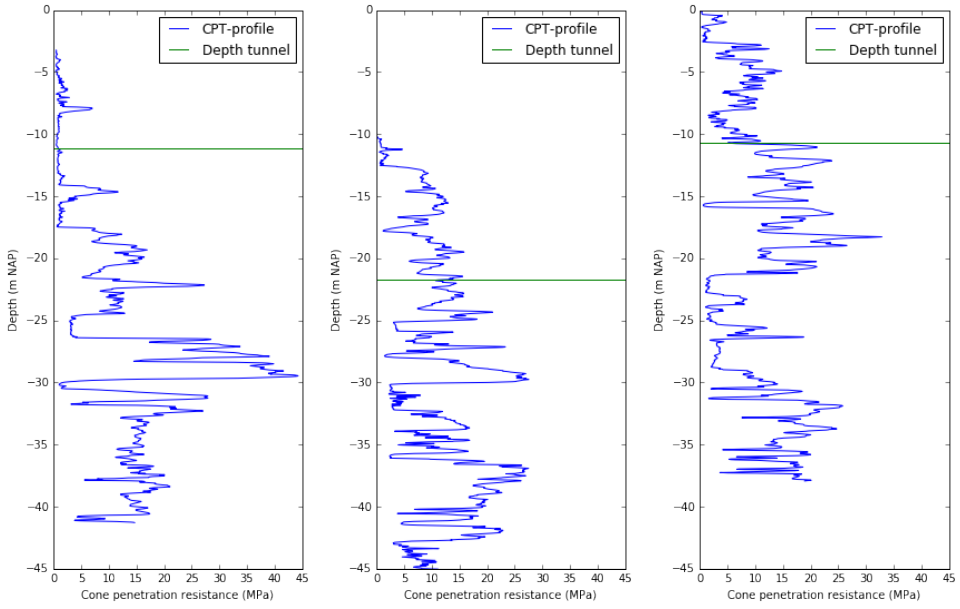

(a) Southwest (b) Middle (c) Northeast

4 Correlations between MASW and CPT

A possible way to characterise the site is to describe the probability of having a certain q_c value when a position has a certain shear wave velocity. This can be used to make a stochastic simulation of CPT profiles at a location based on the MASW profile to calculate the probability of having a certain settlement. The parameters from the CPT measurements are compared to the parameters from MASW to see if this is a possibility.

The steps for this approach would be as follows:

1. Establish the relationship between cone penetration resistance and shear wave velocity or small strain shear stiffness at this site.

2. Determine the loading conditions on the tunnel

3. Compute a Monte Carlo simulation with:

    a) Uncertainties in the soil parameters based on the relations with the shear wave velocity.

    b) Calculation of the settlements of the tunnel for each possible set of soil parameters.

4. Compute the probability of the settlement being a certain value.

This method is tested at the Heinenoord site. This method is not possible at the Kiltunnel site because of the lack of enough CPT data to correlate the both measurement techniques. However, the results at Heinenoord could possibly be used at the Kiltunnel site if the approach is successful.

4.1 Correlations CPT's and MASW

Ideally, when comparing the measurements of the CPT's and the MASW they are at almost the same position or at least within 5 meters because soil parameters vary in space and this would influence the results. The measurements of the CPT's and the MASW are not at exactly the same position at the Heinenoord site. The distances from the 65 CPT's that are used at the Heinenoord site to the nearest MASW profile at the Heinenoord are all smaller than 27.8 meter, about 50% is within 15 meter, and about 25% is within 5 meter.

The interval of the measurement of the MASW and the CPT's in z-direction are different. The interval of the MASW measurement increases with depth from 0.8 up to 4.5 meter while the interval of the CPT's has a constant value of 0.02 meter. The interval of the MASW in z-direction is 40-250 times larger than the interval of the CPT's, so the values from MASW are compared to the average of the CPT over that interval as can be seen in figure 4.1. Figure 4.1 shows a typical CPT profile, from the Northeast element of the Heinenoordtunnel, together with the nearest 1D MASW profile and the same CPT profile averaged over the interval of the MASW profile with the nearest 1D MASW profile.

Fig. 4.1.: Shear wave velocity and cone penetration resistance profile of a CPT at the Northeast entrance of the tunnel

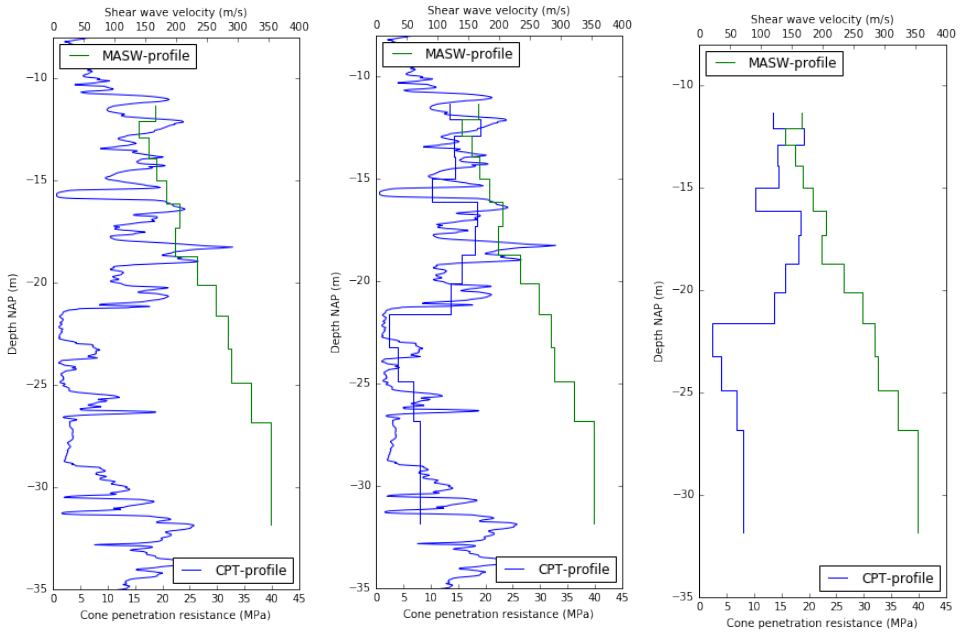

(a) All data from 1 CPT profile

(b) All data from 1 CPT profile and averaged over MASW interval

(c) CPT profile averaged over MASW interval

4.1.1 Correlation shear wave velocity and cone penetration resistance at the Heinenoord site

For the graphs in this section all 65 CPT's that are performed at the Heinenoord site are used. First the shear wave velocity is compared directly to the cone penetration resistance in figure 4.3 using the .

Fig. 4.3.: Shear wave velocity versus cone penetration resistance

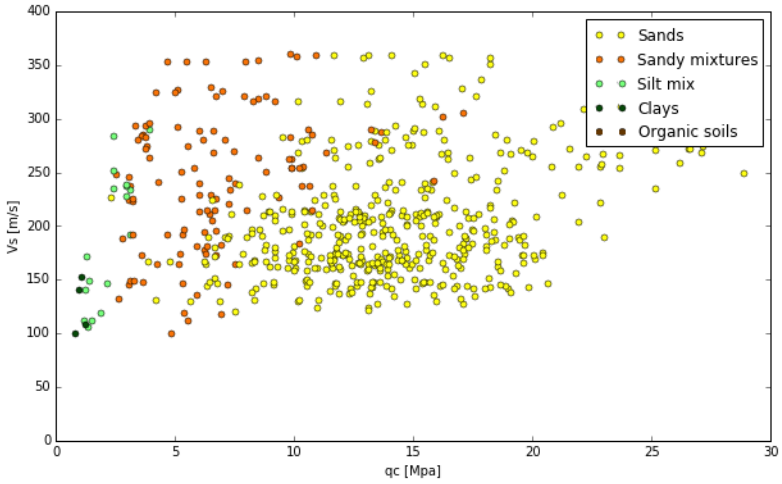

It seems like the correlation between the cone penetration resistance and the shear wave velocity is very weak. For a certain shear wave velocity, especially when higher than 150 m/s, almost the entire range q_c is possible. This causes a large uncertainty when using this correlation in the model. An explanation for this could be because the parameters are stress dependant, to account for this the normalised shear wave velocity is compared to the normalised cone penetration in figure 4.4.

Fig. 4.4.: Normalised shear wave velocity versus normalised cone penetration resistance

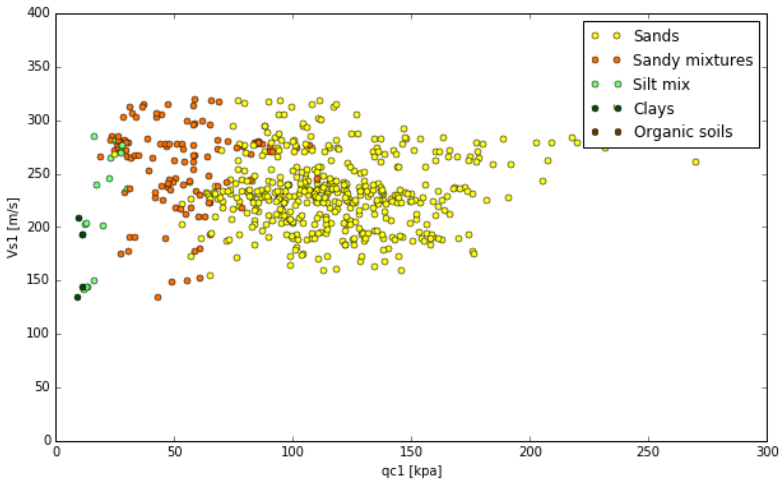

The spread of the data points has become smaller, but the problem of the large uncertainty still exist. This means that other factors influence the correlation as well. Explanations for this could be the distance between the MASW measurement and the CPT's and the fact that the MASW measurement was performed about 40 years after the CPT's have been performed. The static loading has been accounted for by normalising the parameters for the vertical stress but the dynamic loading from the tides and the traffic can have altered the soil beneath the tunnel during these years. Another possibility is that the correlation is just much weaker than presumed.

Something that is often done is to normalise the shear wave velocity with the cone penetration. This is done for the shear wave velocity and for the normalised shear wave velocity in figure 4.5.

Fig. 4.5.: Shear wave velocity and normalised shear wave velocity divided by cone penetration resistance versus normalised cone penetration resistance.

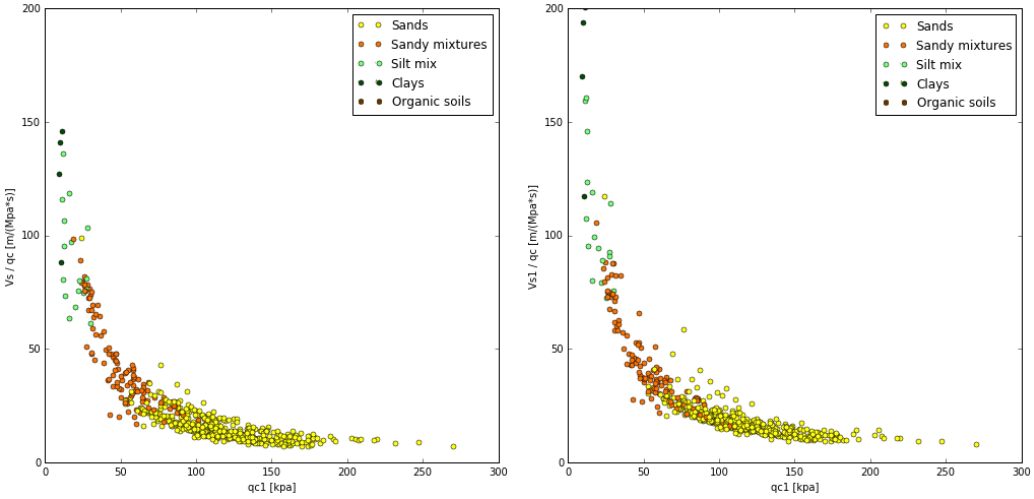

(a) Shear wave velocity

(b) Normalised shear wave velocity

When figure 4.5 is plotted on log-log space it looks like figure 4.7.

Fig. 4.7.: Shear wave velocity and Normalised shear wave velocity divided by cone penetration resistance versus normalised cone penetration resistance.

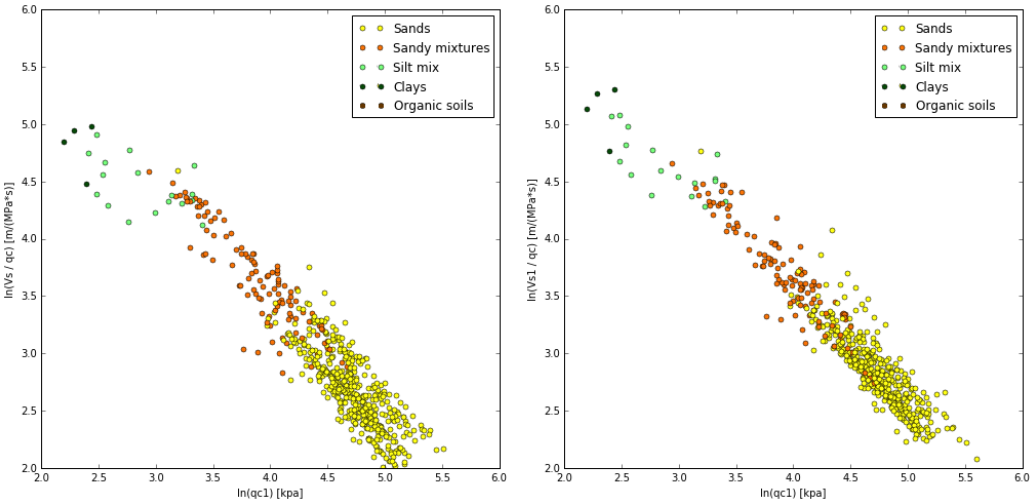

(a) Shear wave velocity

(b) Normalised shear wave velocity

Figures 4.5 and 4.7 seem correlated. But this is mostly due to the normalisation by the cone penetration resistance. When in figure 4.5 a certain V_s/q_c is selected, the difference between the lowest and the highest measured q_{c1} is still around a factor of 2. Adding the uncertainty in the q_c that needs to be selected to calculate V_{s1}/q_c would still cause a large uncertainty when the q_c values would be simulated using the MASW measurements only.

4.1.2 Correlation small strain shear stiffness and cone penetration resistance

Knowing the relationship between the small strain shear stiffness and the cone penetration resistance could prove useful for another site where only CPT data is present. If this small strain shear stiffness is normalised by dividing it by the cone penetration resistance or the normalised cone penetration resistance and this is compared to the normalised cone penetration resistance this gives figure 4.9.

Fig. 4.9.: Small strain shear stiffness divided by the cone penetration resistance versus normalised cone penetration resistance

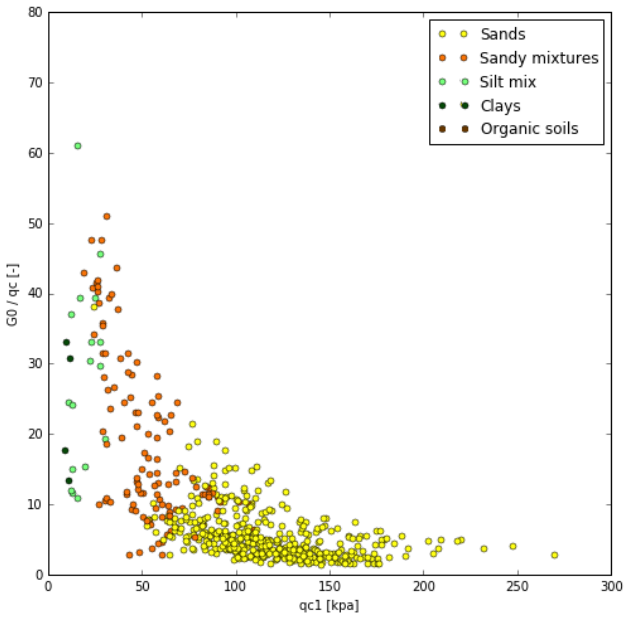

This figure 4.9 shows an even larger spread than the earlier figure 4.5 comparing the shear wave velocity. At a certain q_{c1} the difference between the lowest value and the highest value is a factor 5-10. This means that it hard to create a model that is accurate with this correlation.

4.2 Filtering measurements from multiple layers

One of the reasons why the relationship between the shear wave velocity or the small strain stiffness and the cone penetration resistance is not correlated enough to be useful could be because the measurements of MASW are at such a large interval that often the measurements are not through one layer but through multiple layers.

When looking at the I_c values of the soil in the CPT profile the measurements that are not entirely in soil type can be filtered out. When only looking at sand (other soil types only had a few data points) this results in figure 4.10 for measured values and figure 4.11 for normalised values.

Both figure 4.10 and figure 4.11 look like they have a slightly better correlation than figure 4.3 and 4.4 but at the same time it has the same problem that at a certain value of V_s or V_{s1} almost the entire range of possible q_c or q_{c1} values is possible.

Fig. 4.10.: Shear wave velocity versus cone penetration resistance for measurement entirely in sand layers.

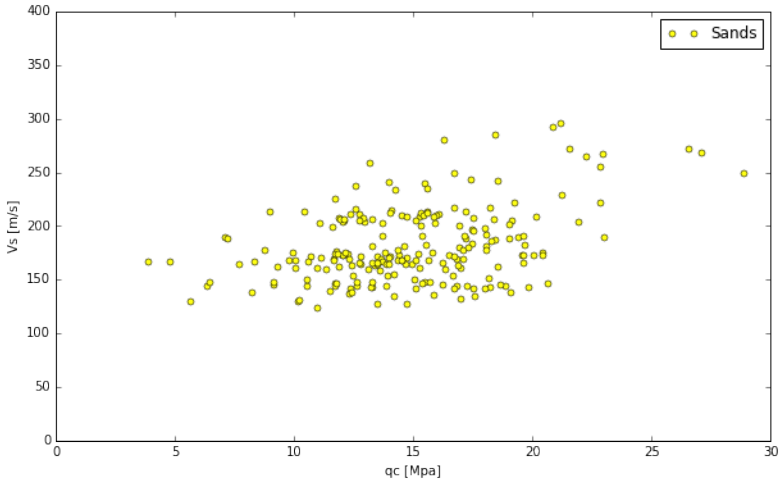

Fig. 4.11.: Normalised shear wave velocity versus normalised cone penetration resistance for measurement entirely in sand layers.

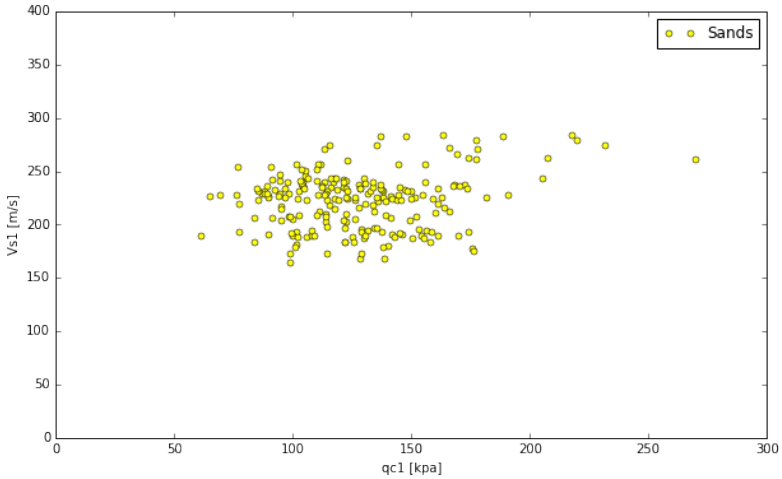

Dividing the V_{s1} values by the q_c gives figure 4.12.

The same trend can be observed as for figure 4.5. When in figure 4.12 a certain V_{s1}/q_c is selected, the difference between the lowest and the highest measured q_{c1} is still around a factor of 2. Adding the uncertainty in the q_c that needs to be selected to calculate V_{s1}/q_c would still cause a large uncertainty when the q_c values would be simulated using the MASW measurements only.

Fig. 4.12.: Normalised shear wave velocity versus normalised cone penetration resistance for measurement entirely in sand layers.

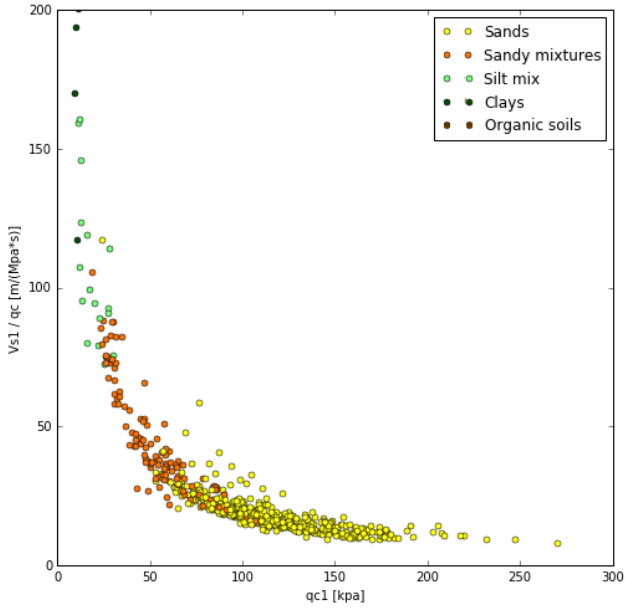

4.3 Comparison to literature

Literature usually focuses on determining the shear wave velocity from the cone penetration resistance instead of determining the cone penetration resistance from the shear wave velocity. This results in a lot of tricks (like dividing V_s/q_c, or V_s/I_c, or multiplying $V_s * D_{50}^{0.115}$) to increase the accuracy of the relationship. As figure 4.13 shows for example.

Fig. 4.13.: Normalised shear wave velocity versus normalised cone penetration resistance using the influence of the mean grain size (Karray et al., (2011)).

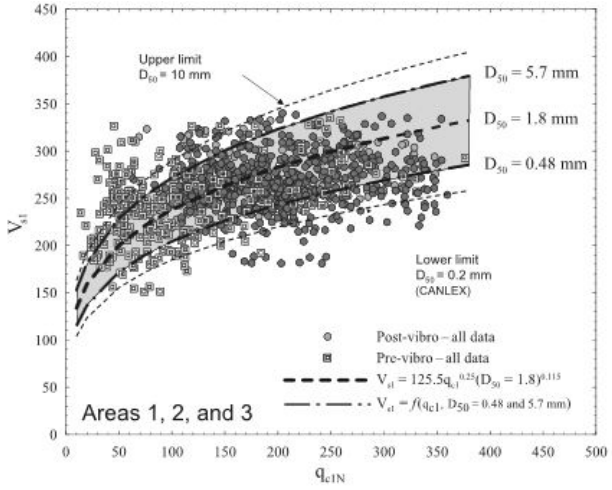

This increases the accuracy of determining the shear wave velocity from the cone penetration resistance but can not be used to increase the accuracy of determining

the cone penetration resistance from the shear wave velocity because of the weak interdependency of the mean grain size and the shear wave velocity according to Karray et al. (2011).

The shape of the relationship of the normalised shear wave velocity compared to the cone penetration in figure 4.13 is however very similar to the shape of the relationship in figure 4.11. This indicates that the relationship between the shear wave velocity and the cone penetration resistance does not increase a lot when other measures are taken to improve the relationship.

4.4 Concluding remarks correlation approach

The approach is based on the simulation of settlement using the MASW measurements to compute both the possible average values for small strain stiffness and cone penetration resistance at each interval of 2.5 meter in horizontal direction. The uncertainty of cone penetration resistance or normalised cone penetration resistance determined based on shear wave velocity or normalised shear wave velocity respectively is almost the same as if you do not correlate the two but just use all possible values of cone penetration resistance.

This means that there is no useful correlation between the cone penetration resistance and the shear wave velocity or the small strain shear modulus for the Heinenoord site.

The filtering of the measurements that are not entirely in one layer does increase the correlation between the shear wave velocity and the cone penetration, but not to a level at which it is useful for the calculation of the settlement at Heinenoord. The possible reasons for this lack of useful correlation are:

1. The distance between the MASW measurement and the cone penetration test are from 1 meter up to almost 28 meter. At those larger distances the layering can be different and even within layers the q_c values experiences large changes over distances of as small as 1.0 meter up to 15.86 meter or more as is shown in the literature study in chapter 2.4.2.

2. There is uncertainty in the shear wave velocity from the data collected with MASW technique. Shear wave velocities obtained from direct borehole measurements could increase the accuracy of the relationship, but this removes the positive properties of the MASW of a measurement every 2.5 meter and the possibility of measurements through the floor of the tunnel.

3. Influence of the geological age on the relationship.

4. Influence of the median grain size on the relationship.

5. Fundamental difference in soil properties. Cone penetration being large strain strength while shear wave velocity is linked to small strain stiffness.

The conclusion is that this method is possible but a large uncertainty is introduced due to a large uncertainty in the correlation between shear wave velocity and cone penetration resistance. It does not increase the accuracy of the model compared to when the entire range of possible q_c values that is found in the CPT profiles is used in the calculations.

5 Stochastic ground model approach

Chapter 4 concluded that there is no usable correlation between the cone penetration resistance and the shear wave velocity or the small strain shear stiffness for the Heinenoord site. Because there was no useful correlation for the Heinenoord site it was decided not to use the MASW as an input and correlate the q_c values from those values but to combined the data from the CPT's and the MASW in the settlement model to determine the parameters used to calculate the settlement.

A stochastic approach is chosen over a deterministic approach because a deterministic approach only gives an indication of the most likely occurring settlement while a stochastic approach gives the probability of the settlement being in a certain range. Given this information it can be determined if it is possible that the occurred settlement is due to the loading that is applied in the model.

At first only the middle (flat) element of both tunnels are investigated because the measurements show that this part is not influenced by the loads induced on the structure by the embankments. The steps for the stochastic ground model approach using both the CPT and MASW data is as follows:

1. Determine all statistical parameters of the CPT's:
    a) The depth trend of the cone penetration resistance.
    b) The standard deviation of the de-trended data.
    c) The vertical and horizontal scale of fluctuation.
2. Determining the loading conditions on the tunnel.
3. Compute a Monte Carlo simulation with:
    a) Simulated CPT profile at that location based on the statistics and vertical and horizontal scale of fluctuation.

b) Uncertainties in the soil parameters based on the relations of small strain shear stiffness with shear wave velocity and the simulated CPT profiles.

c) Calculate the settlements of the tunnel for each possible set of soil parameters.

4. Compute the probability of the settlement being a certain value.

5. Compare the computed probabilities of settlement to the measured settlement.

The settlement initial for each simulation is calculated using the Mayne model shown in equation 5.1.

$$s = \frac{Q_{app} * I_{hrv}}{B * E_0 * [1 - (\frac{Q_{app}}{Q_{ult}})^{0.3}]} \tag{5.1}$$

Where Q_{app} is the applied force in kN, I_hrv is the shape factor of the footing which is 0.85 for a rigid rectangular footing, B is the width of the foundation in m, E_0 is the small strain stiffness of the soil and Q_{ult} is the ultimate bearing resistance of the soil.

In the stochastic ground model approach the Q_{app} is assumed to be known, so no uncertainty is applied over this input parameter. The uncertainty in the model is due to the uncertainty in E_0 and Q_{ult}. Chapter 5.3 explains how the uncertainty of E_0 is taken into account and chapter 5.4 explains that for E_0.

The measurements for the Kiltunnel and the Heinenoord show a clear time dependent settlement. The hypothesis is that this time dependent settlement is due to creep settlement. Lehane et al. (2008, cited by Gavin et al. 2009) proposed the following relationships to describe the creep settlement:

$$s_c/B = m * ln(\frac{t}{t_{ref}}) \tag{5.2}$$

Where s_c is the creep settlement, B is the width of the foundation, m is the creep coefficient, t is the elapsed time and t_{ref} is the reference time that corresponds with the onset of the creep settlement. This t_{ref} is an arbitrary value that is chosen to be

1 day that needs to be consistent over all calculations. The creep coefficient can be calculated using equation 5.3.

$$m = 0.02 * (\frac{q}{q_{ult}})^2 \tag{5.3}$$

Where q is the applied stress on the foundation and q_{ult} is the ultimate bearing resistance of the foundation, which is calculated using $q_{ult} = \alpha * q_c$ using an α value of 0.20.

The relationship in equation 5.2 is used to describe the creep settlement of the Kiltunnel and the Heinenoordtunnel.

5.1 Statistical analysis

In order to model the CPT profile in a stochastic way to obtain an input value for the ultimate bearing capacity Q_{ult}, the CPT's needs the analysed statistically.

The statistical analysis is determined using the cone penetration resistance from the same 13 CPT profiles as from figure 3.9.

Each CPT is divided in layers based the soil type and the depth trend of the cone penetration values of that single CPT. Linearly interpolating between the boundaries of layer between CPT's gives figure 5.5.

Each layer is de-trended and normalised for each individual CPT. The reason that de-trending and normalising is needed is because the input for the estimated correlation function needs normalised CPT data with a mean of 0 and a standard deviation of 1. The procedure is as follows:

1. For each CPT the linear depth trend of q_c is found. This is done using a least squared estimate of the depth trend.

2. The linear depth trend of q_c is then subtracted from each CPT from each layer.

3. The residual standard deviation $\hat{\sigma}_{res}$ has to be calculated for each layer of each CPT.

4. The de-trended is normalised using the residual standard deviation to create a standard normal distributed set of data.

The steps are shown in figure 5.1. At this location the depth of the tunnel is 21.75 m. After these steps the normalised layer has a standard normal distribution, which means that the mean is 0 and the standard deviation is 1.

Fig. 5.1.: Steps de-trending and normalising CPT data

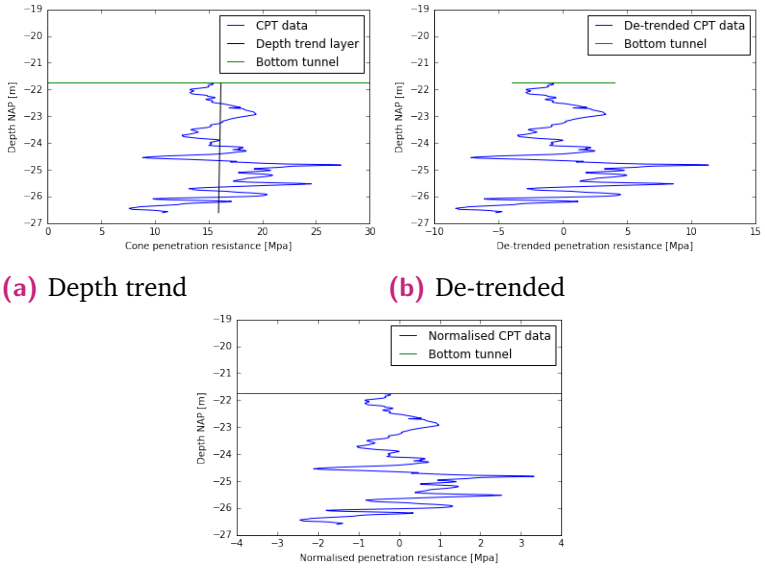

(a) Depth trend **(b)** De-trended

(c) Normalised

The CPT's are divided in layers based the soil type and the depth trend of the cone penetration values. This layer selection is a subjective process that influences the results. It does not change the results significantly but if layers are divided in thicker layers than needed it increases the uncertainty in the answer of your model while if layers are divided in smaller layers than in reality it introduces a decrease in uncertainty in the model that is not accurate.

5.1.1 Vertical scale of fluctuation

The values of the normalised data are then used in equation 2.26 to calculate the estimated correlation function of that layer at the location of that CPT. The error measure of each correlation model is calculated to determine the best type of correlation model. The vertical scale of fluctuation is calculated using the fit of the correlation model with smallest error measure.

The triangular and the circular model were in none of the cases the best model. Sometimes the Gaussian model was the best model, but in most cases the Markov model was the best model to approximate the correlation. An example of the fit of the Markov and the Gaussian model of the normalised layer of figure 5.1 is shown in figure 5.3. The results for each CPT is shown in appendix A along with all other relevant statistical data.

Fig. 5.3.: Estimated vertical correlation function compared to the correlation models

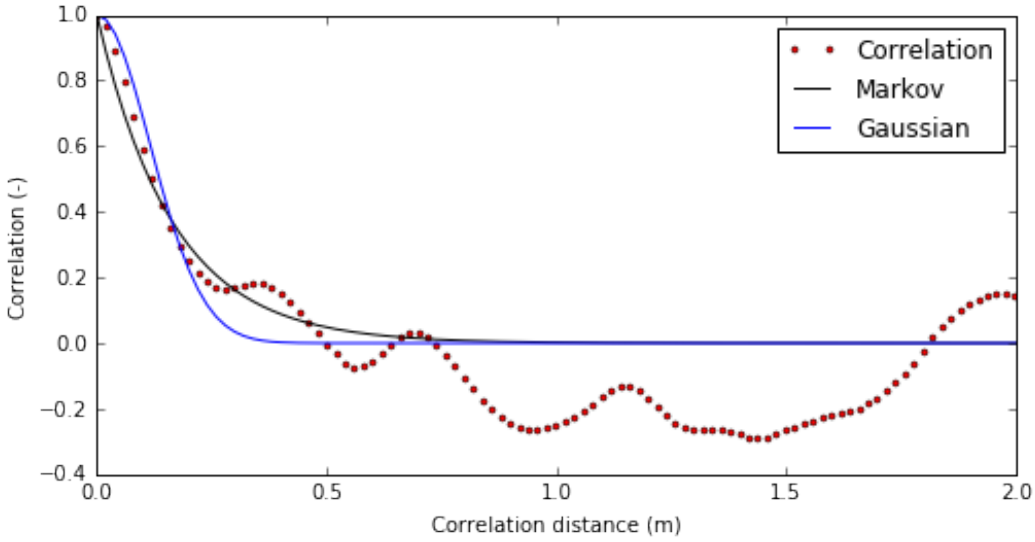

For this particular example shown in figure 5.3 the vertical scale of fluctuation of the Markov fit is 0.59 meter with a summed squared error of 0.06 and the vertical scale of fluctuation of the Gaussian fit 0.54 meter with a summed squared error of 0.37. This means that for this particular example the Markov fit is a better fit than the Gaussian fit.

5.1.2 Horizontal scale of fluctuation

One of the big advantages of MASW over CPT's is that a semi-continues 2D profile can be created of all the 1D profiles because the horizontal spacing between 2 measurements is only 2.5 m in this case. Whereas with CPT's a spacing of about 50 m is used. The large spacing between CPT's can make it difficult to calculate the horizontal scale of fluctuation because the correlation at that distance might already be very close to, or at zero. The horizontal scale of fluctuation is calculated using MASW and CPT's separately to test if the horizontal scale of fluctuation is similar for the shear wave velocity and cone penetration resistance values.

Horizontal scale of fluctuation using MASW

The soil is divided in horizontal layers and the mean of that layer at that x-position is subtracted from all values at that x-position. This value is used in equation 2.26 to calculate the estimated correlation function of that layer at the location of that CPT.

The error measure of each correlation model is calculated to determine the best type of correlation model.

For the horizontal scale of fluctuation using MASW the correlation models represented the estimated correlation function well as is shown in figure 5.4. The values of the horizontal scale of fluctuation for each model and the summed squared error are shown later in this chapter when they are compared to the values of the CPT's.

Fig. 5.4.: Estimated correlation function compared to the correlation models

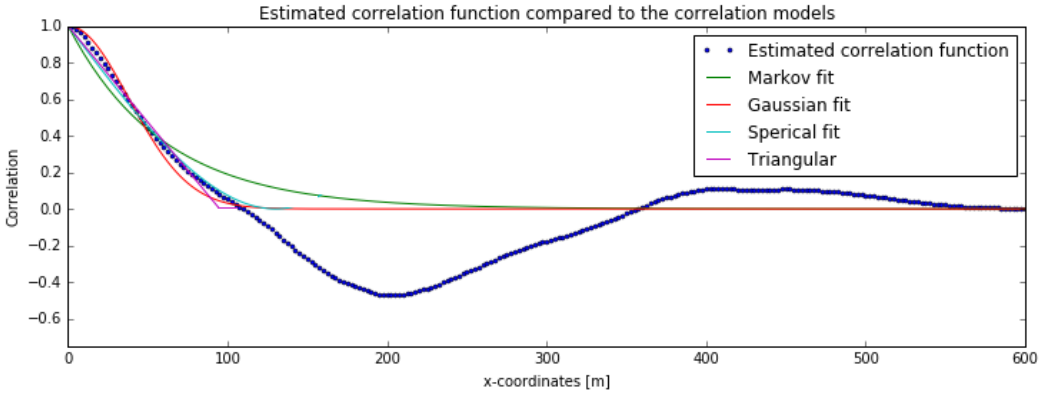

Horizontal scale of fluctuation using CPT's

Each CPT is divided in layers depending on cone penetration value and friction ratio trends. Linearly interpolating between the boundaries of layer between CPT's gives figure 5.5.

Fig. 5.5.: Layers of the Heinenoord site

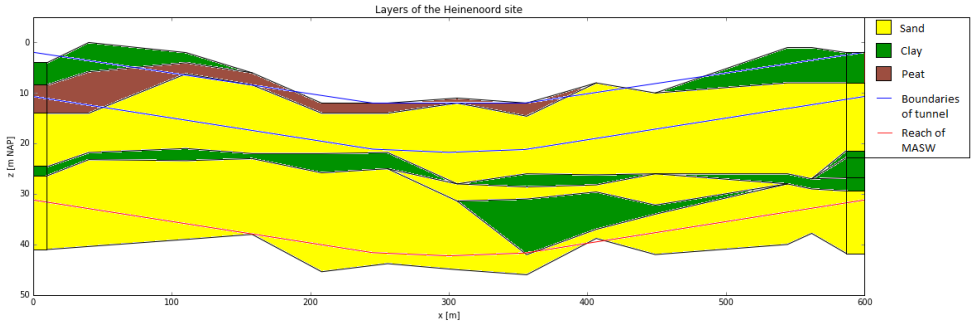

The horizontal scale of fluctuation for CPT's is calculated for each layer of figure 5.5 using the methodology from Lloret Cabot, Fenton and Hicks (2014). This methodology detrends each layer of each CPT with the linear depth trend and divides it by the residual standard deviation to create standard normal fields ($\hat{\mu} = 0$,

$\hat{\sigma} = 1$). The estimation correlation function 2.26 is then changed to equation 5.4, comparing a certain CPT 1, and CPT 2.

$$\hat{\rho}(\tau) = \frac{1}{(\hat{\sigma}_{res_1} * \hat{\sigma}_{res_2}) * k} * \sum_{i=1}^{k} (X_{1,i} - \hat{\mu}_1) * (X_{2,i} - \hat{\mu}_2) \tag{5.4}$$

Equation 5.4 is used for each layer to calculate the horizontal scale of fluctuation for each correlation model. The results of the analysis with the CPT's of the same layer analysed with MASW as in figure 5.4 are shown in figure 5.6.

Fig. 5.6.: Estimated correlation function compared to the correlation models

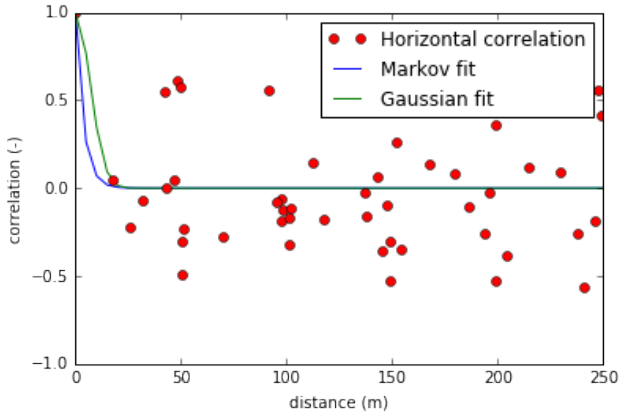

One of the first things that stand out in figure 5.6 is the large spread of the data points which give the first indication that the fit has a high uncertainty. The second problem with this figure is that the fit only goes through 1 data point which is very close to 0.0 correlation. The only conclusion that can be made from this figure is that the horizontal scale of fluctuation is very likely to be equal or smaller than the horizontal scale of fluctuation that is used to make the fit.

Earlier there was mentioned that only 13 CPT's of the 65 CPT's were used for 2D maps and the horizontal scale of fluctuation calculations. 30 of these 65 CPT's were used to map an area where on of the entrances of the tunnel was going to be. The distance between these CPT's range from 1 - 37 meters and the horizontal scale of fluctuation is assumed to be the same in every direction. These CPT's can be used to determine the horizontal scale of fluctuation more accurately. The results of the same layer as figure 5.4 and figure 5.6 are shown in figure 5.7. In the upper part of the figure all measurement points are shown and in the bottom part of the figure only the average of each 1 meter interval is shown.

Fig. 5.7.: Estimated correlation function compared to the correlation models for the closely spaced CPT's

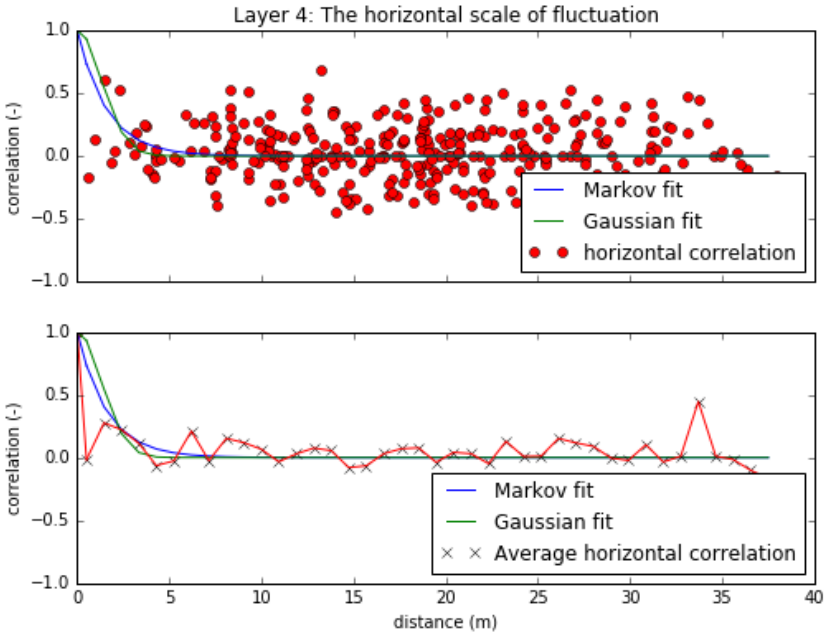

Figure 5.7 provides a better validation for the choice of a horizontal scale of fluctuation even though the scatter of points in the upper part of the figure is quite large.

The large scatter of figure 5.7 gives reason to doubt the method used to determine the scale of fluctuation. To validate the method it is tested at the Blessington which has a very uniform sand deposit. The results are shown in appendix C.1.

The results at Blessington show a larger horizontal scale of fluctuation (14.9 meter) and less scatter, but there is still a lot scatter in individual horizontal scale of fluctuation estimates and averaged estimates. Possible reasons for this scatter can be:

1. Layers being not strictly horizontal but at a (slight) angle.
2. Lack of enough equally spaced CPT's over which can be averaged.
3. Peaks and drops in q_c values due to transition into stronger or weaker zones in the layer.
4. Random noise in measurement values.
5. Rocks or pebbles in the soil.

Due to the small horizontal scale of fluctuation at the Heinenoord site and large uncertainty while obtaining this horizontal scale of fluctuation it is not used in the stochastic ground model.

Comparison horizontal scale of fluctuation from MASW and CPT's

The results for this layer from the analysis for the horizontal scale of fluctuation from the MASW and the CPT's are compared to compare the two methods. The results are shown in table 5.1.

Method of correlation estimation	Correlation model	Horizontal scale of fluctuation (m)
MASW	Markov	109.0
MASW	Gaussian	99.0
CPT's tunnel (far)	Markov	< 7.5
CPT's tunnel (far)	Gaussian	< 17.2
CPT's tunnel entrance (close)	Markov	3.2
CPT's tunnel entrance (close)	Gaussian	3.3

Tab. 5.1.: Comparison horizontal scale of fluctuation from MASW and CPT's

The results in table 5.1 immediately show that the horizontal scale of fluctuation of the shear wave velocity and the horizontal scale of fluctuation of the cone penetration resistance are two different quantities. The horizontal scale of fluctuation of the shear wave velocity is about 30 times larger than the horizontal scale of fluctuation of the cone penetration resistance. This means that scale of fluctuation from the MASW can not be used to determine the scale of fluctuation of the cone penetration resistance.

5.2 Soil profile simulations

The soil profile simulations for the stochastic ground model are based on a method from a paper from Prendergast, Reale and Gavin (2018). It is based on the idea that given the statistical data there is an infinite possible CPT profiles. However, all these CPT profiles are created with an distribution based on the statistical data.

The method starts with constructing a vector containing the z-values for a layer with equally spaced intervals. Then a correlation matrix ρ is created based on the scales of fluctuation and the z-vector. The correlation matrix contains the correlation, according to the Markov or Gaussian fit, between point x_i and x_j. The correlation

matrix is then decomposed in the lower L and upper L^T triangular matrices using the Cholesky decomposition as in equation 5.5.

$$\rho = L * L^T \tag{5.5}$$

In order to do use this Cholesky Decomposition the correlation matrix needs to be a positive definite matrix. This means that the matrix that $z_T * M * z$ is strictly positive for all non-zeros z-columns of real numbers. A property of a positive definite matrix is that all eigenvalues are positive. When the Gaussian function is used for the fit, not all eigenvalues of the correlation matrix are positive, meaning that it is not positive definite, which means that it can not be used in this approach. In 51% of the cases the Markov fit was the best fit and 49% of the cases the Gaussian was. When the Gaussian fit was the best fit the summed squared error was in 78% of the cases less than 25% larger than that of the Markov fit. Based on this it is assumed that the Markov fit for all correlations is a reasonable estimate.

If a vector of standard normal distributed numbers U of the same length as z is created and this is multiplied by the lower Cholesky Decomposition of the correlation matrix the correlated matrix of random processes G is created.

$$G = L * U \tag{5.6}$$

The matrix G has a normal distribution. The data of the CPT's is normally distributed but has a characteristic that is not taken into account using this approach with a normal distribution which is that the q_c values can not be negative. A log-normal distribution is chosen to simulate the CPT's because it gives a similar fit as the normal distribution and it prevents negative values. To transform the normal distribution to a log-normal distribution the parameters need to be transformed as shown in equation 5.7 and 5.8.

$$\sigma_{ln} = \sqrt{ln(1 + \frac{\sigma^2}{\mu^2})} \tag{5.7}$$

$$\mu_{ln} = ln(\mu_{ln}) - 0.5 * \sigma_{ln}^2 \tag{5.8}$$

These parameters can be used to create the simulated CPT profile that takes the statistical data and the vertical spatial variability into account using equation 5.9.

$$q_c = exp(\mu_{ln} + \sigma_{ln} * G) \tag{5.9}$$

5.3 Determining ultimate bearing resistance

The input parameter Q_{ult} for a single simulation is determined based on the cone penetration resistance q_c values of the CPT profile that is simulated in a single Monte Carlo simulation. The representative value of the cone penetration resistance $q_{c,avg}$ for a single simulation is the average q_c value right below the bottom of the tunnel over the zone of influence.

If it is assumed that the load $q_b, 0.1$ is $\alpha * q_c$ at a normalised settlement s/B of 10%, equation 5.1 can be rewritten to equation 5.10.

$$Q_{ult} = \frac{\alpha}{(1 - \frac{10 * \alpha * q_{c,avg} * I_{hrv} * L}{E_0 * B})^{1/0.3}} * (q_{c,avg} * B * L) \tag{5.10}$$

The value for α is assumed to be 0.20 based on the results from the study from Gavin, Adekunte and O'Kelly (2009). The calculated value of Q_{ult} is used as in an input parameter for equation 5.1.

5.4 Determining small strain modulus

The input parameter small strain modulus E_0 for a single simulation is based on the MASW measurement at that location. The uncertainty in E_0 is due to:

1. The uncertainty in the relationship between shear wave velocity from the MASW measurements and the actual shear wave velocity.

2. The uncertainty in the relationship between the shear wave velocity and the wet unit weight of the soil.

The uncertainty in the relationship between the shear wave velocity from the MASW measurement and the actual shear wave velocity is based on a research from Xia et al. (2002) comparing the Comparing shear-wave velocity profiles inverted from

multichannel surface wave with borehole measurements. He concluded that the difference between the two are random and approximately 15% or less. The article does not give an accurate description of the approximate distribution of the differences. For that reason it is assumed that the differences are normally distributed. Using the 3σ-rule with a highest conceived value of +15% and a lowest conceived value of -15% the standard deviation of the actual shear wave velocity is assumed to be 5% of the value obtained from the MASW measurement.

The uncertainty in the relationship between the shear wave velocity and the wet unit weight of the soil is described in chapter 2.1.1. The equation that described the relationship was:

$$\rho_w = a * (V_s)^b \tag{5.11}$$

Where ρ_w is in kN/m^3 and V_s in m/s and a and b are fit parameters of the correlation and have a mean and a standard deviation. Parameter a and b are described by mean μ_a = 4.12 with a standard deviation of σ_a = 0.021 and mean μ_b = 0.262 with a standard deviation of σ_b = 0.0087 for coarse-grained soil. The uncertainties in the fit parameters cause an uncertainty in the determination of small strain shear stiffness G_0 using equation 5.12.

$$G_0 = \rho_w * V_s^2 \tag{5.12}$$

Where the small strain shear stiffness G_0 is in kPa, the wet unit weight ρ_w is in kN/m^3 and the shear wave velocity V_s is in m/s. The small strain stiffness E_0 is then calculated using equation 5.13.

$$E_0 = G_0 * 2 * (1 + \nu) \tag{5.13}$$

Where ν is the Poisson's ratio which is assumed to be 0.1 for small strains. The uncertainty in the relationship is due to the uncertainty in the Poisson's ratio, this uncertainty is not taken into account in the model.

The procedure mentioned in this chapter is done for in each simulation each interval of the MASW measurement. The value for E_0 that is used in equation 5.1 is the average value over the zone of influence.

5.5 Loading conditions

At first, only the static loading conditions are examined. These loading conditions consist of the buoyant weight of the immersed tunnel and the weight of the soil on top of the tunnel. The buoyant weight of the immersed tunnel consists of the weight of the concrete of the structure, the ballast concrete and the asphalt of the road minus the weight of the displaced water.

The loading is calculated for each segment, because based on the differential settlement in figure 1.1 it is assumed that each segment settles individually. The loading is calculated for the middle element, because that is where the weight of the dike does not have an influence on the loading conditions.

5.5.1 Static loading Kiltunnel

The cross-section of the tunnel is assumed to be constant over the entire length of the tunnel. The cross-section of the Kiltunnel is shown in figure 5.8. The weight of the concrete is 24 kN/m^3, the weight of the water is 10 kN/m^3 and the weight of the sand on top is assumed to be 20 kN/m^3 with a thickness of 2 meter. The length of a segment is 22.3 meter. The space between the tunnel element and the road is assumed to be filled with ballast concrete. The cross-section in figure 5.8 shows the thickness of the ballast concrete. This means that on average the concrete is 2.63 meter thick from the bottom of the tunnel.

Fig. 5.8.: cross-section Kiltunnel.

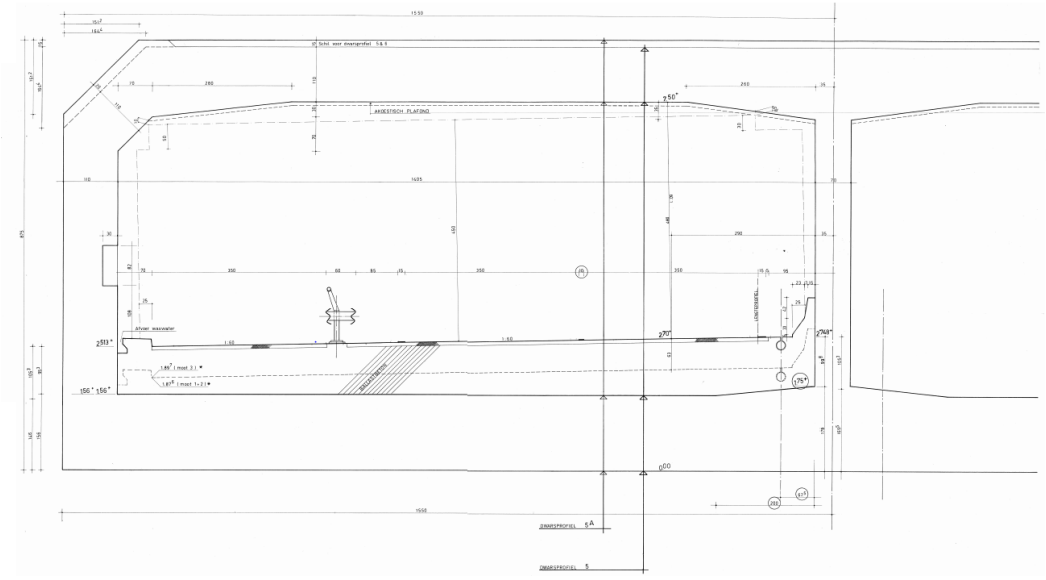

The total static loading on a segment of the foundation of the immersed tunnel is then the buoyant weight of the tunnel plus the buoyant weight of the soil on top of the tunnel. Which can be calculated using equation 5.14.

$$Q_{app} = A_c * L * \rho_c - A_w * L * \rho_{water} + A_s * L * (\rho_s - \rho_{water}) \tag{5.14}$$

Where A_c is area of the concrete, L is the length of the segment, ρ_c is the unit weight of the concrete, A_w is the area of the total cross section of the tunnel, ρ_{water} is unit weight of water, A_s is the area of the soil on top of the tunnel and $\rho_s - \rho_{water}$ is the buoyant unit weight of the soil.

The total area of the cross-section of the immersed tunnel is 268.53 m^2, the area of the concrete is 133.99 m^2 and the length of the segment is 22.3 meter and the width the tunnel is 31.0 meter. The thickness of the soil on top is assumed to be 2 meter and have buoyant unit weight of 10 kN/m^3. This gives a Q_{app} of 24,800 kN per segment. This gives an applied stress of 35.9 kPa. The calculation is shown in appendix B.2.

5.5.2 Static loading Heinenoordtunnel

The cross-section of the tunnel is assumed to be constant over the entire length of the tunnel. The cross-section of the Heinenoordtunnel is shown in figure 5.9.

Fig. 5.9.: cross-section Heinenoordtunnel.

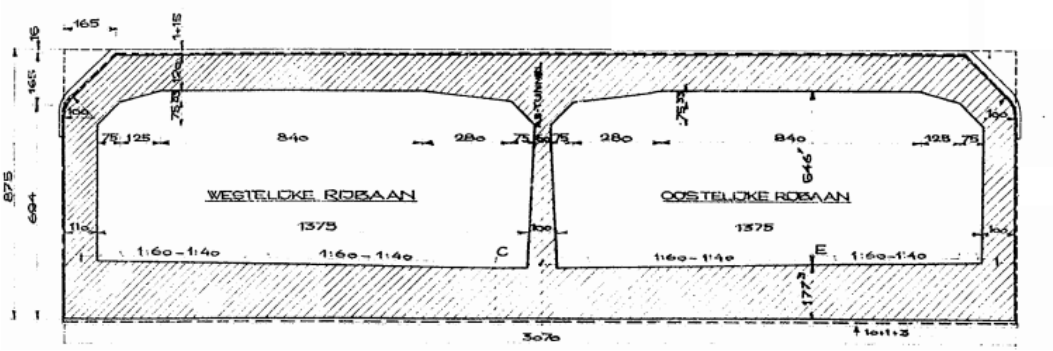

The weight of the concrete is 24 kN/m^3, the weight of the water is 10 kN/m^3 and the weight of the sand on top is assumed to be 20 kN/m^3 with a thickness of 1 meter. The length of a segment is 24.0 meter and the width of the tunnel is 30.7 meter. Because of lack on information of the ballast concrete in the Heinenoordtunnel it is assumed to be the same thickness as the Kiltunnel as the design of the Heinenoordtunnel

is based on that of the Kiltunnel. This means that on average the concrete is 2.63 meter thick from the bottom of the tunnel.

The total static loading on a segment of the foundation of the immersed tunnel is calculated using equation 5.14. The total area of the cross-section of the immersed tunnel is 267.26 m^2, the area of the concrete is 132.16 m^2, the length of the segment is 24.0 meter and the width of the tunnel is 30.7 meter. The thickness of the soil on top is assumed to be 1 meter and have buoyant unit weight of 10 kN/m^3. This gives a Q_{app} of 19,350 kN per segment. This gives an applied stress of 26.3 kPa. The calculation is shown in appendix B.3.

5.6 Settlement calculations

The initial settlement calculations are done using a Monte Carlo simulation. This means that the initial settlement is calculated N times using equation 2.13. In this equation Q_{app}, I_{hrv} and B are constant, while Q_{ult} changes based on the simulated CPT profiles and E_0 changes based on the uncertainty in shear wave velocity based on the MASW measurement and the uncertainty in the relationship between E_0 and V_s. Each calculation in the Monte Carlo simulation gives a value for the settlement. The probability of a certain settlement is the amount of times the settlement is calculated divided by N.

5.6.1 Verification at Blessington site

In order to show if the model for the initial settlement is accurate, it is tested and compared to plate load tests that are performed in a sand quarry in Blessington, Ireland. The sand was deposited at the bottom of a glacial lake and had a median grain size D_{50} of 0.10 (silty sand) to 0.32 (coarse sand). Glacial loading and removal of 15 meter of overburden material causes the sand to be heavily overconsolidated. For more details about the site see Gavin, Adekunte and O'Kelly (2009) and Gavin and O'Kelly (2007).

The size of the plate load test is 0.25 x 0.25 meter. For this very small plate load test the determination of the zone of influence using a rule of thumb for square footings is accurate enough. This means that the zone of influence = 2B = 0.50 meter. In this zone of influence the average q_c value is approximately 13750 kPa and the average G_0 value is approximately 80000 kPa. The plate is loaded up to a level of around 2750 kPa, which is around 0.2 * q_c. The CPT profiles and the G_0 profiles are shown in appendix C.

The shear wave velocity is back-figured from the average G_0 value using equation 5.11 and 5.12. The same uncertainty procedures are used as described in chapter 5.3 and 5.4. The results of the comparison of the normalised settlement s/B versus the normalised loading q/q_c of plate load test versus the model are shown in figure 5.10. The figure shows the boundaries of the probability of the normalised settlement being smaller than a certain value after a certain normalised loading.

Note that for the measured load settlement response only initial settlement is measured. This is according to model which only takes initial settlement into account. This means that it does not take creep or time dependent loading into account.

Fig. 5.10.: Data points load-settlement response Blessington versus probability boundaries of normalised settlement being larger according to the model.

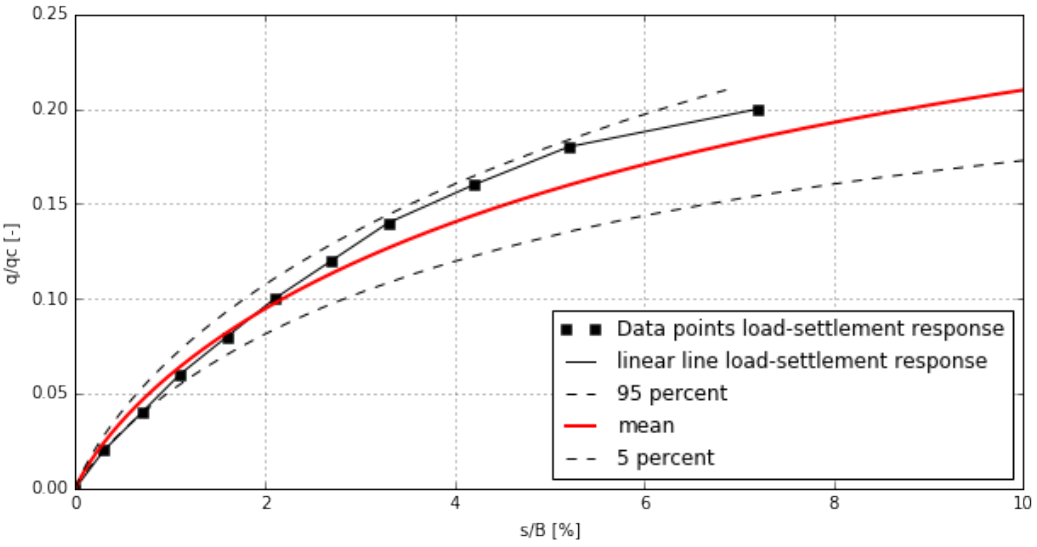

Figure 5.10 show that the occurred settlement at the plate load test site in Blessington are within the probability ranges of 90% (between 5% and 95%). In the range of s/B of 0-1 % the load-settlement response it is approximately the same as the 95% settlement response. After that, when s/B is in the range of 1 - 8 % the values vary around the mean response.

The comparison between the plate load test and the model shows that the model works for initial settlement of small scale plate tests at the Blessington site. The literature study in chapter 2.3.2 arguments that the model can be scaled up to at least 2.5 x 2.5 meter but indicates that it can be scaled up to even larger dimensions.

5.6.2 Settlement calculations Heinenoordtunnel site

The model that is verified at the Blessington site is first going to be used at the Heinenoord site because of the deeper and higher amount of CPT's. The dimension of 1 segment, which is assumed to be settling independently, is 24.0 x 30.7 meter.

At the location of the middle element, 3 CPT's were performed. The calculations and figures that are shown in this chapter are performed using the middle CPT of the middle element and the nearest 1D MASW profile to this CPT. The CPT that is used is in this chapter highlighted in figure 5.11 with yellow, the CPT that are used for the calculations in appendix D are highlighted with brown.

Fig. 5.11.: Locations of the CPT's used (yellow for this chapter, brown in appendix).

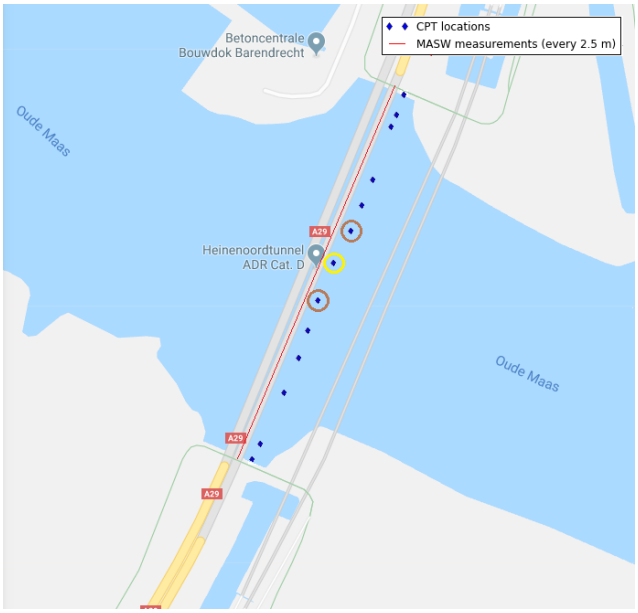

Zone of influence

An important parameter that influences the results of the model is the zone of influence. The input parameters E_0 and Q_{ult} are averaged over this zone of influence. The maximum zone of influence that can be taken into account is a zone of influence of 20 meter, because this is the maximum depth of the MASW. The influence of the zone of influence is shown in figure 5.12. In this figure the zone of influence is varied from 2.0 to 20.0 meter with an interval of 1.0 meter. For each interval of 1.0 meter 100,000 simulations of the soil parameters were performed. The probabilities of settlement being smaller than the plotted values is shown for these zones of influence.

Fig. 5.12.: Probability of settlement being smaller versus zone of influence using 100,000 simulations for each 1.0 meter interval.

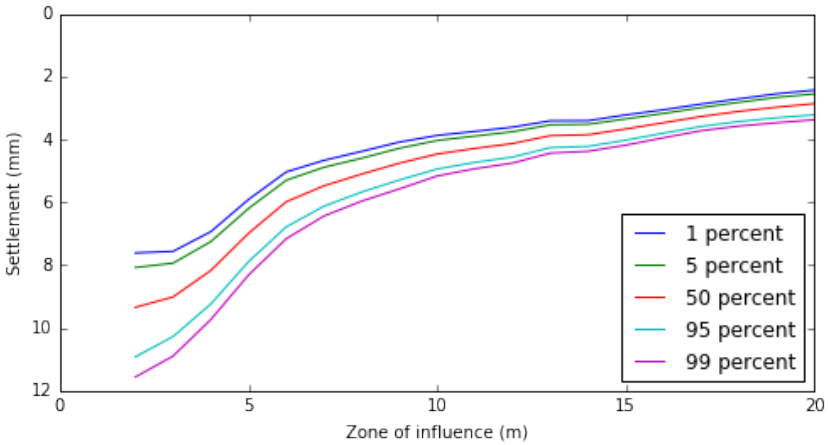

Figure 5.12 shows that the zone of influence has a large influence on the results of the model and illustrates the importance of an accurately determined zone of influence. The initial settlement tends to be smaller at a larger zone of influence. This is because all over the site the shear wave velocity, and with that the estimated small strain modulus, increases with depth.

The method used to determine the zone of influence is described in chapter 2.3.4. The Boussinesq equation used is repeated in equation 5.15.

$$q_v = \frac{3Q}{2\pi z^2} * \frac{1}{(1 + (r/z)^2)^{\frac{5}{2}}} \tag{5.15}$$

Where q_v is the vertical stress increase at the location chosen in the subsurface, Q is the force of the point load in kN, z is the depth below the point load, r is the horizontal distance from the point load to the location chosen in the subsurface which means that $r = (x^2 + y^2)^{0.5}$.

Using the static loading of the Heinenoordtunnel of 26.3 kPa, the width of the segment of 30.7 meter, the length of the segment of 24.0 meter and the dividing of the loading in point loads of area's of 0.25 x 0.25 meter gives the distribution of stresses shown in figure 5.13. Figure 5.13 gives a cross section of the increase in stress in the soil beneath the tunnel.

The zone of influence is defined in Eurocode 7 as the depth at which the increase of stress due to the loading of the tunnel is larger than 25%. Because the actual effective unit weight of the soil is unknown it assumed to be 8 kPa/m^3. The centre of the tunnel is used as the representative stress increase for the determining of the

Fig. 5.13.: Cross section of the Boussinesq solution of the increase of stress in the soil beneath the Heinenoordtunnel under the static loading of the tunnel.

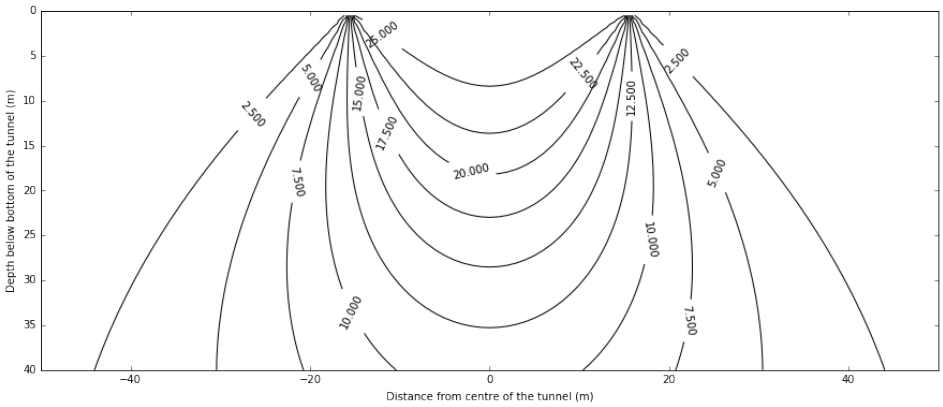

zone of influence. Given the rule from Eurocode 7 the following equation can be used to determine the zone of influence:

$$q_v(Z_i) = 0.25 * 8 * Z_i \tag{5.16}$$

Using equation 5.16 and the solution of the Boussinesq calculation the zone of influence can be determined at a certain location in the tunnel as the intersection between equation 5.16 and the increase in stress calculated using the Boussinesq solution. This is shown in figure 5.14 for the middle of the segment.

Fig. 5.14.: Boussinesq solution in depth compared to 25% of the in situ vertical stress at the middle of the segment.

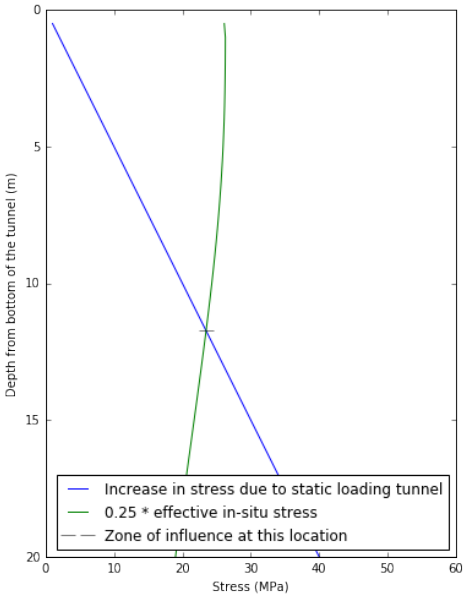

If this is done for each location over the width of the segment it creates figure 5.15 This figure includes the average zone of influence over the width of the tunnel.

Fig. 5.15.: Zone of influence over the width of the segment and the average zone of influence over the width of the segment.

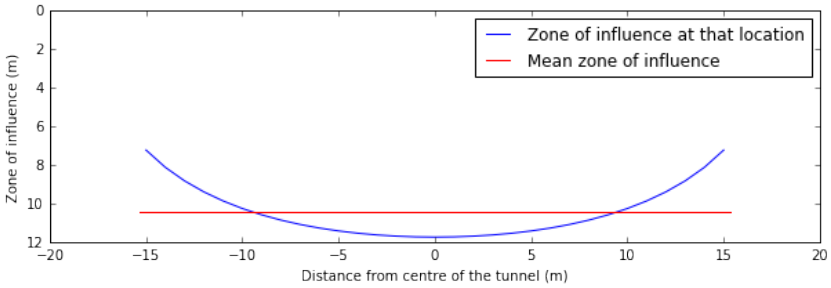

The zone of influence is on average 10.41 meter for the Heinenoordtunnel.

Initial settlement calculations Heinenoordtunnel

Using this zone of influence of 10.41 meter the settlement can be calculated using the described procedure. The initial settlement is calculated for the middle element using the middle CPT using 100,000 simulations. The probability density plot is shown in figure 5.16 and the cumulative density function is plotted in figure 5.17.

Fig. 5.16.: Probability density plot of the initial settlement of the middle CPT of the middle element of Heinenoord.

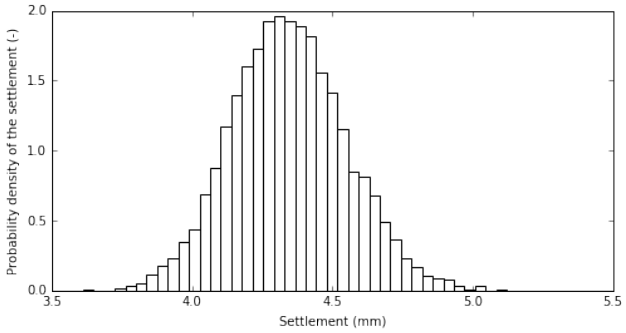

The 5% and 95% boundaries of the initial settlement at the middle element of the Heinenoordtunnel are 4.04 - 4.68 mm. These initial settlements that are calculated can not be compared to the measured settlements at the Heinenoordtunnel. This is because the measurements started after the Heinenoordtunnel was being built and the first measurement is a zero measurement. This means that at the moment of the zero measurement, the initial settlement have already occurred.

Fig. 5.17.: Cumulative density function of the initial settlement of the middle CPT of the middle element of Heinenoord.

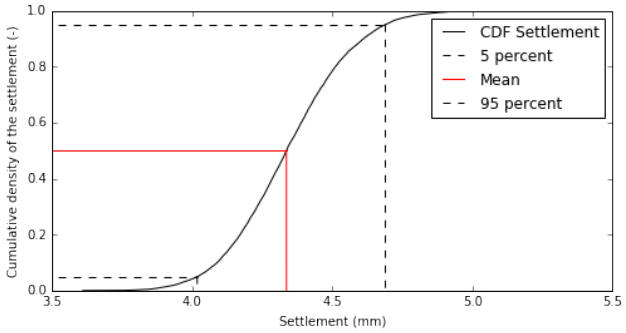

Creep settlement calculations Heinenoordtunnel

The next step is to introduce the creep settlement in the model. This is done using equations 5.2 and 5.3. No real investigation has been done in the factors in these two equations. The calculated creep settlements are merely to show an order of magnitude of the creep settlements. The calculated creep settlement is plotted in figure 5.18 without the initial settlement, because the initial settlement is not measured.

Fig. 5.18.: Estimated probability boundaries of the creep settlement at the middle section of the Heinenoordtunnel

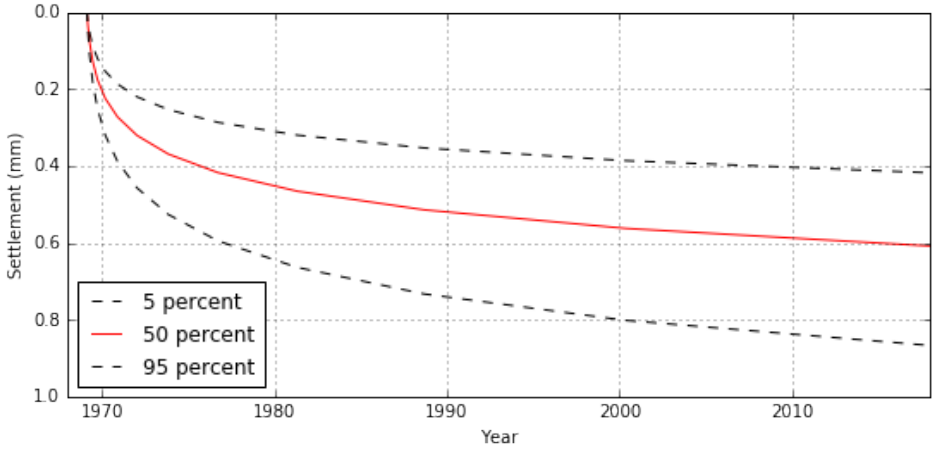

The 5% and 95% boundaries of the creep settlements that are calculated for the middle element of the Heinenoordtunnel are 0.39 - 0.80 mm in 1996. This is much smaller than the measured settlement of around 7 mm. The settlement calculations are using assumed parameters, but the difference is so large that this can not be the only contributor to the difference between the predicted settlements and the measured settlements.

5.6.3 Settlement calculations Kiltunnel site

The same calculations are performed at the middle element of the Kiltunnel. The advantage of the Kiltunnel is the much more accurate measurements that are measured in every joint in the tunnel instead of only at the immersion joint, which is the case at the Heinenoordtunnel.

The problem at the Kiltunnel was the very limited information of the CPT measurements. These CPT measurement are the only input parameter from the site characterisation for the creep model. This means that the predictions that are made for the creep settlement for the Kiltunnel are not very accurate. The second problem is that the three CPT measurements that are available are performed before the installation of the Kiltunnel. Before the Kiltunnel was built the soil beneath the Kiltunnel was dredged to an unknown depth and backfilled with sand. This means that these three CPT's do not give an indication of the q_c values of the backfilled soil beneath the Kiltunnel.

Zone of influence Kiltunnel

Using equation 5.15, the static loading of the Kiltunnel of 35.9 kPa, the width of the segment of 31.0 meter, the length of the segment of 22.3 meter and the dividing of the loading in point loads of area's of 0.25 x 0.25 meter gives the distribution of stresses shown in figure 5.19. Figure 5.19 gives a cross section of the increase in stress in the soil beneath the tunnel.

Fig. 5.19.: Cross section of the Boussinesq solution of the increase of stress in the soil beneath the Kiltunnel under the static loading of the tunnel.

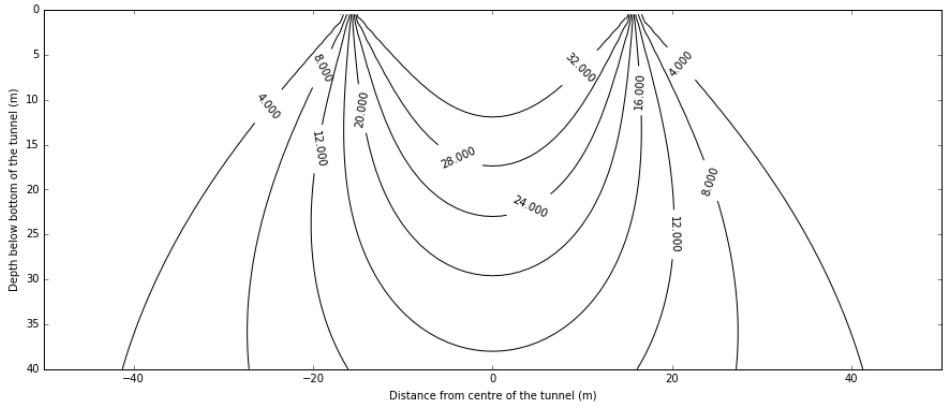

The zone of influence is defined in Eurocode 7 as the depth at which the increase of stress due to the loading of the tunnel is larger than 25%. Because the actual effective unit weight of the soil is unknown it assumed to be 8 kPa/m^3. The centre

of the tunnel is used as the representative stress increase for the determining of the zone of influence. Given the rule from Eurocode 7 the following equation can be used to determine the zone of influence:

$$q_v(Z_i) = 0.25 * 8 * Z_i \tag{5.17}$$

Using equation 5.16 and the solution of the Boussinesq calculation the zone of influence can be determined at a certain location in the tunnel as the intersection between equation 5.16 and the increase in stress calculated using the Boussinesq solution. This is shown in figure 5.20 for the middle of the segment.

Fig. 5.20.: Boussinesq solution in depth compared to 25% of the in situ vertical stress at the middle of the segment.

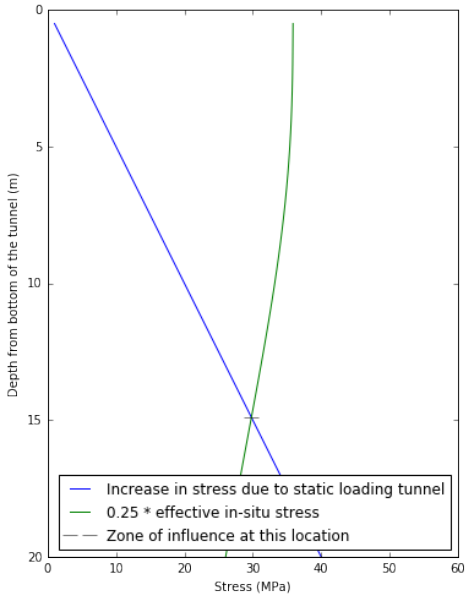

If this is done for each location over the width of the segment it creates figure 5.21 This figure includes the average zone of influence over the width of the tunnel.

Fig. 5.21.: Zone of influence over the width of the segment and the average zone of influence over the width of the segment.

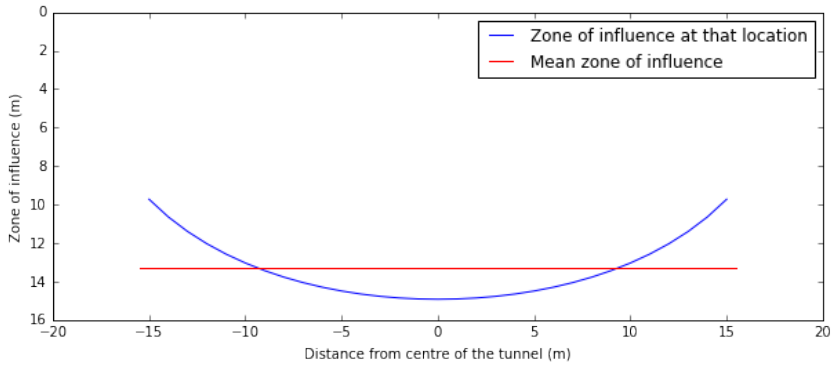

The zone of influence is on average 13.30 meter for the Kiltunnel.

Initial settlement calculations Kiltunnel

For the settlement calculations for the Kiltunnel CPT31 (see figure 3.4) is used because it is the CPT that goes to the greatest depth. The calculations are not very accurate for the two problems mentioned earlier in this section and the fact that there is been no thorough investigation in the in the creep parameters for these sites, but they do give an order of magnitude of the creep settlement of the middle section of the Kiltunnel.

Using this zone of influence of 13.30 meter the settlement can be calculated using the described procedure. The initial settlement is calculated for the middle element using the middle CPT using 100,000 simulations. The probability density plot is shown in figure 5.22 and the cumulative density function is plotted in figure 5.23.

Fig. 5.22.: Probability density plot of the initial settlement of the middle CPT of the middle element of the Kiltunnel.

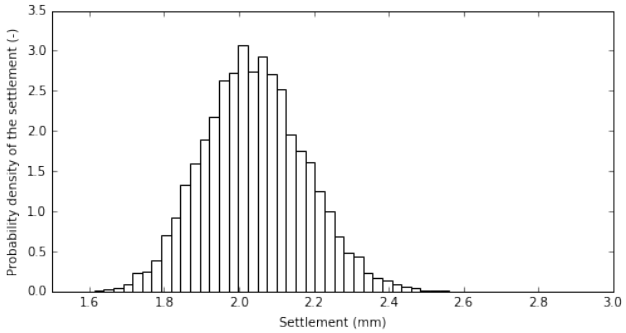

The 5% and 95% boundaries of the initial settlement at the middle element of the Kiltunnel are 1.82 - 2.27 mm. These initial settlements that are calculated can not

Fig. 5.23.: Cumulative density function of the initial settlement of the middle CPT of the middle element of The Kiltunnel.

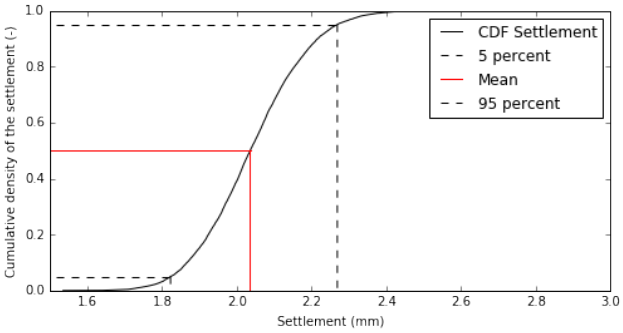

be compared to the measured settlements at the Kiltunnel. This is because the measurements started after the Kiltunnel was being built and the first measurement is a zero measurement. This means that at the moment of the zero measurement, the initial settlement have already occurred.

Creep settlement calculations Kiltunnel

For the creep calculation for the Kiltunnel the same CPT31 is used as for the initial settlement, because of the earlier mentioned problems it is still to give an order of magnitude rather than an accurate calculation.

The results of the creep settlement calculations are shown in figure 5.24.

Fig. 5.24.: Estimated probability boundaries of the creep settlement at the middle section of the Kiltunnel

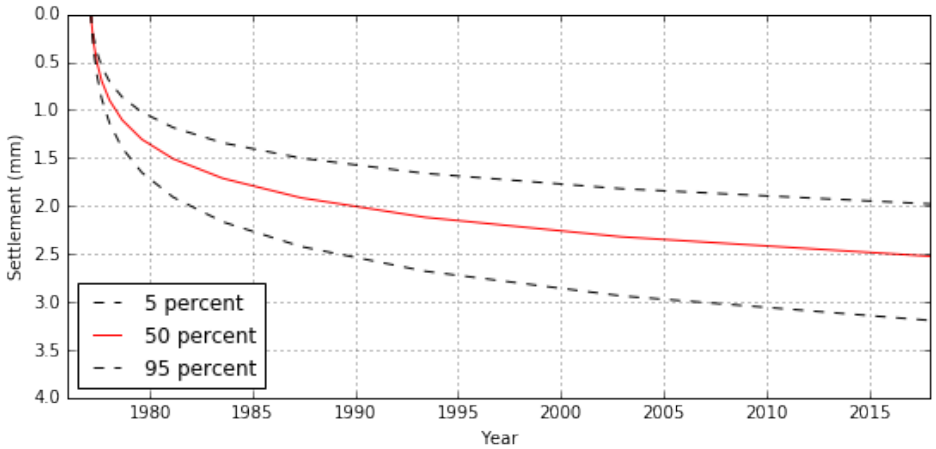

The creep settlements that are calculated for the middle element of the Kiltunnel are in the order magnitude of 1.98 - 3.19 mm in 2018. This is much smaller than the measured settlement of around 7.5 - 18.1 mm in 2018. The settlement calculations

are using assumed parameters, but the difference is so large that this can not be the only contributor to the difference between the predicted settlements and the measured settlements.

5.7 Concluding remarks stochastic ground model approach

The approach is based on the simulation of settlement using both MASW measurements and CPT measurements. The cone penetration resistance profiles are modelled stochastically based on the statistical data and the scales of fluctuations from the CPT's.

The vertical scale of fluctuation ranges from 0.06 - 1.44 meter for sands and 0.19 - 1.37 meter for clays. The horizontal scale of fluctuation of the shear wave velocity is a different quantity than the horizontal scale of fluctuation of the cone penetration resistance because it has been shown that it is at least a factor 10 larger for the Heinenoord site. This means that they can not be used interchangeably. The horizontal scale of fluctuation of the CPT's over the length of the tunnel could not be determined accurately enough to use in a model due to lack of data within the correlation length.

The static loading of the tunnels is due to buoyant weight of the concrete and the soil on top of the tunnel. The static loading of the middle element of the Kiltunnel is 24,800 kN and the static loading of the middle element of the Heinenoordtunnel is 19,350 kN.

The 5% and 95% boundaries of the initial settlement at the middle element of the Heinenoordtunnel are 4.04 - 4.68 mm, this settlement can not be compared to the measured settlement because it has occurred before the start of the measurements. The 5% and 95% boundaries of the creep settlements that are calculated for the middle element of the Heinenoordtunnel are 0.39 - 0.80 mm in 1996. This is much smaller than the measured settlement of around 7 mm.

The 5% and 95% boundaries of the initial settlement at the middle element of the Kiltunnel are 1.82 - 2.27 mm. The creep settlements that are calculated for the middle element of the Kiltunnel are in the order magnitude of 1.98 - 3.19 mm in 2018. This is much smaller than the measured settlement of around 7.5 - 18.1 mm in 2018.

The conclusion that can be drawn from these calculations is that even though the creep calculations are not very accurate it can be concluded that creep is not the main driver of the time dependant settlements at the Heinenoord and the Kiltunnel. It does contribute to the settlement that is being measured, but other factors have a larger influence on the settlement behaviour.

6 Cyclic loading

Chapter 5 concluded that the measured settlement can not be a result from only the static loading and creep. This means that to model the settlement the cyclic loads have to be taken into account as well.

In this report two different types of cyclic loading have been taken into account. These two types are:

1. Thermal expansion and contraction.

2. Tidal loading.

6.1 Thermal expansion and contraction of the tunnel lining

Thermal expansion and contraction of the tunnel lining can load and unload the tunnel. When the elements that are at an angle are expanding, they push the middle segment into the soil and when they contract they release the soil.

The temperature of the tunnel lining is assumed to be predominately influenced by the soil temperature and not by the air temperature. This means that the temperature changes are small and can be approached a sinusoidal function with a period of 1 year.

For the thermal expansion and contraction the tunnel is modelled as a beam. At small changes in temperature the linear thermal expansion model is an accurate approximation of the change in length of a beam. The linear expansion model is shown in equation 6.1.

$$\Delta L = L_0 * \alpha * (T_1 - T_0) \tag{6.1}$$

Where ΔL is the change in length of the tunnel section, L_0 is the initial length of the tunnel, α is the linear coefficient of thermal expansion, T_1 is the temperature after the temperature change and T_0 is the temperature before the temperature change.

The linear coefficient of thermal expansion is the expansion of a material per meter for each increment of 1 Kelvin. The linear coefficient of thermal expansion of the concrete α_c is mostly dependant on the linear coefficient of thermal expansion of the cement and the aggregate, the percentage of the volume of the two and the temperature of the concrete. For a typical concrete containing about 60 - 75 % of aggregate the linear coefficient of thermal expansion of concrete α_c will be in the range of 7 - 12 * 10^{-6} K^{-1} and is around 10 * 10^{-6} K^{-1} on average according to Hobbs (1971).

Florides (2004) measured the temperature in the soil at different depths in Cyprus. He concluded that fluctuation in temperature at a depth of 3 meters is between 15 and 25 $°C$, and remains constant at a depth larger than 25 meter. The difference in average temperature in the Netherlands is similar but slightly smaller than in Cyprus. This means that these results can be used and will even slightly overestimate the fluctuation in temperature in the subsurface in the Netherlands. Given the exponential decrease of the temperature fluctuation in depth it assumed that an average temperature fluctuation of 5 degrees is a safe estimate for the temperature fluctuation in both of the tunnels.

It is assumed that one Gina Gasket is compressed due to the temperature fluctuation of the half of the element on either side. This gives a total length of the tunnel that loads a single Gina Gasket of 120.0 meter. When an α of 10 * 10^{-6} K^{-1} and a temperature fluctuation of 5 degrees is used it gives a range of -3 mm to 3 mm over the year.

Figure 6.1 from the research of van Montfort (2018) on immersion joints shows the force per meter that is needed on the Gina Gasket to cause a certain compression in the Gina Gasket.

Fig. 6.1.: Force per meter in of types of Gina Gaskets at different compressions.

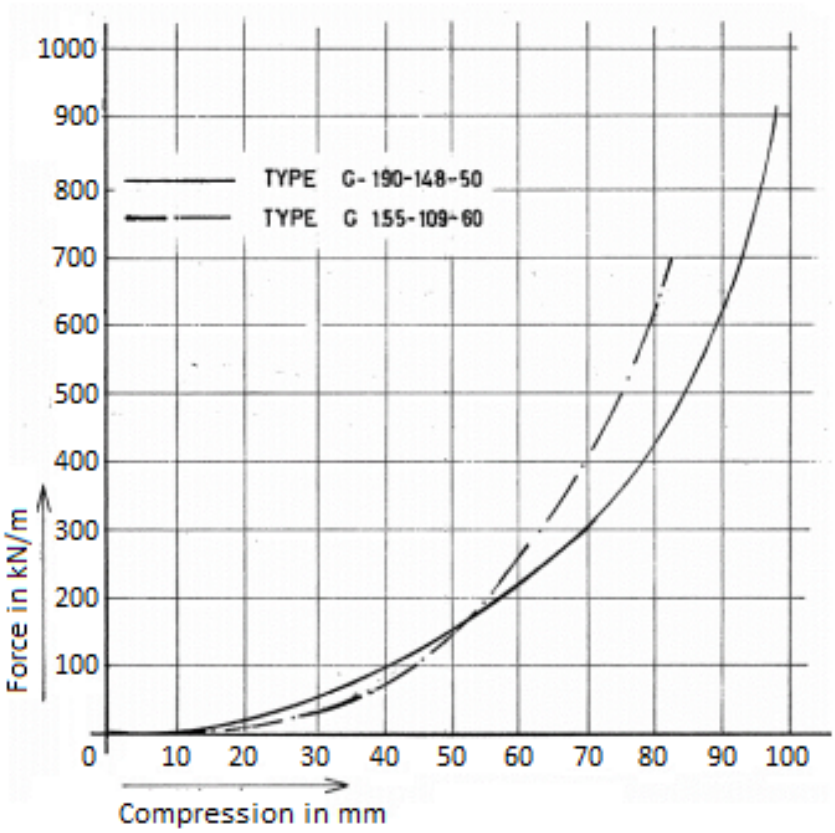

Because of the non-linearity of the relation in figure 6.1 the initial compression of the Gina gasket needs be known to determine the increase force per meter of Gina Gasket.

The Gina Gaskets that are used in the middle element of the Kiltunnel are of type G-190. The design compression of the Gina Gasket to ensure the water tightness of the joints. The design compression of the Gina Gasket of the middle element of the Kiltunnel is 80 mm (reported in van Montfort (2018)). Because the lack of information on the type of Gina Gasket and the design compression of the Gina Gasket in the Heinenoordtunnel it is assumed to be the same as for the Kiltunnel.

At this initial compression the initial force in the Gina Gasket is 427.6 kN/m. The compression in the Gina Gasket ranges from about 77 to 83 mm during the year due the temperature fluctuation. This means that the force in the Gina Gasket ranges from 389.4 - 468.4 kN/m. This gives a fluctuation of the force in the Gina Gasket of 79.0 kN/m.

The Gina Gasket seals all around the immersed tunnel, this means that length of the Gina Gasket can be approximated by the circumference of the tunnel. This means

that the length of the Gina Gasket of the Heinenoordtunnel is $2*8.0+2*30.7 = 77.4m$. This means that the fluctuation in the force in the total Gina Gasket is 6,115 kN.

This force is in the direction of the slope. The slope is at a slight angle. In the length of the two elements of 240 meter, the tunnel descents 10.52 meter. The force can be separated in the vertical component and the horizontal component. The fluctuation of the force in the total Gina Gasket in the vertical direction can then be calculated by:

$$\Delta F_v = \frac{F_{total} * \Delta H}{L} \tag{6.2}$$

This gives 268 kN of fluctuation in force in vertical direction at the joints at the immersion joints of the middle element each year.

6.1.1 Settlement of Heinenoordtunnel due temperature fluctuation

The temperature fluctuation mentioned in the previous paragraph occurs every year, which means that vertical load that is calculated loads the edges of the middle element each year.

The cyclic loading is modelled using a simplified settlement model for cyclic loading from chapter 2.3.6. The equation that is being used is:

$$s_N = s_e * A^{ln(N)} \tag{6.3}$$

Where s_N is the settlement after N loading cycles, s_e is the elastic settlement from one loading cycle, A is a constant and N is the number of loading cycles that have occurred.

Some calculations were performed to see if the settlement caused by the loading of the tides is in the order of magnitude of the measured settlements. For these calculations the elastic settlement is calculated using the Mayne model, which presented in chapter 2.3.3 and the constant A is assumed to be 1.6, which is a typical value for sand.

To calculate the initial settlement the area on which the force acts needs to be known. Pul et al. (2017) conducted experiments on the cohesion and the internal friction

angle of conventional concretes. The friction angles that were determined were between 29.8 and 41.7 degrees. The average friction angle was around 35 degrees. The area on which the force works is approximated using this angle, the height of the tunnel and the width of the tunnel as shown in figure 6.2.

Fig. 6.2.: Projection force in Gina Gasket on bottom of tunnel

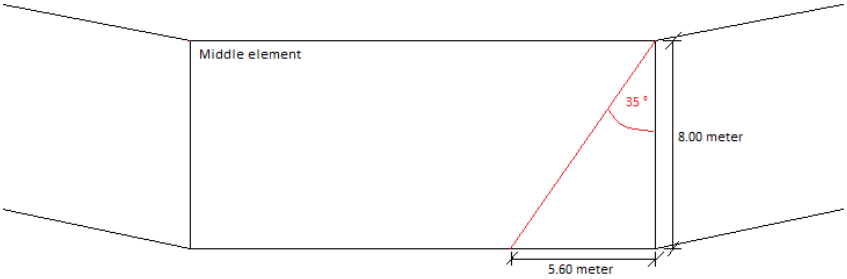

The width of the projected area of 5.60 meter is multiplied by the width of the segment of 30.7 meter to get the projected area of 171.92 m^2

The extra settlement at the edges of the middle element of the Heinenoordtunnel over the years is shown below in figure 6.3.

Fig. 6.3.: Settlement at edges of the middle element of the Heinenoordtunnel due to compression of the Gina due to temperature effects.

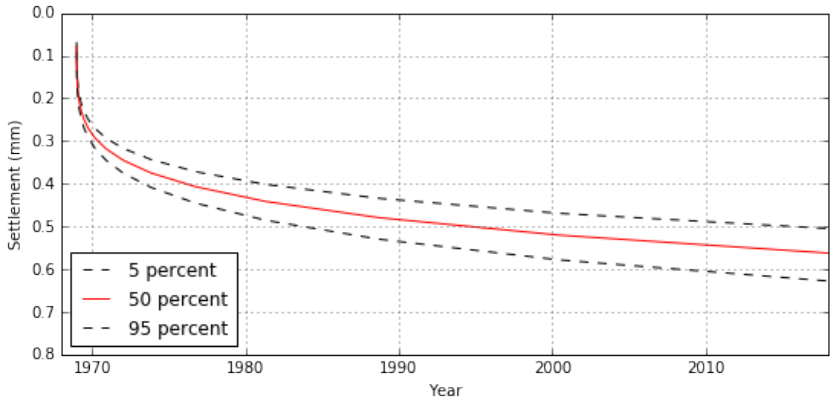

The initial settlement at the edges of the middle element of the Heinenoordtunnel due to temperature fluctuation is between 0.07 and 0.09 mm and the settlement at the edges of the middle element of the Heinenoordtunnel in 1996 is between 0.47 and 0.58 mm. This means that it does have a small influence on the settlement measured at these immersion joints but does not explain all occurred settlement.

6.1.2 Settlement of Kiltunnel due temperature fluctuation

The same vertical load occurs at the Kiltunnel because of the almost exact same dimensions of the elements. The same calculations were performed using the site characterisation data from the Kiltunnel.

The settlement at the edges of the middle element of the Kiltunnel over the years is shown below in figure 6.4.

Fig. 6.4.: Settlement at edges of the middle element of the Kiltunnel due to compression of the Gina due to temperature effects.

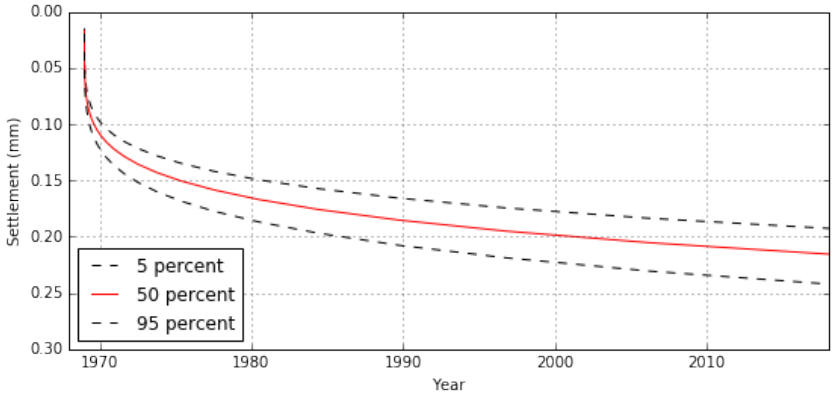

The initial settlement at the edges of the middle element of the Kiltunnel due to temperature fluctuation is between 0.06 and 0.08 mm and the settlement at the edges of the middle element of the Kiltunnel in 2018 is between 0.42 and 0.55 mm. This means that it does have a small influence on the settlement measured at these joints but does not explain all occurred settlement.

6.2 Tidal loading

Both the Kiltunnel and the Heinenoordtunnel are built in an estuary. The water level in these estuaries are influenced by the tides. The water level for the Kiltunnel and the Heinenoordtunnel are shown in figure 6.5 and figure 6.6 for a period of 28 days.

The tide loads both tunnels because there is a layer of sludge on the bottom of the rivers that could cause a decay and a lag in the fluctuation of the pore pressures in the deeper sand layers. This means that the effective stress in the deeper sand layers can increase and decrease due to the tides.

Fig. 6.5.: Tides at the Kiltunnel over a period of 28 days.

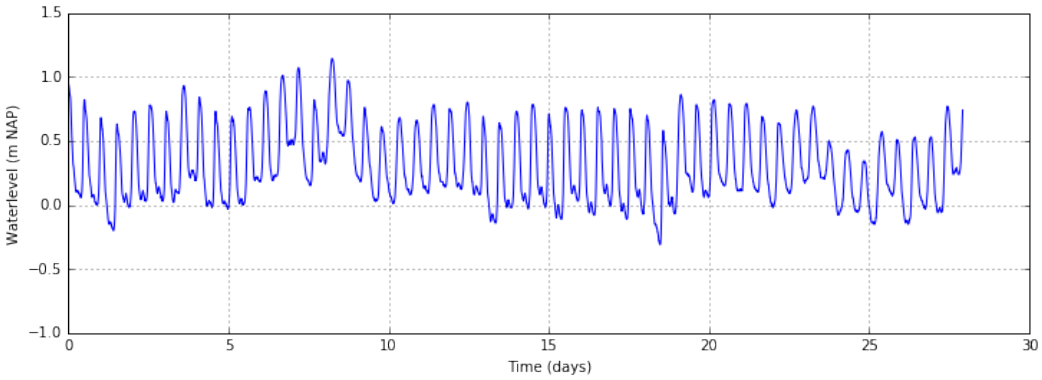

Fig. 6.6.: Tides at the Heinenoordtunnel over a period of 28 days.

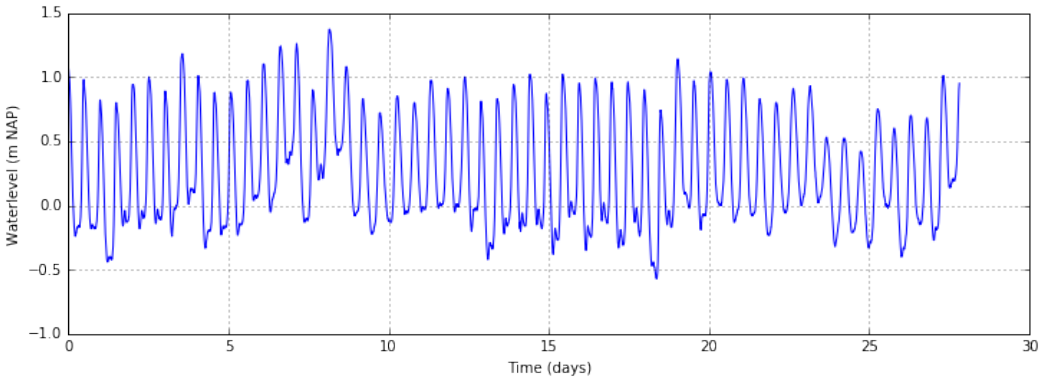

The difference between the lowest water level and the highest water level of each cycle changes with each cycle. On average this difference is around 8 kPa for the Kiltunnel and 12 kPa for the Heinenoordtunnel. This difference fluctuates between 6 and 10 kPa for the Kiltunnel and between 9 and 15 kPa for the Heinenoordtunnel.

This fluctuation in water level loads the soil because in the estuaries near Rotterdam a layer of sludge is formed on the bottom of the river. This sludge provides a low permeable layer on the bottom of the river. This causes a lag and a decay in the pore pressure changes in the deeper sand layers causing it to be loaded and unloaded by each cycle of the tides.

Some calculations were performed to see if the settlement caused by the loading of the tides is in the order of magnitude of the measured settlements. The settlement from the cyclic loading is calculated again using equation 6.3. For these calculations the elastic settlement is calculated using the Mayne model, which presented in chapter 2.3.3 and the constant A is assumed to be 1.6, which is a typical value for sand.

The main problem for the calculation of the settlement due to the tidal wave loading is the uncertainty in the fluctuations of the pore pressure in the deeper sand layers. As mentioned before, the sludge cause a lag and a decay in the increase and decrease in pore pressure in the deeper sand layer. However, there is little information about the magnitude of the lag and the decay of the pore pressures and therefore it is not possible to obtain an accurate determination of the magnitude of the loading by tidal loading.

The only measurements that indicate the pore pressure fluctuation in the deeper sand layers are measurements from the influence of the boring process of the second Heinenoordtunnel, a bored tunnel around 100 meter from the Heinenoordtunnel, on the pore pressures in a deeper sand layer. The measurements are shown below in figure 6.7.

Fig. 6.7.: Influence boring process on the pore pressure in a deeper sand layer from Broere (2001).

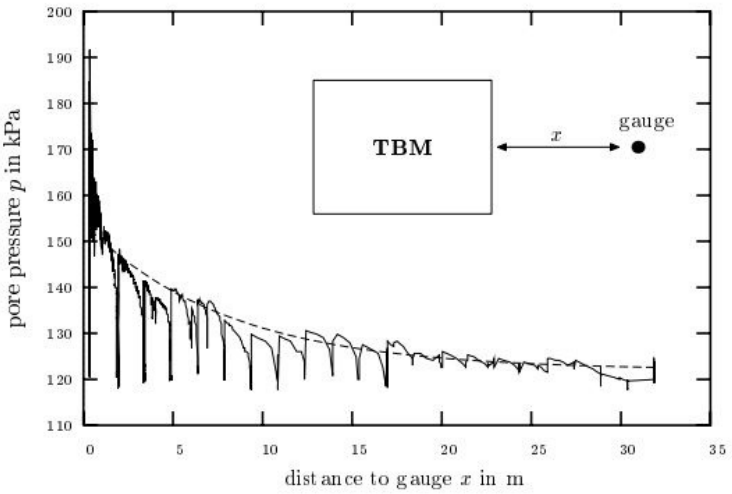

Each vertical peak in figure 6.7 is due to a stop in the boring process. The vertical peak at the largest distance from the gauge is the start of the measurements where the pore pressures are measured for about the entire day before the start of the boring process. This can not be seen in this figure 6.7 but was observed by prof. W. Broere from the TU Delft (personal communication, December 11, 2018), who worked on the measurements. This means that the height of this peak indicates the fluctuation of the pore pressures in the deeper sand layers. In figure 6.8 the determination of the fluctuation in the pore pressure is shown.

Based on figure 6.8 the fluctuation of the pore pressure in a deeper sand layer is assumed to be at least 4 kPa at this location.

Fig. 6.8.: Fluctuation of the pore pressure in a deeper sand layer from Broere (2001).

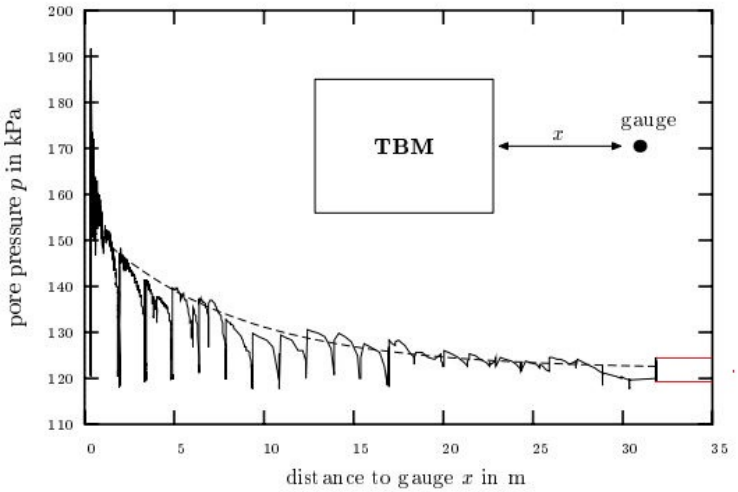

The measurements of figure 6.8 are at an estimated 100 meter of the river Oude Maas. This means that there has been a decay of the influence of the tide on the pore pressure in the sand layer, but the magnitude of this decay is unknown.

The tidal fluctuation at the time of the measurements of figure 6.8 are unknown. So there is a possibility that the layer of sludge also cause a lag in the in the fluctuation of the pore pressure of the deeper sand layers.

For the calculations 2 situation are described:

1. A lower bound scenario where all relevant parameters are added together in a realistic way that results in the estimated lowest possible loading of the soil beneath the tunnel due to the fluctuations in the tides.

2. An upper bound situation where all relevant parameters are added together in a realistic way that results in the estimated lowest possible loading of the soil beneath the tunnel due to the fluctuations in the tides.

6.2.1 Lower bound scenario

The lower bound scenario uses the following assumptions to lead to the assumed lowest possible loading of the soil:

1. Using the upper and lower bound of the observed fluctuation of the water level over 28 days in figure 6.6 of 9 to 15 kPa and the 3σ-rule it can be estimated

that each day there is a 95% probability that the fluctuation of the tide is larger than 10 kPa.

2. The decay of the fluctuation of the tide in the deeper sand layer from the middle element to the measurement point is assumed to be smaller than 2 kPa. This gives a fluctuation of the tides of 6 kPa at the location of the middle element of the Heinenoordtunnel.

3. The delay of the fluctuation of the tide in the deeper sand layer at the location of the middle element is assumed to be 0 hours.

The delay of 0 hours means the total peak of the fluctuation of the tide in the deeper sand layers can be subtracted from the load from the tides on the immersed tunnel. This gives a load of $10 - 6 = 4kPa$. This means that 40% of the fluctuation of the tide loads the tunnel.

Because of a lack of any information about the pore pressures fluctuation at the Kiltunnel the same assumptions are used for this location.

6.2.2 Upper bound scenario

The upper bound situation uses the following assumptions to lead to the assumed lowest possible loading of the soil:

1. Using the upper and lower bound of the observed fluctuation of the water level over 28 days in figure 6.6 of 9 to 15 kPa and the 3σ-rule it can be estimated that each day there is a 95% probability that the fluctuation of the tide is smaller than 14 kPa.

2. The decay of the fluctuation of the tide in the deeper sand layer from the middle element to the measurement point is assumed to be around 0 kPa. This gives a fluctuation of the tides of 4 kPa at the location of the middle element of the Heinenoordtunnel.

3. The delay of the fluctuation of the tide in the deeper sand layer at the location of the middle element is assumed to be 2 hours.

The delay of 2 hours means that the fluctuation in the deeper sand layer can not be simply subtracted from the fluctuation of the tide but the time also needs to be taken into account. The subtraction is shown in figure 6.9.

Fig. 6.9.: Fluctuation of the pore pressure relative to the mean.

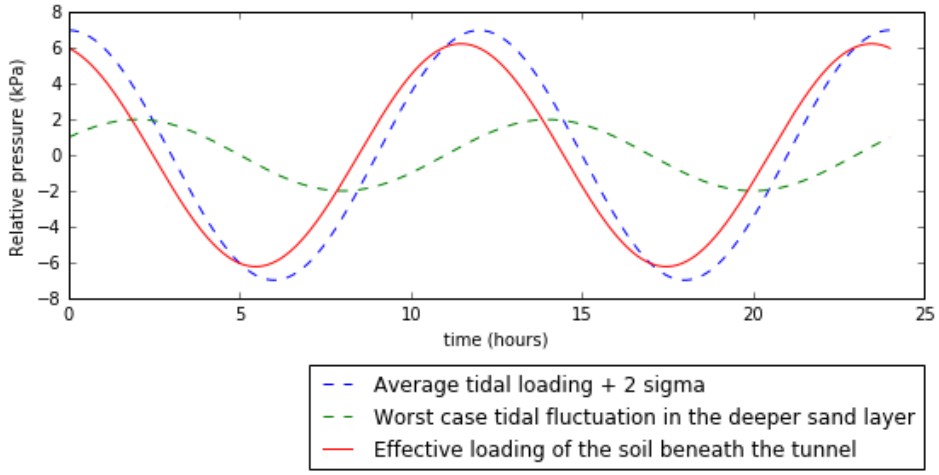

The amplitude of the effective loading of the soil beneath the tunnel is 12.48 kPa. This means that 89.2% of the fluctuation loads the soil beneath the tunnel. This is rounded to 90%.

There is a very huge difference in the load of the lower bound scenario and the upper bound situation which will cause a large uncertainty in the calculated settlement, but without more accurate measurement data it is impossible to make a more accurate estimate without making assumptions that might not be realistic.

Because of a lack of any information about the pore pressures fluctuation at the Kiltunnel the same assumptions are used for this location.

6.2.3 Settlement calculations Heinenoordtunnel

The loading for each load cycle of the tide at the Heinenoordtunnel is assumed to be between 40% and 90% of the fluctuation in the water level. Using the lower bound of 9 kPa and the upper bound of 15 kPa of water level fluctuation based on figure 6.6, the water level is assumed to fluctuate 12 kPa on average with a standard deviation of 1 kPa using the 3-σ rule. This fluctuation is multiplied by factor of 0.4 for the lower bound scenario and 0.9 for the upper bound situation.

Settlement calculations lower bound scenario Heinenoord

The calculations are performed using 40% of the fluctuation of the tides as a load on the soil beneath the tunnel. The results from the calculations are shown in figure 6.10.

Fig. 6.10.: Settlement of middle element of the Heinenoordtunnel due to tidal loading in lower bound scenario.

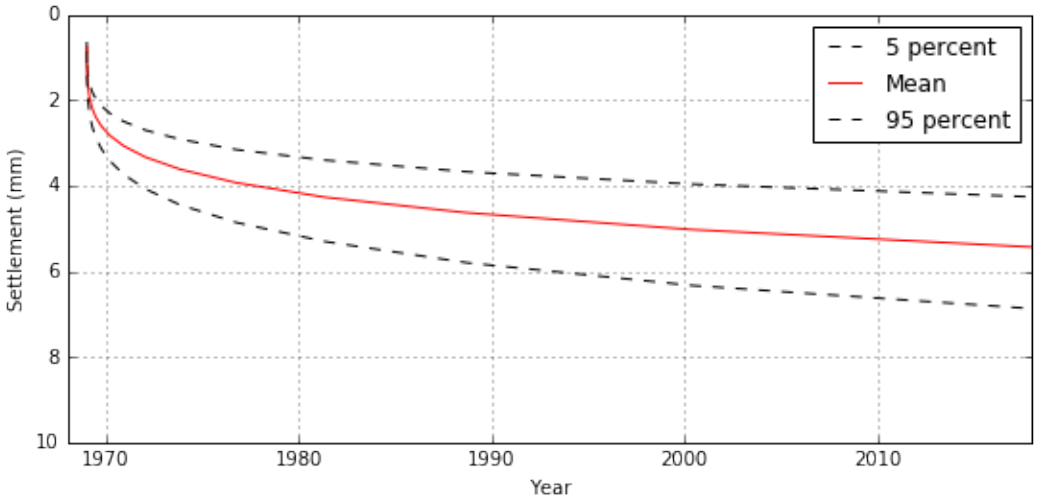

If the calculated settlement from the tidal loading is plotted together with the creep settlement from figure 5.18 and the temperature effects from figure 6.3 it gives figure 6.11.

Fig. 6.11.: Settlement in the edges of middle element of the Heinenoordtunnel due to tidal loading, creep and temperature fluctuation in lower bound scenario.

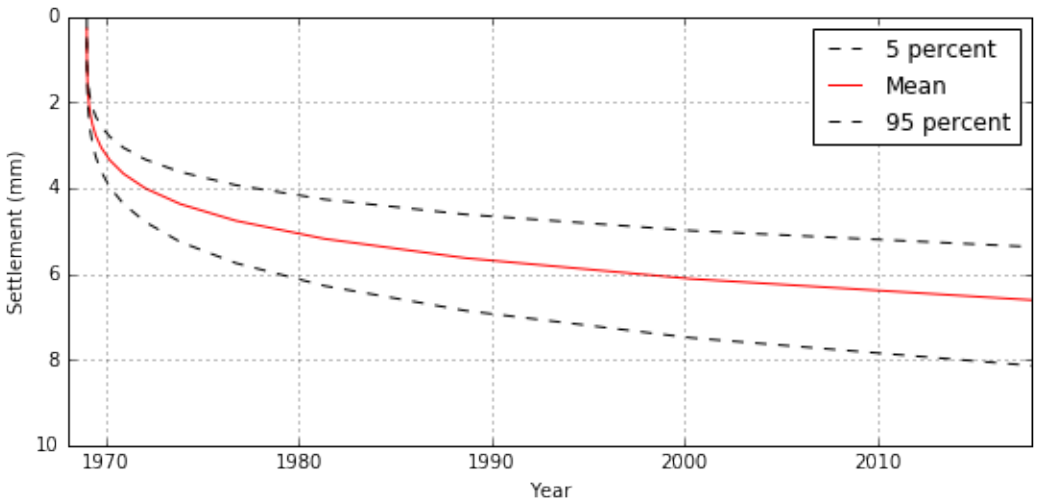

The initial settlements are not included because they have occurred before start of the measurements.

The settlements of the Heinenoordtunnel that are calculated that could be measured using the lower bound scenario calculations have a 5% probability of being larger

than 4.99 mm and a 95% probability of being smaller than 7.51 mm in 1996 according to this model.

The measured settlement of around 7 mm falls within this range that is calculated. This means that the lower bound scenario could explain the settlements that are occurring at the middle element of the Heinenoordtunnel.

Settlement calculations upper bound scenario Heinenoord

The calculations are performed using 90% of the fluctuation of the tides as a load on the soil beneath the tunnel. The results from the calculations are shown in figure 6.12.

Fig. 6.12.: Settlement of the edges of the middle element of the Heinenoordtunnel due to tidal loading in upper bound scenario.

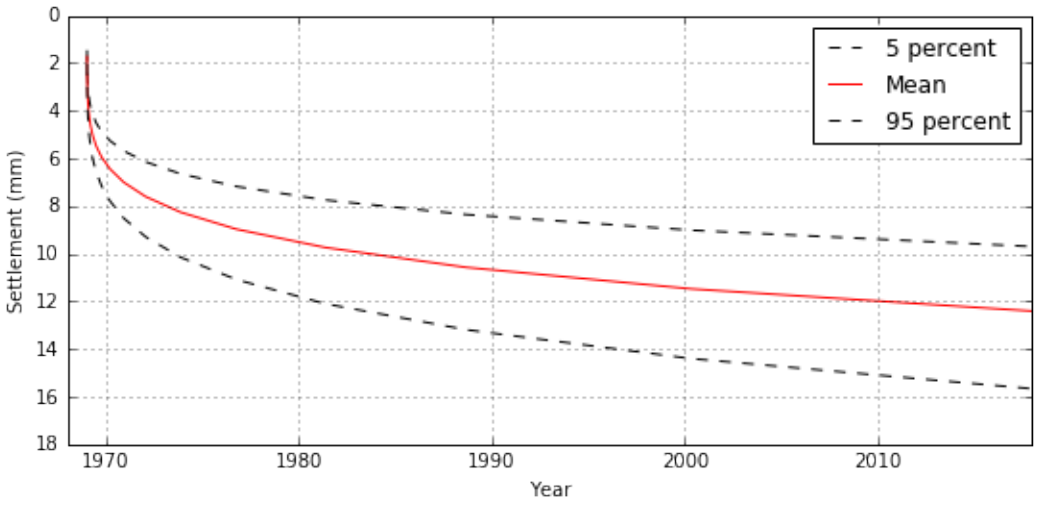

If the calculated settlement from the tidal loading is plotted together with the creep settlement from figure 5.18 and the temperature effects from figure 6.3 it gives figure 6.13.

The initial settlements are not included because they have occurred before start of the measurements.

The settlements of the Heinenoordtunnel that are calculated that could be measured using the upper bound scenario calculations have a 5% probability of being larger than 10.05 mm and a 95% probability of being smaller than 15.57 mm in 1996 according to this model.

Fig. 6.13.: Settlement in the edges of middle element of the Heinenoordtunnel due to tidal loading, creep and temperature fluctuation in upper bound scenario.

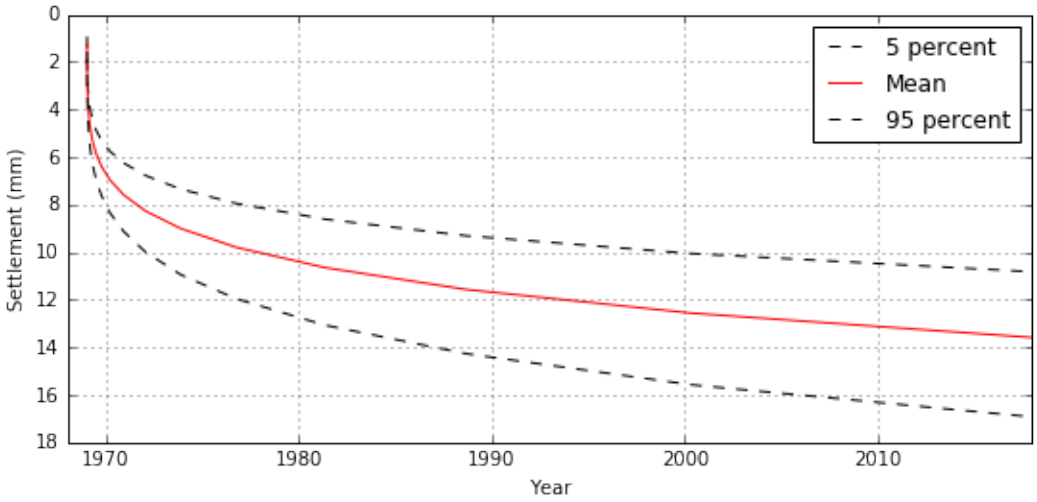

This is larger than the measured settlement of around 7 mm. This means that the lower bound scenario is a more accurate estimation of the loading of the tides of the soil beneath the Heinenoordtunnel.

6.2.4 Settlement calculation Kiltunnel

The loading for each load cycle of the tide at the Kiltunnel is assumed to be between 40% and 90% of the fluctuation in the water level. Using the lower bound of 6 kPa and the upper bound of 10 kPa of water level fluctuation based on figure 6.5, the water level is assumed to fluctuate 8 kPa on average with a standard deviation of 0.67 kPa using the 3-σ rule. This fluctuation is multiplied by factor of 0.4 for the lower bound scenario and 0.9 for the upper bound situation.

The settlement of the Kiltunnel is calculated for each measurement location of the middle element, indicated in figure 6.14 as location 19 - 29.

Fig. 6.14.: Measurement locations Kiltunnel.

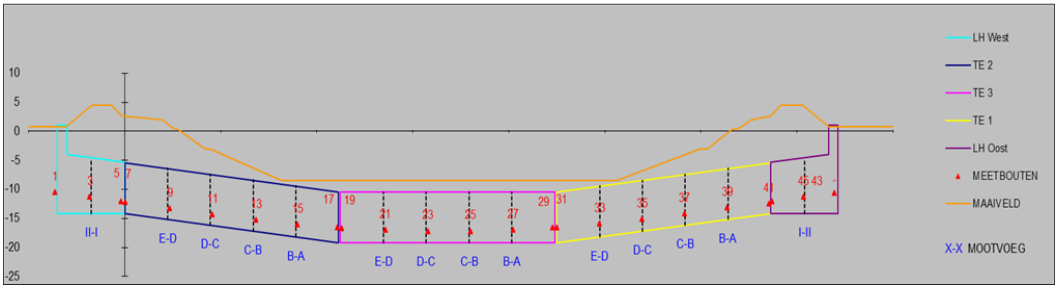

All the results from the calculations of both the lower and the upper bound scenario for each measurement location in the middle element are shown in appendix D in figure D.2 - D.13 together with the creep settlement from figure 5.24. For measurement locations 19 and 29 the temperature effects from figure 6.4 are added. The figures include the measurement points as well.

The initial settlements are not included because they have occurred before start of the measurements.

Example: results location 29

As an example the results from location 29 are shown in figure 6.15 (lower bound) and 6.16 (upper bound).

Fig. 6.15.: Probability boundaries of modelled settlement of measurement location 29 of the middle element of the Kiltunnel due to tidal loading, creep and temperature effects in lower bound scenario compared to the measured settlement.

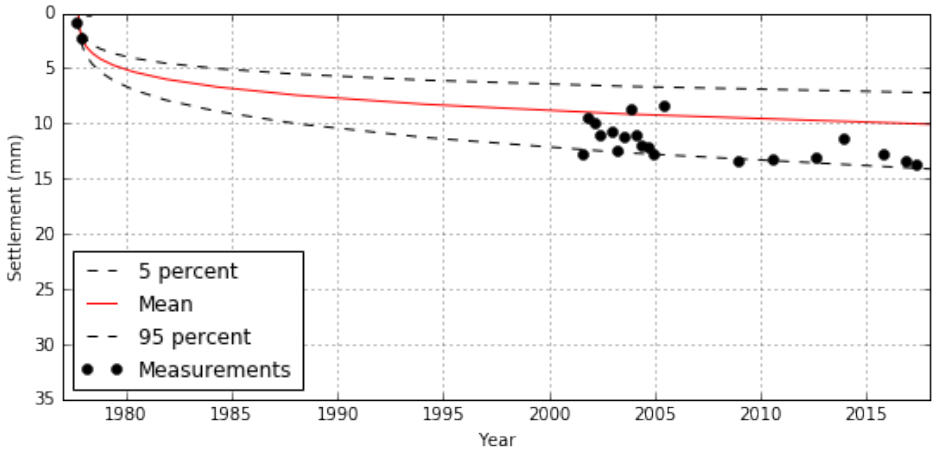

The calculated settlement of location 29 using the lower bound scenario has a 5% probability of being smaller than 7.24 mm and a 95% of being smaller than 14.20 mm in 2018. The measured settlement at location 29 of around 14 mm in 2018 is within the calculated range of the lower bound.

The calculated settlement of location 29 using the upper bound scenario has a 5% probability of being smaller than 12.61 mm and a 95% of being smaller than 28.11 mm in 2018. The measured settlement at location 29 of around 14 mm in 2018 is within the calculated range of the upper bound.

Fig. 6.16.: Probability boundaries of modelled settlement of measurement location 29 of the middle element of the Kiltunnel due to tidal loading, creep and temperature effects in upper bound scenario compared to the measured settlement.

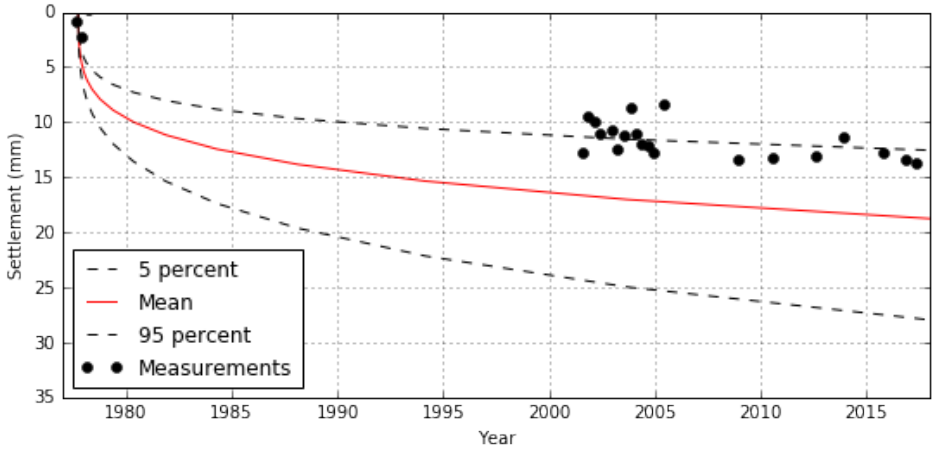

Summary results at all locations of the Kiltunnel

The settlement calculations of locations 19 - 29 are summarised in table 6.1.

Tab. 6.1.: Summary settlement results lower and upper bound scenario Kiltunnel

		5 %	95 %	Measured	Within range?
Location 19	LB	5.96	11.16	34	Too small
	UB	9.94	21.34	34	Too small
Location 21	LB	4.97	9.08	8	Yes
	UB	8.23	17.23	8	Too large
Location 23	LB	4.79	8.69	8	Yes
	UB	7.87	16.33	8	Yes
Location 25	LB	5.20	9.52	17	Too small
	UB	8.77	18.65	17	Yes
Location 27	LB	6.00	11.66	18	Yes
	UB	10.52	23.13	18	Yes
Location 29	LB	7.24	14.20	14	Yes
	UB	12.61	28.11	14	Yes

There are two interesting results in table 6.1. First there is no real trend of which bound is more accurate compared to the measured settlements. At location 21 and 23 the lower bound is more accurate, at location 19, 25 and 27 the upper bound is more accurate while for location 29 the measured settlement is somewhere in between the two bounds.

The second result is that at location 19 even the 95 % of the upper bound is much smaller than the measured settlement. The difference in shear wave velocity is not that large and can not explain the large difference in settlement while the

information from the CPT's is so limited that it is not possible to determine if there is a difference between location 19 and the other locations.

Possible reasons why the measured settlements at location 19 is larger than the calculated settlements are:

1. The upper bound scenario could be even worse than assumed. If this is the case it is most likely due to a larger lag than assumed. This could case a smaller reduction of the load on the soil of the tunnel or even a larger load than the load of the fluctuation of the tides.

2. The creep could be larger than calculated. The creep is calculated using a CPT profile that is performed before the dredging en backfilling of the soil beneath the Kiltunnel. Also, the CPT is to a smaller depth than the zone of influence of the Kiltunnel. This means that the information from the CPT profile is inaccurate.

3. Part of the load of the embankment could be transferred through the tunnel to location 19 causing a larger settlement.

4. The backfilled material at this location is a much poorer condition than at the other measurement locations. A counterargument against this is that if this is the case it should be observable in the MASW profile.

6.3 Concluding remarks cyclic loading

This chapter focused on the influence of cyclic loading on the settlement of the middle element of the Heinenoordtunnel and the Kiltunnel.

The thermal expansion and contraction of the elements at an angle loaded the middle element. The expansion of the Gina Gaskets between the flat element and the elements at an angle is between -3 and 3 mm. This expansion and contraction of the Gina Gasket causes a vertical load on each of the edges of the middle element of 268 kN. This causes a settlement of 0.47 - 0.58 mm in 1996 at the edges of the middle element of the Heinenoordtunnel and a settlement of 0.42 - 0.55 mm in 2018 of the edges of the middle element of the Kiltunnel. This means that it does have a small influence on the settlement of both tunnels measured at these joints but does not explain all occurred settlement.

The water levels at the Heinenoord and the Kiltunnel are measured accurately, but the decay and the lag of the pore pressure in the deeper sand layers has not been measured accurately. The best indication for this fluctuation of pore pressure is the measurements of the of the pore pressure under the influence of the boring of the TBM (Tunnel boring machine) for the nearby second Heinenoordtunnel. These measurements show at least 4 kPa of pore pressure fluctuation during a cycle of the tide.

For an indication of the settlement of the Heinenoordtunnel and the Kiltunnel under the loading of the tides a few calculations have been performed using a lower bound of 40% and an upper bound of 90% of loading of the tides.

At the Heinenoord the lower bound scenario gave results between 4.99 - 7.51 mm, which means that the measured values of around 7 mm are within the range of the results, while the upper bound scenario gave results between 10.05 and 15.57 mm which is larger than the measured values.

At the Kiltunnel there is no real trend of which bound is more accurate compared to the measured settlements. At location 21 and 23 the lower bound is more accurate, at location 19, 25 and 27 the upper bound is more accurate while for location 29 the measured settlement is somewhere in between the two bounds.

The second result is that at location 19 even the 95 % of the upper bound (21.34 mm) is much smaller than the measured settlement (around 34 mm). The difference in shear wave velocity is not that large and can not explain the large difference in settlement while the information from the CPT's is so limited that it is not possible to determine if there is a difference between location 19 and the other locations.

To see how much effect the cyclic loading really has more investigation needs to be done on the parameter A of the cyclic loading equation or a more accurate model needs to be used. More importantly measurements of the fluctuation of the pore pressures in the deeper sand layers in combination of the fluctuations of the tides at that time are needed to accurately determine the loading of the soil due to the tides.

7 Conclusions

The most important conclusions that can drawn from the results of this thesis can be divided in two sections: the conclusions for the characterisation of the sites and the conclusions for the settlement calculations of both tunnels.

The conclusions for the characterisation of the sites are:

1. The correlation between the cone penetration resistance and shear wave velocity or small strain shear stiffness at the Heinenoord site is so weak that it practically means that almost all possible q_c values should be considered. This means that when this correlation is used by only using the shear wave velocity as an input parameter, and correlating q_c to this value, it does not increase the accuracy of the model compared to using just all possible q_c values. Even if only the values of the measurements that are entirely in one layer are used.

2. The horizontal scale of fluctuation of the shear wave velocity is a different quantity than the horizontal scale of fluctuation of the cone penetration resistance. This can be concluded because it is at least a factor 10 larger for the Heinenoord site. This means that they can not be used interchangeably. The horizontal scale of fluctuation of the CPT's over the length of the tunnel could not be determined accurately enough to use in a model due to lack of data within the correlation length.

The conclusions for the settlement calculations of both tunnels are:

1. Initial settlement cause a few mm of settlement. However, it can not have caused the measurements that have been measured because the measurements started after the tunnel was installed so the initial settlements had already occurred.

2. Even though the creep calculations are not very accurate it can be concluded that creep is not the main driver of the time dependant settlements at the Heinenoord and the Kiltunnel because the measured settlements are not in the range of the calculated. It does contribute to the settlement, but other factors have a larger influence on the settlement behaviour.

3. The thermal expansion and contraction of the elements at an angle load the middle element because the expansion of the two elements together is between -3 and 3 mm. This expansion and contraction of the Gina Gasket causes a vertical load on the edges middle element. This causes a settlement a few tenths of millimetres of settlement at the edges of the middle elements of both tunnels. This means that it does have a small influence on the settlement of both tunnels measured at the joints at the edges of the middle elements but does not explain all occurred settlement.

4. For an indication of the settlement of the middle element of the Heinenoordtunnel and the Kiltunnel under the loading of the tides, the settlement is calculated using assumed lower and upper bound scenarios. For the Heinenoord the measured settlement was in range of the calculations of the lower bound scenario. For the Kiltunnel the measured settlement were sometimes in the range the lower bound scenario, sometimes in the range of upper bound scenario and at location 19 larger than the upper bound scenario.

These conclusions show that there is a possibility that the settlements have occurred through a combination of the creep, the temperature effects and the loading of the tides but it does not conclude that all settlements occur because of these loading conditions.

The measured settlement at measurement location 19 of the Kiltunnel was, even in the upper bound scenario, not in the range of calculated measurements. Reasons why this is not the case could be:

1. At the Kiltunnel the weight of the embankment could be pushing the elements on the slopes into the middle (flat) element. At the Heinenoordtunnel there could be a similar effect but in a smaller magnitude because of the embankment not being directly on top of the tunnel.

2. Poor quality of the backfilled material after the digging of the trench of the immersed tunnels

3. The creep could be larger than calculated. The creep is calculated using a CPT profile that is performed before the dredging en backfilling of the soil beneath the Kiltunnel. Also, the CPT is to a smaller depth than the zone of influence of the Kiltunnel. This means that the information from the CPT profile is inaccurate.

8 Recommendations

Because this thesis does not give definitive solution for the research question further investigation and site characterisation need to be performed to work towards a solution. The recommendations are summarised.

1. Performing CPT measurements at the Kiltunnel at least every 50 meter. Preferably the CPT measurements are performed as close to the tunnel as possible because it gives more accurate information and hopefully it includes information about the backfilled soil.

2. Pore pressure measurements needs to be performed at both the Kiltunnel and the Heinenoordtunnel to be able to determine the decay and the lag of the fluctuation of the pore pressure in the deeper sand layers. This is needed to see if, and how much, the fluctuation of the tides contributes to the settlement of the tunnel.

3. Investigation needs to be performed into the influence of the embankment on the loading of the tunnel. It needs to be checked if there is a possibility that the embankments push the elements on the slope into middle (flat) element, causing a settlement of the middle element.

4. Investigation into the parameters of the creep model and the cyclic model needs to be performed in order to get a more accurate prediction of the settlement due to creep and cyclic loading or a more accurate model should be used (for example FEM). But in order to get a more accurate answer from this new model the input parameters need to be more accurate, starting with recommendations 1-3, because otherwise the new model still can not give accurate answers.

5. Continuous measurement data, both in time and x-direction, of the settlement in both tunnels could increase the knowledge of the settlement processes going on in the tunnels. This can for example be done by installing glass fiber cables in the tunnels.

Bibliography

[Ana+03] A. Anagnostopoulos, G. Koukis, N. Sabatakakis, and G. Tsiambaos. „Empirical correlations of soil parameters based on Cone Penetration Tests (CPT) for Greek soils“. In: *Geotechnical and Geological Engineering* 21.4 (2003), pp. 377–387.

[Anb+16] P. Anbazhagan, A. Uday, S. S. R. Moustafa, and N. S. N. Al-Arifi. „Correlation of densities with shear wave velocities and SPT N values“. In: *Journal of Geophysics and Engineering* 13.3 (2016), pp. 320–341.

[And+07] R. D. Andrus, N. P. Mohanan, P. Piratheepan, B. S. Ellis, and T. L. Holzer. „Predicting shear-wave velocities from cone penetration resistance“. In: *Proceedings of the 4th international Conference on earthquake Geotechnics* (2007), p. 1454.

[Bri07] J. L. Briaud. „Spread Footings in Sand: Load Settlement Curve Approach“. In: *Journal of Geotechnical and Geoenvironmental Engineering* 133.8 (2007), pp. 905–920.

[Bro01] W. Broere. „Tunnel Face Stability and New CPT Applications“. In: *TU Delft repository* (2001).

[CB03] J. T. Christian and G. B. Baecher. „Discussion of “Probabilistic Foundation Settlement on Spatially Random Soil” by Gordon A. Fenton and D. V. Griffiths“. In: *Journal of Geotechnical and Geoenvironmental Engineering* 129.9 (2003), pp. 866–866.

[DB93] D. J. Degroot and G.B. Baecher. „Estimating autocovariance of in-situ soil properties“. In: *International Journal of Rock Mechanics and Mining Sciences & Geomechanics Abstracts* 30.4 (1993).

[Fel17] B. Fellenius. *BASICS OF FOUNDATION DESIGN*. LULU COM, 2017.

[Fir+15] S. Firouzianbandpey, D. V. Griffiths, L. B. Ibsen, and L. V. Andersen. „Corrigendum: Spatial correlation length of normalized cone data in sand: case study in the north of Denmark“. In: *Canadian Geotechnical Journal* 52.8 (2015), pp. 1195–1197.

[FK04] G. Florides and S. Kalogirou. „Measurements of Ground Temperature at Various Depths“. In: *Proceedings of the SET 2004, 3rd International Conference on Sustainable Energy Technologies on CD-ROM, Nottingham, UK* 3 (2004).

[GAO09] K. G. Gavin, A. Adekunte, and B. Okelly. „A field investigation of vertical footing response on sand“. In: *Proceedings of the Institution of Civil Engineers - Geotechnical Engineering* 162.5 (2009), pp. 257–267.

[Gar13] Garnier. „Advances in lateral cyclic pile design: contribution of the SOLCYP project“. In: *Proceedings of the TC 209 Workshop: 18th ICSMGE – Design for Cyclic Loading: Piles and Other Foundations, Paris, France* (2013), pp. 59–68.

[Gav18] K.G. Gavin. „Use of CPT for the design of shallow and deep foundations on sand“. In: *Proceedings of the 4th International Symposium on Cone Penetration Testing* (2018).

[GMC03] C. I. Giasi, P. Masi, and C. Cherubini. „Probabilistic and fuzzy reliability analysis of a sample slope near Aliano“. In: *Engineering Geology* 67.3-4 (2003), pp. 391–402.

[GO07] K. G. Gavin and B. C. O'Kelly. „Effect of Friction Fatigue on Pile Capacity in Dense Sand“. In: *Journal of Geotechnical and Geoenvironmental Engineering* 133.1 (2007), pp. 63–71.

[HK16] M. N. Hussien and M. Karray. „Shear wave velocity as a geotechnical parameter: an overview“. In: *Canadian Geotechnical Journal* 53.2 (2016), pp. 252–272.

[Hob71] D. W. Hobbs. „The dependence of the bulk modulus, Youngs modulus, creep, shrinkage and thermal expansion of concrete upon aggregate volume concentration“. In: *Matériaux et Constructions* 4.2 (1971), pp. 107–114.

[JBK97] M. B. Jaksa, P. I. Brooker, and W. S. Kaggwa. „Modelling the Spatial Variability of the Undrained Shear Strength of Clay Soils Using Geostatistics“. In: *Geostatistics Wollongong' 96 Quantitative Geology and Geostatistics* (1997), pp. 1284–1295.

[Kar+11] M. Karray, G. Lefebvre, Y. Ethier, and A. Bigras. „Influence of particle size on the correlation between shear wave velocity and cone tip resistance“. In: *Canadian Geotechnical Journal* 48.4 (2011), pp. 599–615.

[LFH14] M. Lloret-Cabot, G.A. Fenton, and M.A. Hicks. „On the estimation of scale of fluctuation in geostatistics“. In: *Georisk: Assessment and Management of Risk for Engineered Systems and Geohazards* 8.2 (Feb. 2014), pp. 129–140.

[Mon18] R. van Montfort. „Insufficiency of immersion joints in existing immersed tunnels“. In: *TU Delft repository* (2018).

[MP99] P. W. Mayne and H. G. Poulos. „Approximate displacement influence factors for elastic shallow foundations“. In: *Journal of Geotechnical and Geoenvironmental Engineering* 125.6 (1999), pp. 453–460.

[Mur03] V. N. S. Murthy. *Geotechnical engineering: principles and practices of soil mechanics and foundation engineering*. Marcel Dekker, 2003.

[Nwo+17] C.U. Nwoji, Onah H.N., Mama B.O., and C.C. Ike. „Solution of the Boussinesq Problem of Half Space using Green and Zerna Displacement Potential Function Method“. In: *Electronic Journal of Geotechnical Engineering* (2017), pp. 4305–4314.

[Par+07] C. B. Park, R. D. Miller, J. Xia, and J. Ivanov. „Multichannel analysis of surface waves (MASW)—active and passive methods“. In: *The Leading Edge* 26.1 (2007), pp. 60–64.

[PMX99] C. B. Park, R. D. Miller, and J. Xia. „Multichannel analysis of surface waves“. In: *Geophysics* 64.3 (1999), pp. 800–808.

[PRG18] L. J. Prendergast, C. Reale, and K. G. Gavin. „Probabilistic examination of the change in eigenfrequencies of an offshore wind turbine under progressive scour incorporating soil spatial variability“. In: *Marine Structures* 57 (2018), pp. 87–104.

[Pul+17] Selim Pul, Amir Ghaffari, Ertekin Öztekin, Metin Hüsem, and Serhat Demir. „Experimental Determination of Cohesion and Internal Friction Angle on Conventional Concretes“. In: *ACI Materials Journal* 114.3 (2017).

[RC15] P. K. Robertson and K.L. Cabal. „Guide to Cone Penetration Testing for Geotechnical Engineering 6th edition“. In: *Gregg Drilling & Testing, Inc.* (2015).

[RC83] P. K. Robertson and R. G. Campanella. „Interpretation of cone penetration tests. Part I: Sand“. In: *Canadian Geotechnical Journal* 20.4 (1983), pp. 718–733.

[Rob90] P. K. Robertson. „Soil classification using the cone penetration test“. In: *Canadian Geotechnical Journal* 27.1 (1990), pp. 151–158.

[Ter43] K. Terzaghi. „Theoretical Soil Mechanics“. In: (Jan. 1943).

[UM11] Marco Uzielli and Paul W. Mayne. „Serviceability limit state CPT-based design for vertically loaded shallow footings on sand“. In: *Geomechanics and Geoengineering* 6.2 (2011), pp. 91–107.

[UM12] M. Uzielli and P. W. Mayne. „Load-displacement uncertainty of vertically loaded shallow footings on sands and effects on probabilistic settlement estimation“. In: *Georisk: Assessment and Management of Risk for Engineered Systems and Geohazards* 6.1 (2012), pp. 50–69.

[Van77] E. H. Vanmarcke. „Probabilistic modeling of soil profiles“. In: *Journal of the Geotechnical Engineering Division* 103.11 (1977), pp. 1227–1246.

[Xia+02] J. Xia, R. D. Miller, C. B. Park, et al. „Comparing shear-wave velocity profiles inverted from multichannel surface wave with borehole measurements“. In: *Soil Dynamics and Earthquake Engineering* 22.3 (2002), pp. 181–190.

Websites

[Cho18] Choon Park. *MASW Data acquisition*. 2018. URL: `http://www.masw.com/DataAcquisition.html` (visited on Dec. 4, 2018) (cit. on p. 8).

[Weg18a] Wegenwiki, Inc. *Heinenoord tunnel*. 2018. URL: `https://www.wegenwiki.nl/Heinenoordtunnel` (visited on May 27, 2018) (cit. on p. 3).

[Weg18b] Wegenwiki, Inc. *Kiltunnel*. 2018. URL: `https://www.wegenwiki.nl/Kiltunnel` (visited on May 27, 2018) (cit. on p. 1).

Appendices

Appendix A: Statistical data CPT's Heinenoord

A

This appendix contains all statistical data for the Heinenoord site for each layer. Table A.1 and table A.2 contain all statistical data for each layer for each individual CPT, 0 being the CPT at Southwest end and 12 being the CPT at the Northeast end. Table A.3 until table A.6 contain the mean and the ranges of the statistical data for each layer.

Tab. A.1.: All statistical data for each layer for each individual CPT (Part 1)

CPT	0	1	2	3	4	5	6	7	8	9	10	11	12
Layer 1: [m below NAP]	4.0 – 8.4	0.0 – 5.8	2.0 - 4.0										
μ [MPa]	1.60	1.48	1.49										
σ [Mpa]	1.45	1.63	1.26										
σres [Mpa]	1.20	1.27	1.24										
atrend [MPa/m]	0.64	0.61	0.39										
btrend [MPa]	-2.35	-0.31	0.30										
Θv [m] (Markov)	0.23	0.55	0.35										
SSE [-] (Markov)	1.35	0.27	6.63										
Θv [m] (Gaussian)	0.26	0.55	0.44										
SSE [-] (Gaussian)	0.89	0.21	5.74										
Layer 2: [m below NAP]	8.4 – 14.0	5.8 – 14.0	4.0 – 6.2	6.0 – 8.4	12.0 – 14.0	12.0 – 14.0	11.0 – 12.0	12.0 – 14.6					
μ [MPa]	0.91	1.01	0.44	0.78	0.71	0.89	1.91	1.13					
σ [Mpa]	0.29	0.43	0.14	0.45	0.18	0.49	0.62	0.57					
σres [Mpa]	0.27	0.32	0.12	0.25	0.14	0.42	0.57	0.56					
atrend [MPa/m]	0.07	0.12	0.13	0.54	0.19	0.44	-0.83	-0.14					
btrend [MPa]	0.12	-0.19	-0.21	-3.13	-1.72	-4.82	11.47	3.03					
Θv [m] (Markov)	0.52	0.58	0.19	0.25	0.26	0.20	0.14	0.27					
SSE [-] (Markov)	0.31	0.29	1.11	0.53	1.33	1.23	1.59	3.57					
Θv [m] (Gaussian)	0.53	0.50	0.18	0.22	0.26	0.21	0.14	0.32					
SSE [-] (Gaussian)	0.30	1.43	1.38	0.64	1.49	1.34	1.59	3.60					
Layer 3: [m below NAP]											1.0 – 8.0	1.0 – 8.0	2.0 – 8.0
μ [MPa]											6.82	8.45	8.42
σ [Mpa]											3.75	2.86	2.50
σres [Mpa]											3.67	2.86	2.29
atrend [MPa/m]											0.38	-0.09	-0.57
btrend [MPa]											5.11	8.87	11.27
Θv [m] (Markov)											1.10	0.31	0.21
SSE [-] (Markov)											0.22	0.97	0.67
Θv [m] (Gaussian)											1.00	0.33	0.21
SSE [-] (Gaussian)											1.21	0.67	0.53
Layer 4: [m below NAP]	14.0 – 24.6	14.0 – 21.8	6.2 – 21.0	8.4 - 22.0	14.0 – 22.0	14.0 – 21.8	12.0 – 28.0	14.6 – 26.0	8.0 – 26.2	10.0 – 26.0	8.0 – 26.0	8.0 – 27.0	8.0 – 21.4
μ [MPa]	8.65	12.10	8.91	10.80	8.75	9.05	11.83	13.37	9.58	9.55	12.18	14.40	11.51
σ [Mpa]	5.49	4.06	4.69	5.15	4.01	3.58	4.49	4.96	6.65	5.63	5.35	6.29	6.47
σres [Mpa]	4.44	4.06	4.15	4.36	3.66	2.40	3.78	4.33	3.32	4.66	5.11	6.10	5.00
atrend [MPa/m]	1.03	-0.04	0.51	0.69	0.71	1.18	0.53	0.76	1.10	0.69	0.30	0.28	1.05
btrend [MPa]	-11.2	12.91	1.96	0.20	-4.09	-12.1	1.23	-2.25	-9.34	-2.92	6.99	9.51	-3.96
Θv [m] (Markov)	0.67	0.38	0.52	1.04	0.70	0.30	0.66	1.44	0.60	1.30	0.83	0.59	0.51
SSE [-] (Markov)	0.16	0.67	0.68	0.39	0.21	0.66	0.11	0.02	0.15	0.03	0.04	0.07	0.14
Θv [m] (Gaussian)	0.62	0.38	0.53	0.94	0.66	0.32	0.55	1.18	0.54	1.10	0.73	0.55	0.49
SSE [-] (Gaussian)	0.13	0.57	0.25	0.16	0.15	0.40	0.75	0.42	0.32	0.35	0.56	0.27	0.11
Layer 5: [m below NAP]	24.6 – 26.4	21.8 – 23.2	21.0 – 23.4	22.0 – 23.0	22.0 – 25.8	21.8 – 25.0							
μ [MPa]	3.31	3.27	2.88	3.56	3.03	2.92							
σ [Mpa]	0.35	0.69	0.42	0.40	0.42	0.38							
σres [Mpa]	0.34	0.56	0.40	0.34	0.36	0.26							
atrend [MPa/m]	-0.06	-0.99	-0.19	0.76	0.19	0.31							
btrend [MPa]	4.82	25.65	7.19	-13.5	-1.51	-4.22							
Θv [m] (Markov)	0.13	0.16	0.16	0.07	0.26	0.27							
SSE [-] (Markov)	0.28	2.44	1.37	0.56	3.90	1.13							
Θv [m] (Gaussian)	0.12	0.19	0.15	0.07	0.28	0.29							
SSE [-] (Gaussian)	0.33	2.18	1.52	0.61	3.59	0.74							
Layer 6: [m below NAP]													21.4 – 22.8
μ [MPa]													3.08
σ [Mpa]													0.93
σres [Mpa]													0.75
atrend [MPa/m]													-1.32
btrend [MPa]													32.21
Θv [m] (Markov)													0.06
SSE [-] (Markov)													0.17
Θv [m] (Gaussian)													0.05
SSE [-] (Gaussian)													0.20

Tab. A.2.: All statistical data for each layer for each individual CPT (Part 2)

CPT	0	1	2	3	4	5	6	7	8	9	10	11	12
Layer 7: [m below NAP]													21.4 – 22.8
μ [MPa]													3.08
σ [Mpa]													0.93
σres [Mpa]													0.75
atrend [MPa/m]													-1.32
btrend [MPa]													32.21
Θv [m] (Markov)													0.06
SSE [-] (Markov)													0.17
Θv [m] (Gaussian)													0.05
SSE [-] (Gaussian)													0.20
Layer 8: [m below NAP]								26.0 – 28.6	26.2 – 28.2		26.0 – 28.0	27.0 – 29.0	26.8 – 29.4
μ [MPa]								11.54	3.80		7.95	3.42	15.29
σ [Mpa]								6.64	2.00		4.35	0.61	5.23
σres [Mpa]								5.32	1.97		1.73	0.57	4.08
atrend [MPa/m]								-5.25	-0.59		-7.03	-0.36	0.92
btrend [MPa]								154.9	19.86		197.7	13.47	-17.4
Θv [m] (Markov)								0.16	0.15		0.16	0.25	0.19
SSE [-] (Markov)								5.48	1.64		1.61	1.75	0.42
Θv [m] (Gaussian)								0.20	0.17		0.16	0.28	0.18
SSE [-] (Gaussian)								4.90	1.41		1.48	1.56	0.31
Layer 9: [m below NAP]							28.0 – 31.4	28.6 – 31.0	28.2 – 29.6	26.0 – 32.2			
μ [MPa]							18.27	33.67	22.48	18.28			
σ [Mpa]							9.93	9.35	10.78	6.12			
σres [Mpa]							9.90	9.32	8.87	5.54			
atrend [MPa/m]							0.70	-1.13	14.97	1.45			
btrend [MPa]							-2.59	67.25	-410.2	-23.9			
Θv [m] (Markov)							0.69	0.30	0.18	0.25			
SSE [-] (Markov)							0.90	0.52	1.67	0.68			
Θv [m] (Gaussian)							0.69	0.30	0.19	0.27			
SSE [-] (Gaussian)							0.35	0.51	1.52	0.25			
Layer 10: [m below NAP]								31.0 – 42.0	29.6 – 37.0	32.2 – 34.0			
μ [MPa]								5.13	3.53	3.65			
σ [Mpa]								3.26	0.90	0.43			
σres [Mpa]								3.24	0.88	0.41			
atrend [MPa/m]								-0.11	0.10	-0.27			
btrend [MPa]								9.06	0.24	12.75			
Θv [m] (Markov)								0.30	0.19	0.23			
SSE [-] (Markov)								1.17	0.62	1.03			
Θv [m] (Gaussian)								0.26	0.15	0.25			
SSE [-] (Gaussian)								1.26	0.73	0.99			
Layer 11: [m below NAP]	26.4 – 41.0	23.2 – 40.4	23.4 – 39.0	23.0 – 38.0	25.8 – 45.4	25.0 – 43.8	31.4 – 45.0	42.0 – 46.0	37.0 – 38.8	34.0 – 42.0	28.0 – 40.0	29.0 – 37.8	29.4 – 41.8
μ [MPa]	18.77	15.71	18.13	18.48	13.08	12.63	12.60	15.31	16.17	12.51	13.52	16.77	15.29
σ [Mpa]	9.50	7.53	7.90	8.38	8.49	7.36	8.06	10.92	2.58	3.70	6.90	6.01	5.23
σres [Mpa]	8.17	7.04	7.84	8.35	8.45	7.32	6.96	8.00	2.50	2.77	5.53	4.81	4.08
atrend [MPa/m]	-1.13	-0.54	-0.22	-0.16	-0.14	-0.15	1.05	-6.09	-1.15	1.10	1.20	1.36	0.92
btrend [MPa]	56.82	32.30	24.67	23.42	18.26	17.75	-27.3	282.4	59.80	-29.0	-27.1	-28.6	-17.4
Θv [m] (Markov)	0.60	0.72	0.67	0.77	0.82	0.72	0.59	0.25	0.18	0.38	1.20	0.40	0.19
SSE [-] (Markov)	0.20	0.16	1.70	0.45	0.24	0.08	0.06	0.96	0.75	0.23	0.06	0.20	0.42
Θv [m] (Gaussian)	0.56	0.68	0.70	0.75	0.77	0.66	0.54	0.26	0.16	0.31	1.05	0.32	0.18
SSE [-] (Gaussian)	0.18	0.32	0.87	0.27	0.25	0.42	0.37	0.81	1.04	0.53	0.84	0.82	0.31

Tab. A.3.: Ranges and mean values of the statistical data of each layer. (Part 1)

Property	Range	Mean value
Layer 1: 0.0 m to 8.4 m (3 CPT's) Clay with some sandlayers		
Mean (μ): MPa	1.48 – 1.60	1.52
Standard deviation (σ): Mpa	1.26 – 1.63	1.47
Standard deviation (σres): Mpa (de-trended)	1.20 – 1.27	1.24
Slope of the linear depth trend (atrend): MPa/m	0.39 – 0.64	0.55
Intercept of the linear depth trend (btrend): MPa	-2.35 – 0.30	-0.79
Vertical scale of fluctuation (θh): m (Markov)	0.23 – 0.55	0.38
Summed Squared Error: - (Markov)	0.27 – 6.63	2.75
Vertical scale of fluctuation (θh): m (Gaussian)	0.26 – 0.55	0.42
Summed Squared Error: - (Gaussian)	0.21 – 5.74	2.28
Layer 2: 4.0 m to 14.6 m (8 CPT's) Peat with some clay layers		
Mean (μ): MPa	0.44 – 1.91	0.98
Standard deviation (σ): Mpa	0.14 – 0.62	0.40
Standard deviation (σres): Mpa (de-trended)	0.12 – 0.57	0.33
Slope of the linear depth trend (atrend): MPa/m	-0.83 – 0.54	0.07
Intercept of the linear depth trend (btrend): MPa	-4.82 – 11.47	0.57
Vertical scale of fluctuation (θh): m (Markov)	0.14 – 0.58	0.30
Summed Squared Error: - (Markov)	0.29 – 3.57	1.25
Vertical scale of fluctuation (θh): m (Gaussian)	0.14 – 0.53	0.30
Summed Squared Error: - (Gaussian)	0.30 – 3.60	1.47
Layer 3: 1.0 m to 8.0 m (3 CPT's) Clay		
Mean (μ): MPa	6.82 – 8.45	7.90
Standard deviation (σ): Mpa	2.50 – 3.75	3.04
Standard deviation (σres): Mpa (de-trended)	2.29 – 3.67	2.94
Slope of the linear depth trend (atrend): MPa/m	-0.57 – 0.38	-0.09
Intercept of the linear depth trend (btrend): MPa	5.11 – 11.27	8.42
Vertical scale of fluctuation (θh): m (Markov)	0.21 – 1.10	0.54
Summed Squared Error: - (Markov)	0.22 – 0.97	0.62
Vertical scale of fluctuation (θh): m (Gaussian)	0.21 – 1.00	0.51
Summed Squared Error: - (Gaussian)	0.53 – 1.21	0.80

Tab. A.4.: Ranges and mean values of the statistical data of each layer. (Part 2)

Property	Range	Mean value
Layer 4: 6.2 m to 28.0 m (12 CPT's) Sand with some clay layers		
Mean (μ): MPa	8.65 – 14.40	10.82
Standard deviation (σ): Mpa	3.58 – 6.65	5.14
Standard deviation (σres): Mpa (de-trended)	2.40 – 6.10	4.26
Slope of the linear depth trend (atrend): MPa/m	-0.04 – 1.18	0.68
Intercept of the linear depth trend (btrend): MPa	-12.1 – 12.91	-1.00
Vertical scale of fluctuation (θh): m (Markov)	0.30 – 1.44	0.73
Summed Squared Error: - (Markov)	0.02 – 0.68	0.26
Vertical scale of fluctuation (θh): m (Gaussian)	0.32 – 1.18	0.66
Summed Squared Error: - (Gaussian)	0.11 – 0.75	0.34
Layer 5: 21.0 m to 26.4 m (6 CPT's) Clay		
Mean (μ): MPa	2.88 – 3.56	3.16
Standard deviation (σ): Mpa	0.38 – 0.69	0.44
Standard deviation (σres): Mpa (de-trended)	0.26 – 0.56	0.38
Slope of the linear depth trend (atrend): MPa/m	-0.99 – 0.76	0.00
Intercept of the linear depth trend (btrend): MPa	-13.5 – 25.65	3.07
Vertical scale of fluctuation (θh): m (Markov)	0.07 – 0.27	1.05
Summed Squared Error: - (Markov)	0.28 – 3.90	1.61
Vertical scale of fluctuation (θh): m (Gaussian)	0.07 – 0.29	0.18
Summed Squared Error: - (Gaussian)	0.33 – 3.59	1.50
Layer 6: 21.4 m to 22.8 m (1 CPT) Clay		
Mean (μ): MPa	-	3.08
Standard deviation (σ): Mpa	-	0.93
Standard deviation (σres): Mpa (de-trended)	-	0.75
Slope of the linear depth trend (atrend): MPa/m	-	-1.32
Intercept of the linear depth trend (btrend): MPa	-	32.21
Vertical scale of fluctuation (θh): m (Markov)	-	0.06
Summed Squared Error: - (Markov)	-	0.17
Vertical scale of fluctuation (θh): m (Gaussian)	-	0.05
Summed Squared Error: - (Gaussian)	-	0.20

Tab. A.5.: Ranges and mean values of the statistical data of each layer. (Part 3)

Property	Range	Mean value
Layer 7: 22.8 m to 26.8 m (1 CPT) Clay with some peat layers		
Mean (μ): MPa	-	13.3
Standard deviation (σ): Mpa	-	9.44
Standard deviation (σres): Mpa (de-trended)	-	8.58
Slope of the linear depth trend (atrend): MPa/m	-	3.46
Intercept of the linear depth trend (btrend): MPa	-	-72.5
Vertical scale of fluctuation (θh): m (Markov)	-	0.30
Summed Squared Error: - (Markov)	-	1.92
Vertical scale of fluctuation (θh): m (Gaussian)	-	0.34
Summed Squared Error: - (Gaussian)	-	1.55
Layer 8: 26.0 m to 29.4 m (5 CPT's) Clay		
Mean (μ): MPa	3.80 – 15.29	8.40
Standard deviation (σ): Mpa	0.61 – 6.64	3.77
Standard deviation (σres): Mpa (de-trended)	0.57 – 5.32	2.73
Slope of the linear depth trend (atrend): MPa/m	-7.03 – 0.92	-2.46
Intercept of the linear depth trend (btrend): MPa	-17.4 – 197.7	73.71
Vertical scale of fluctuation (θh): m (Markov)	0.15 – 0.25	0.18
Summed Squared Error: - (Markov)	0.42 – 5.48	2.18
Vertical scale of fluctuation (θh): m (Gaussian)	0.16 – 0.28	0.20
Summed Squared Error: - (Gaussian)	0.31 – 4.90	1.93
Layer 9: 26.0 m to 32.2 m (4 CPT's) Sand		
Mean (μ): MPa	18.27 – 33.67	23.18
Standard deviation (σ): Mpa	6.12 – 10.78	9.05
Standard deviation (σres): Mpa (de-trended)	5.54 – 9.90	8.41
Slope of the linear depth trend (atrend): MPa/m	-1.13 – 14.97	4.00
Intercept of the linear depth trend (btrend): MPa	-410.2 – 67.25	-92.36
Vertical scale of fluctuation (θh): m (Markov)	0.18 – 0.69	0.36
Summed Squared Error: - (Markov)	0.52 – 1.67	0.94
Vertical scale of fluctuation (θh): m (Gaussian)	0.19 – 0.69	0.36
Summed Squared Error: - (Gaussian)	0.25 – 1.52	0.66

Tab. A.6.: Ranges and mean values of the statistical data of each layer. (Part 4)

Property	Range	Mean value
Layer 10: 29.6 m to 42.0 m (3 CPT's) Clay		
Mean (μ): MPa	3.53 – 5.13	4.10
Standard deviation (σ): Mpa	0.43 – 3.26	1.53
Standard deviation (σres): Mpa (de-trended)	0.41 – 3.24	1.51
Slope of the linear depth trend (atrend): MPa/m	-0.27 – 0.10	-0.09
Intercept of the linear depth trend (btrend): MPa	0.24 – 12.75	7.35
Vertical scale of fluctuation (θh): m (Markov)	0.19 – 0.30	0.24
Summed Squared Error: - (Markov)	0.62 – 1.17	0.94
Vertical scale of fluctuation (θh): m (Gaussian)	0.15 – 0.26	0.19
Summed Squared Error: - (Gaussian)	0.73 – 1.26	0.99
Layer 11: 23.0 m to 46.0 m (13 CPT's) Sand with very thin clay layers		
Mean (μ): MPa	12.51 – 18.77	15.31
Standard deviation (σ): Mpa	2.58 – 10.92	7.12
Standard deviation (σres): Mpa (de-trended)	2.50 – 8.17	6.29
Slope of the linear depth trend (atrend): MPa/m	-6.09 – 1.36	-0.30
Intercept of the linear depth trend (btrend): MPa	-29.0 – 282.4	29.69
Vertical scale of fluctuation (θh): m (Markov)	0.18 – 1.20	0.58
Summed Squared Error: - (Markov)	0.06 – 1.70	0.50
Vertical scale of fluctuation (θh): m (Gaussian)	0.16 – 1.05	0.53
Summed Squared Error: - (Gaussian)	0.18 – 1.04	0.54

Appendix B: Hand calculations

B

This chapter contains hand calculations that were performed for this report.

B.1 Determining ultimate bearing resistance for the Mayne equation

The Mayne equation that is used to calculate the initial settlement needs an input value for the ultimate bearing resistance Q_{ult}. The equation for the model is shown in equation B.1.

$$s = \frac{Q_{app} * I_{hrv}}{B * E_0 * [1 - (\frac{Q_{app}}{Q_{ult}})^{0.3}]} \tag{B.1}$$

Where Q_app is the applied force in kN, I_hrv is the shape factor of the footing, which is 0.85 for a rigid rectangular footing, B is the width of the foundation in m, E_0 is the small strain stiffness of the soil and Q_{ult} is the ultimate bearing resistance of the soil. The model is similar to the linear settlement model of equation 2.10. However, it takes the degradation of the secant linear stiffness at higher loading into account.

At a normalised settlement s/B of 10% the applied load can be written as $\alpha * q_c$. If equation B.1 is divided by B:

$$s/B = \frac{Q_{app} * I_{hrv}}{B^2 * E_0 * [1 - (\frac{Q_{app}}{Q_{ult}})^{0.3}]} \tag{B.2}$$

If $s/B = 0.1$ and $Q_{app} = \alpha * q_c * B * L$ is filled into the equation it gives:

$$0.1 = \frac{\alpha * q_c * B * L * I_{hrv}}{B^2 * E_0 * [1 - (\frac{\alpha * q_c * B * L}{Q_{ult}})^{0.3}]} \tag{B.3}$$

$$\frac{E_0 * B}{10 * \alpha * q_c * L * I_{hrv}} = \frac{1}{[1 - (\frac{\alpha * q_c * B * L}{Q_{ult}})^{0.3}]} \tag{B.4}$$

$$\frac{10 * \alpha * q_c * L * I_{hrv}}{E_0 * B} = 1 - (\frac{\alpha * q_c * B * L}{Q_{ult}})^{0.3} \tag{B.5}$$

$$1 - \frac{10 * \alpha * q_c * L * I_{hrv}}{E_0 * B} = (\frac{\alpha * q_c * B * L}{Q_{ult}})^{0.3} \tag{B.6}$$

$$(1 - \frac{10 * \alpha * q_c * L * I_{hrv}}{E_0 * B})^{1/0.3} = \frac{\alpha * q_c * B * L}{Q_{ult}} \tag{B.7}$$

$$\frac{Q_{ult}}{\alpha * q_c * B * L} = \frac{1}{(1 - \frac{10 * \alpha * q_c * L * I_{hrv}}{E_0 * B})^{1/0.3}} \tag{B.8}$$

The ultimate bearing resistance can be calculated with equation B.9.

$$Q_{ult} = \frac{\alpha}{(1 - \frac{10 * \alpha * q_c * I_{hrv} * L}{E_0 * B})^{1/0.3}} * (q_c * B * L) \tag{B.9}$$

B.2 Determining the applied load on the middle section of the Kiltunnel

The cross-section of the tunnel is assumed to be constant over the entire length of the tunnel. The cross-section of the Kiltunnel is shown in figure B.1. The weight of the concrete is 24 kN/m^3, the weight of the water is 10 kN/m^3 and the weight of the sand on top is assumed to be 20 kN/m^3 with a thickness of 2 meter. The length of a segment is 22.3 meter. The space between the tunnel element and the road is assumed to be filled with ballast concrete. The cross-section in figure B.1 shows the thickness of the ballast concrete. This means that on average the concrete is 2.63 meter thick from the bottom of the tunnel.

Fig. B.1.: Cross-section Kiltunnel.

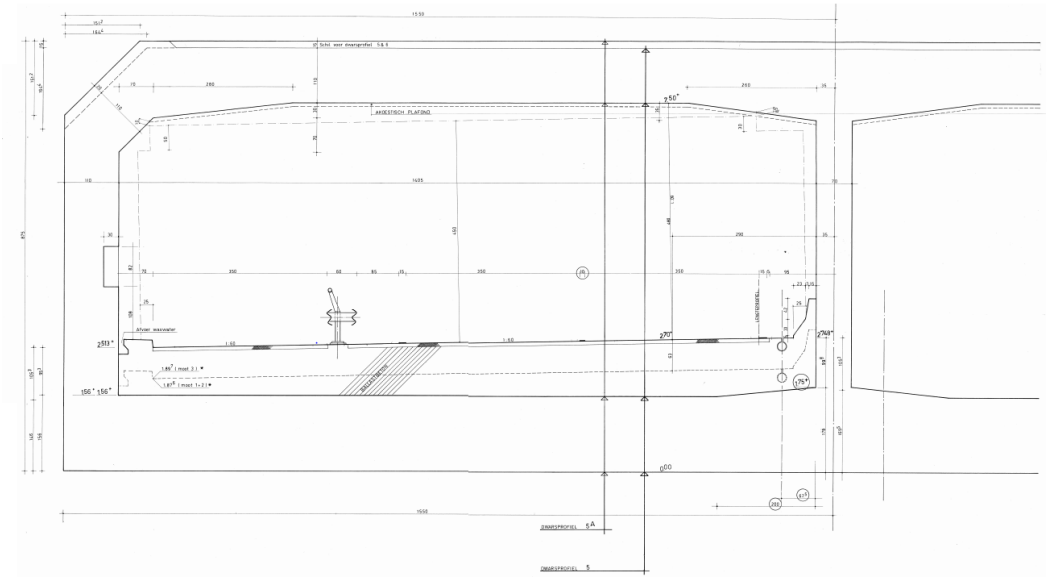

The total static loading on a segment of the foundation of the immersed tunnel is then the buoyant weight of the tunnel plus the buoyant weight of the soil on top of the tunnel. Which can be calculated using equation B.10.

$$Q_{app} = A_c * L * \rho_c - A_w * L * \rho_{water} + A_s * L * (\rho_s - \rho_{water}) \tag{B.10}$$

Where A_c is area of the concrete, L is the length of the segment, ρ_c is the unit weight of the concrete, A_w is the area of the total cross section of the tunnel, ρ_{water} is unit weight of water, A_s is the area of the soil on top of the tunnel and $\rho_s - \rho_{water}$ is the buoyant unit weight of the soil.

The area of the concrete can be calculated as:

$$\begin{aligned} A_c = {} & 2.63 * 31.00 + 1.10 * 31.00 + (2 * 1.10 + 0.70) * (8.75 - 1.10 - 2.63) \\ & + 2 * 0.5 * 0.50 * 0.70 + 2 * 0.35 * 0.70 + 4 * 0.5 * 2.80 * 0.35 \\ & - 2 * 0.5 * 1.65 * 1.65 = 133.99 m^2 \end{aligned} \tag{B.11}$$

The area of the water that the tunnel occupies can be calculated as:

$$A_w = 31.00 * 8.75 - 2 * 0.5 * 1.65 * 1.65 = 268.53m^2 \tag{B.12}$$

The area of the soil on top of the tunnel can be calculated as:

$$A_s = 31.00 * 2.00 = 62.00m^2 \tag{B.13}$$

The applied load of the middle section of the Kiltunnel tunnel can then be calculated as:

$$Q_{app,Kiltunnel} = 133.99 * 21.3 * 24.0 - 268.53 * 21.3 * 10 + 62.00 * 21.3 * 10 \tag{B.14}$$

$$Q_{app,Kiltunnel} = 24,800kN \tag{B.15}$$

The applied stress can then be calculated as:

$$q_{app,Kiltunnel} = 24,800/(31.0 * 22.3) = 35.9kPa \tag{B.16}$$

B.3 Determining the applied load on the middle section of the Heinenoordtunnel

The cross-section of the tunnel is assumed to be constant over the entire length of the tunnel. The cross-section of the Heinenoordtunnel is shown in figure B.2.

Because of lack on information of the ballast concrete in the Heinenoordtunnel it is assumed to be the same thickness as the Kiltunnel as the design of the Heinenoordtunnel is based on that of the Kiltunnel. This means that on average the concrete

Fig. B.2.: Cross-section Heinenoordtunnel.

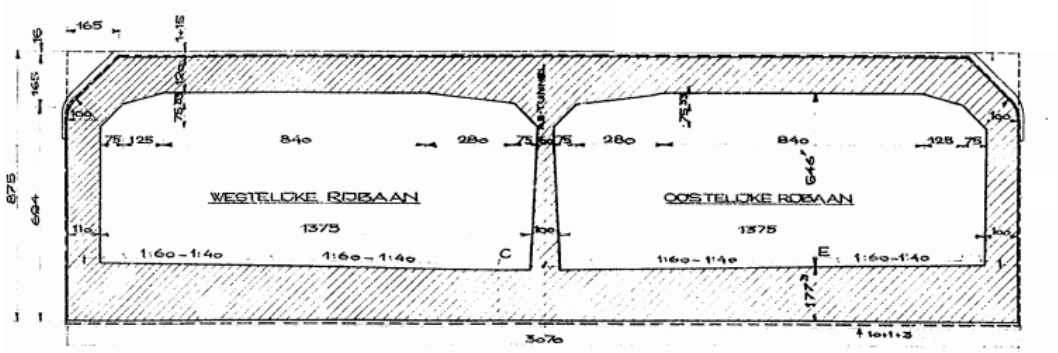

is 2.63 meter thick from the bottom of the tunnel. The area of the concrete can be calculated as:

$$\begin{aligned} A_c = {} & 2.63 * 30.70 + 1.20 * 30.70 + (2 * 1.10 + 0.80) * (8.75 - 1.20 - 2.63) \\ & + 4 * 0.5 * 0.75 * 0.75 + 2 * 0.5 * 1.25 * 0.35 + 2 * 0.5 * 2.80 * 0.35 \\ & - 2 * 0.5 * 1.65 * 1.65 = 132.16 m^2 \end{aligned} \tag{B.17}$$

The area of the water that the tunnel occupies can be calculated as:

$$A_w = 30.70 * 8.75 - 2 * 0.5 * 1.65 * 1.65 = 267.26 m^2 \tag{B.18}$$

The area of the soil on top of the tunnel can be calculated as:

$$A_s = 30.70 * 1.00 = 30.70 m^2 \tag{B.19}$$

The applied load of the middle section of the Heinenoordtunnel can then be calculated as:

$$Q_{app,Heinenoord} = 132.16 * 24.0 * 24.0 - 267.26 * 24.0 * 10 + 30.70 * 24.0 * 10 \tag{B.20}$$

$$Q_{app,Heinenoord} = 19,350kN \tag{B.21}$$

The applied stress can then be calculated as:

$$q_{app,Heinenoord} = 19,350/(31.0 * 24.0) = 26.0kPa \tag{B.22}$$

Appendix C: Blessington site

C

The Blessington site is a sand quarry in Blessington, Ireland. The sand was deposited at the bottom of a glacial lake and had a median grain size D_{50} of 0.10 (silty sand) to 0.32 (coarse sand). Glacial loading and removal of 15 meter of overburden material causes the sand to be heavily overconsolidated. For more details about the site see Gavin, Adekunte and O'Kelly (2009) and Gavin and O'Kelly (2007).

The CPT's and the average of the CPT's of the Blessington site is shown in figure C.1 and the G_0 profiles of the Blessington site are shown in figure C.2.

Fig. C.1.: CPT's and average of the CPT's of the Blessington site

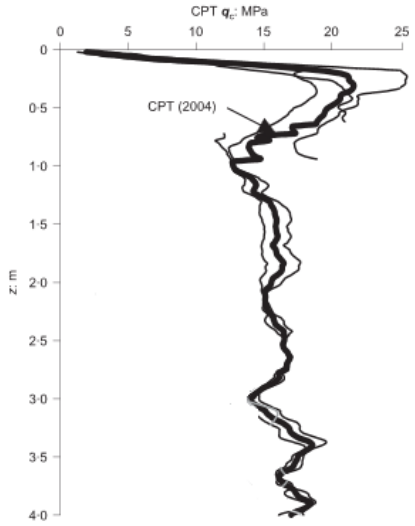

Fig. C.2.: G_0 profiles of the Blessington site

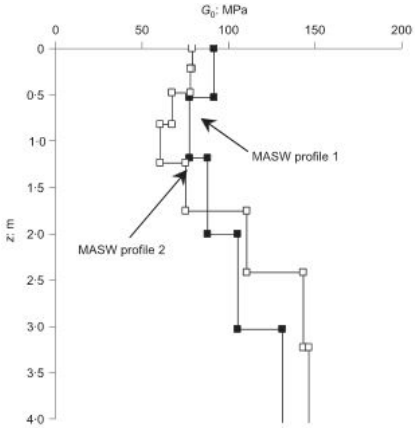

C.1 horizontal scale of fluctuation

Because of the lack of demonstrable horizontal scale of fluctuation at the Heinenoord site, the methodology is tested at the Blessington site because the Blessington site is known for its homogeneity. CPT's were performed at the Blessington site for the plate load test and for pile tests as well. The locations of the CPT's correspond with pile test S1 - S6, where 2 CPT's were performed for S1 - S4, 1.5 meter from the centre, and one for S5 and S6. The locations are shown in figure C.3.

Fig. C.3.: Locations of the CPT's at the Blessington site.

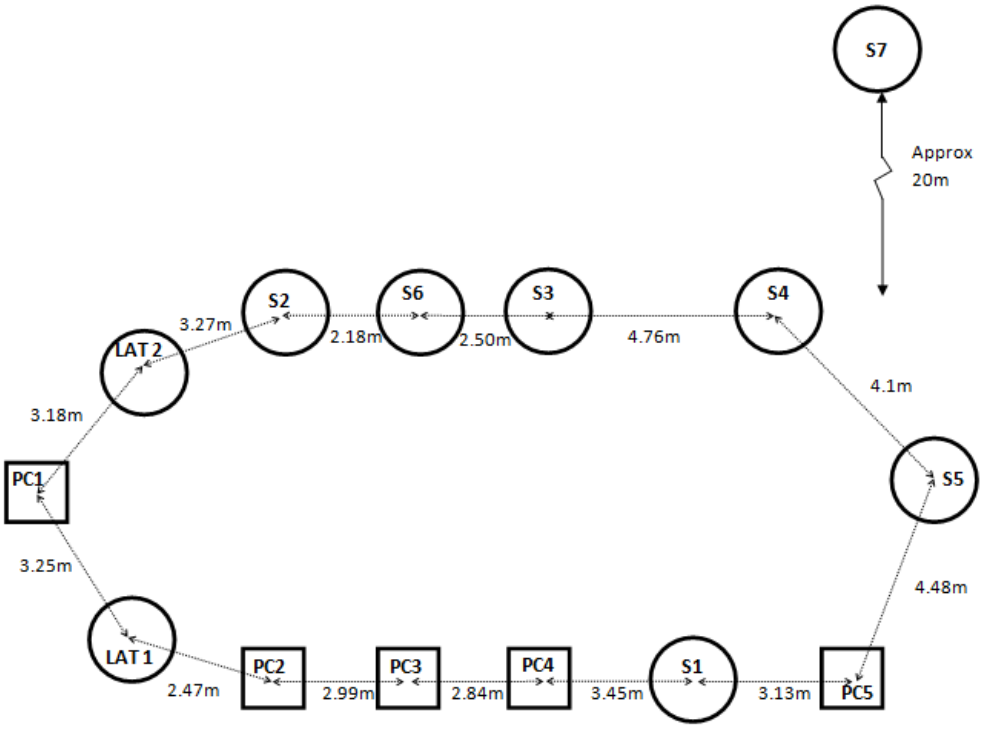

The horizontal scale of fluctuation at the Blessington site is determined using the same methodology as described in chapter 5.1.2. The results for the horizontal scale of fluctuation estimation for all CPT's together with the Markov and the Gaussian fit is shown in figure C.4. The results for the average horizontal scale of fluctuation estimation for different intervals together with the Markov and the Gaussian fit is shown in figure C.5.

The horizontal scale of fluctuation determined using a least squared estimate is 4.27 meter for the Markov fit with a summed squared error of 1.64 and is 5.01 meter for the Gaussian fit with a summed squared error of 1.59.

The results at Blessington show a larger horizontal scale of fluctuation (4.27/5.01 meter) and less scatter than the results at the Heinenoord site, but there is still a lot

Fig. C.4.: Horizontal scale of fluctuation estimation for all CPT's.

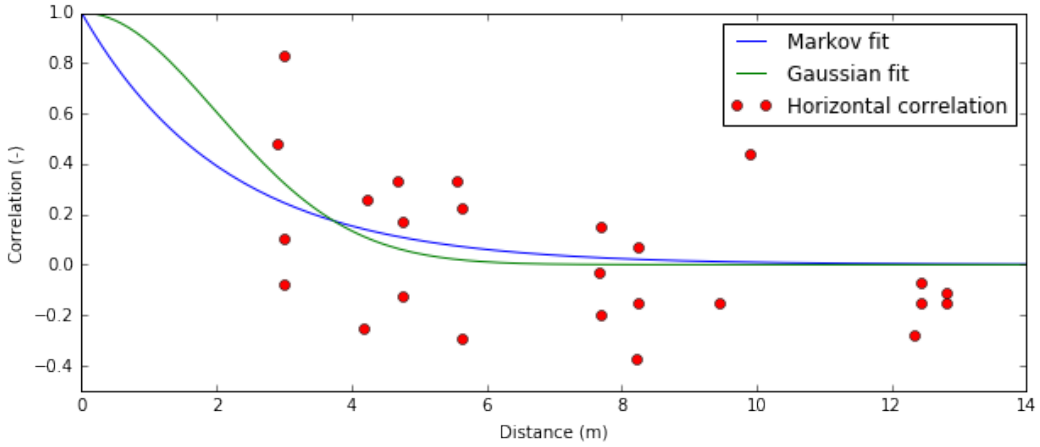

Fig. C.5.: Average horizontal scale of fluctuation estimation for different intervals.

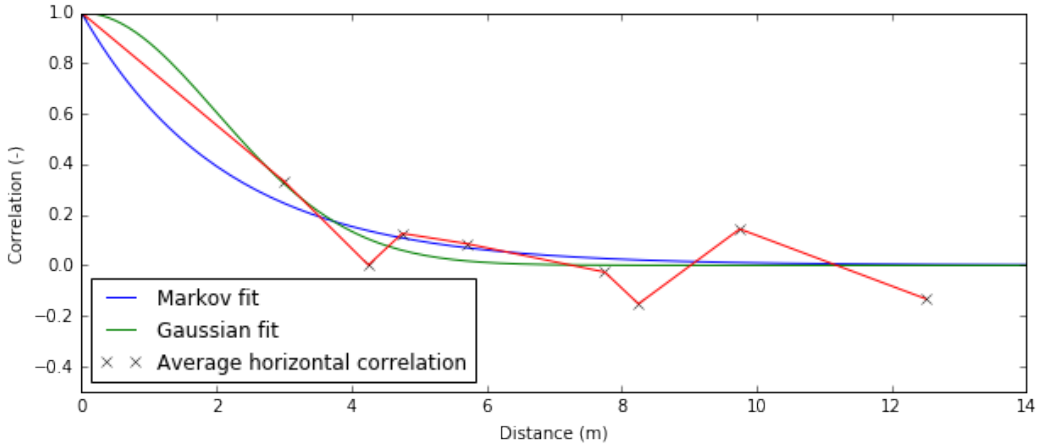

scatter in individual horizontal scale of fluctuation estimates and also some with the averaged estimates. Possible reasons for this scatter can be:

1. Layers being not strictly horizontal but at a (slight) angle.
2. Lack of enough equally spaced CPT's over which can be averaged.
3. Peaks and drops in $q_c$values due to transition into stronger or weaker zones in the layer.
4. Random noise in measurement values.
5. Rocks or pebbles in the soil.

C.1.1 Demonstration of scatter in horizontal correlation at a horizontal lag of 3.0 meter

The scatter can be shown for the CPT's from pile test S1 - S4. For each test 2 CPT's were done 1.5 meter from the centre, 3.0 meter from each other. This is the smallest distance between 2 CPT's at this site. The CPT's are named 1 and 1a for pile test S1. The q_c values of the CPT's are shown in figure C.6.

Fig. C.6.: CPT's q_c values Blessington site S1-S4.

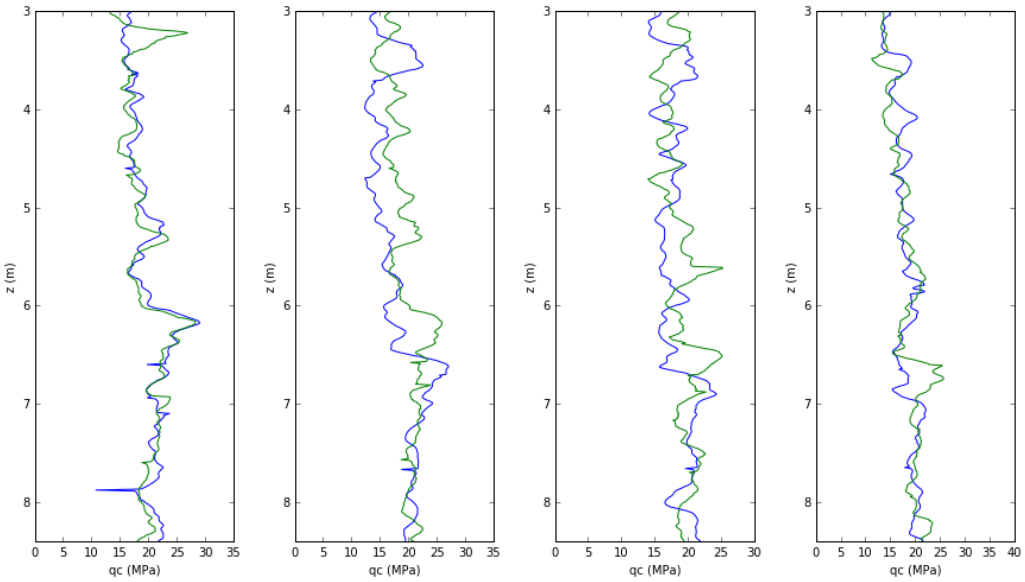

(a) CPT 1 and 1a **(b)** CPT 2 and 2a **(c)** CPT 3 and 3a **(d)** CPT 4 and 4a

Figure C.6 already shows that for this layer CPT 1 and 1a and CPT 4 and 4a are much more correlated than CPT 2 and 2a and CPT 3 and 3a. These values are not directly used as input value. The values are normalised first to get a standard normal distribution ($\mu = 0$, $\sigma = 1$). The normalised q_c values of the CPT's are shown in figure C.8.

Fig. C.8.: CPT's normalised q_c values Blessington site S1-S4.

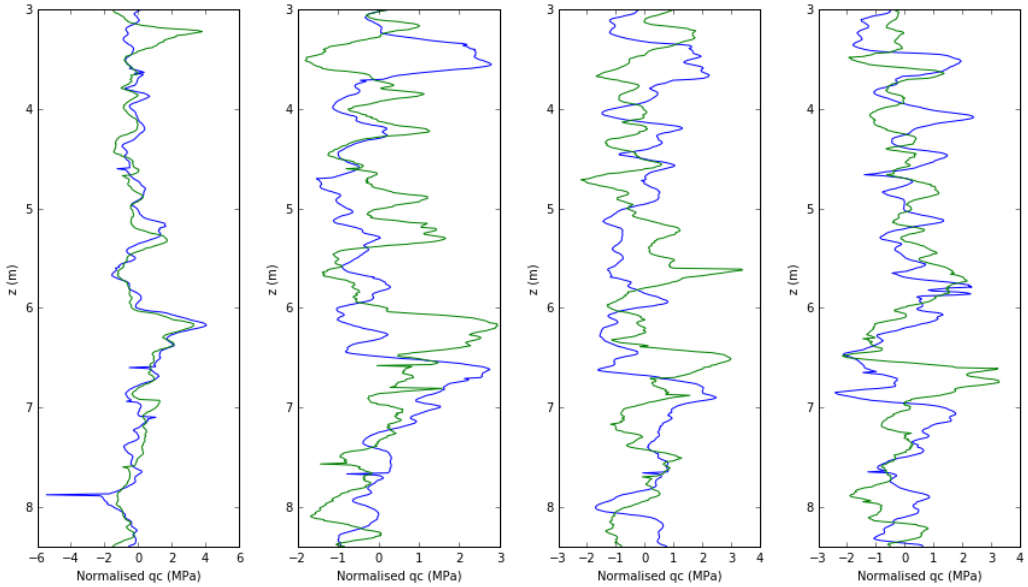

(a) CPT 1 and 1a **(b)** CPT 2 and 2a **(c)** CPT 3 and 3a **(d)** CPT 4 and 4a

Figure C.8 show that there is a large difference in horizontal correlation between CPT's that have the same horizontal lag of 3.0 meter with CPT 1 and 1a being almost 100% correlated and CPT 4 and 4a being slightly less correlated and CPT 2 and 2a and CPT 3 and 3a even less. This causes the spread in the horizontal correlation at a horizontal lag of 3.0 meter. The best way to solve this is to have a lot of CPT's in one row that have the same horizontal lag, preferably as small as possible (e.g. 1.0 meter).

C.2 Plate load test Blessington

The plate load test of a plate of 0.25 x 0.25 meter to which the model is compared in chapter 5.6.1 is performed by Gavin, Adekunte and O'kelly (2009). The results of this test is shown in figure C.10.

Fig. C.10.: Plate load-settlement response Blessington site.

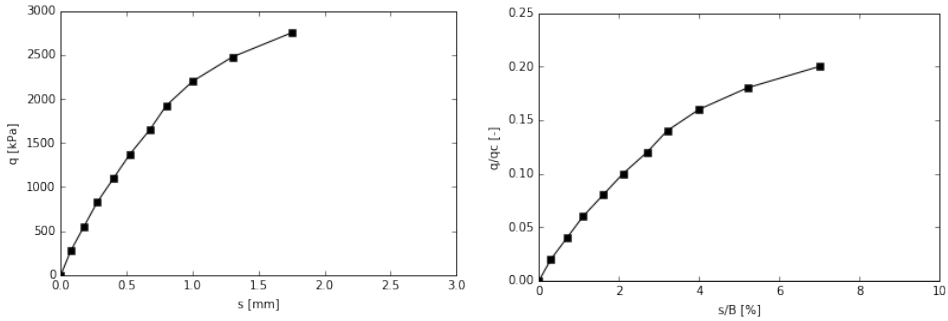

(a) Load vs settlement

(b) Normalised load vs normalised settlement

Appendix D: Results settlement calculations Kiltunnel

D

The loading for each load cycle of the tide at the Kiltunnel is assumed to be between 40% and 90% of the fluctuation in the water level. Using the lower bound of 6 kPa and the upper bound of 10 kPa of water level fluctuation based on figure 6.5, the waterlevel is assumed to fluctuate 8 kPa on average with a standard deviation of 0.67 kPa using the 3-σ rule. This fluctuation is multiplied by factor of 0.4 for the lower bound scenario and 0.9 for the upper bound situation.

The initial settlements are not included because they have occurred before start of the measurements.

D.1 Settlement calculations Kiltunnel

The settlement of the Kiltunnel is calculated for each measurement location of the middle element, indicated in figure D.1 as location 19 - 29.

Fig. D.1.: Measurement locations Kiltunnel.

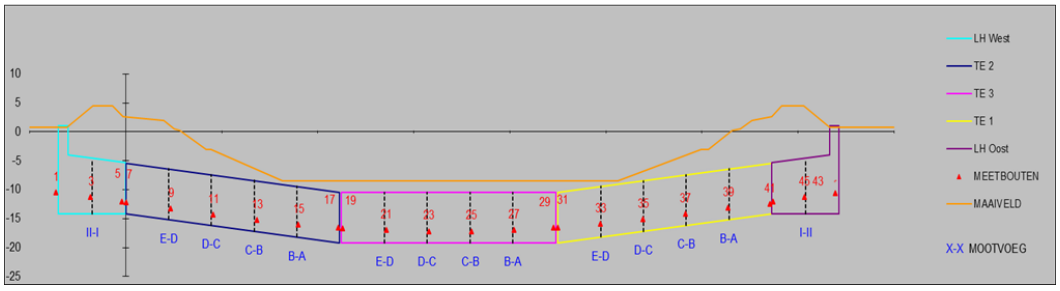

The results from the calculations of both the lower and the upper bound scenario for each measurement location in the middle element are shown in figure D.2 - D.13 together with the creep settlement from figure 5.24. For measurement locations 19 and 29 the temperature effects from figure 6.4 are added.

D.1.1 Settlement Kiltunnel Location 19

Fig. D.2.: Probability boundaries of modelled settlement of measurement location 19 of the middle element of the Kiltunnel due to tidal loading, creep and temperature effects in lower bound scenario compared to the measured settlement.

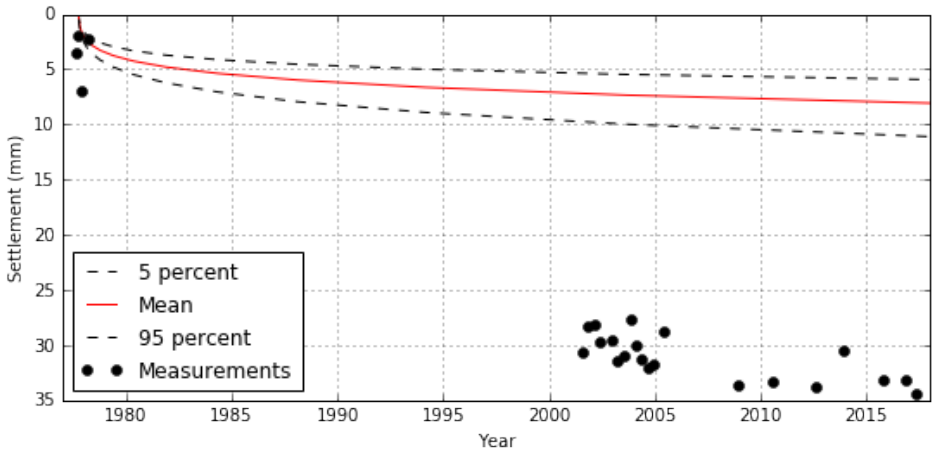

The calculated settlement of location 19 using the lower bound scenario has a 5% probability of being smaller than 5.96 mm and a 95% of being smaller than 11.16 mm in 2018. This is much smaller than the measured settlements at location 19 of around 34 mm in 2018.

Fig. D.3.: Probability boundaries of modelled settlement of measurement location 19 of the middle element of the Kiltunnel due to tidal loading, creep and temperature effects in upper bound scenario compared to the measured settlement.

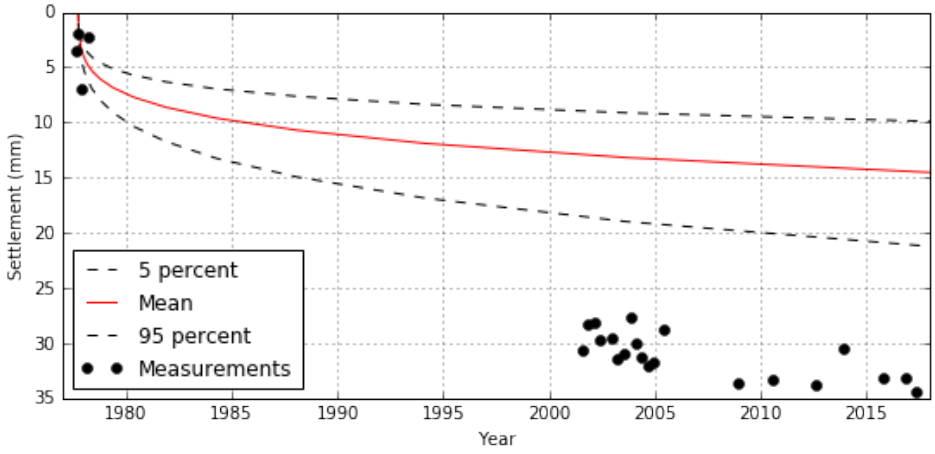

The calculated settlement of location 19 using the upper bound scenario has a 5% probability of being smaller than 9.94 mm and a 95% of being smaller than 21.34 mm in 2018. This is still much smaller than the measured settlements at location 19 of around 34 mm in 2018.

This can have different reasons:

1. The upper bound scenario could be even worse than assumed. If this is the case it is most likely due to a larger lag than assumed. This could case a smaller reduction of the load on the soil of the tunnel or even a larger load than the load of the fluctuation of the tides.

2. The creep can be larger than calculated. The creep is calculated using a CPT profile that is performed before the dredging en backfilling of the soil beneath the Kiltunnel. Also the CPT is to a smaller depth than the zone of influence of the Kiltunnel. This means that the information from the CPT profile is inaccurate.

3. Part of the load of the embankment could be transferred through the tunnel to location 19 causing a larger settlement.

4. The backfilled material at this location is a much poorer condition than at the other measurement locations. A counterargument against this is that if this is the case it should be observable in the MASW profile.

D.1.2 Settlement Kiltunnel Location 21

Fig. D.4.: Probability boundaries of modelled settlement of measurement location 21 of the middle element of the Kiltunnel due to tidal loading, creep in lower bound scenario compared to the measured settlement.

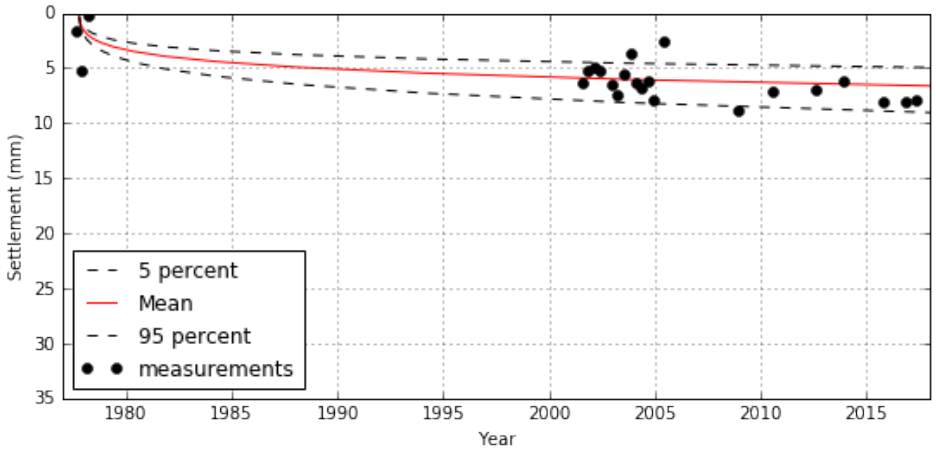

The calculated settlement of location 21 using the lower bound scenario has a 5% probability of being smaller than 4.97 mm and a 95% of being smaller than 9.08 mm in 2018. The measured settlement at location 21 of around 8 mm in 2018 is within this calculated range of the lower bound.

Fig. D.5.: Probability boundaries of modelled settlement of measurement location 21 of the middle element of the Kiltunnel due to tidal loading, creep in upper bound scenario compared to the measured settlement.

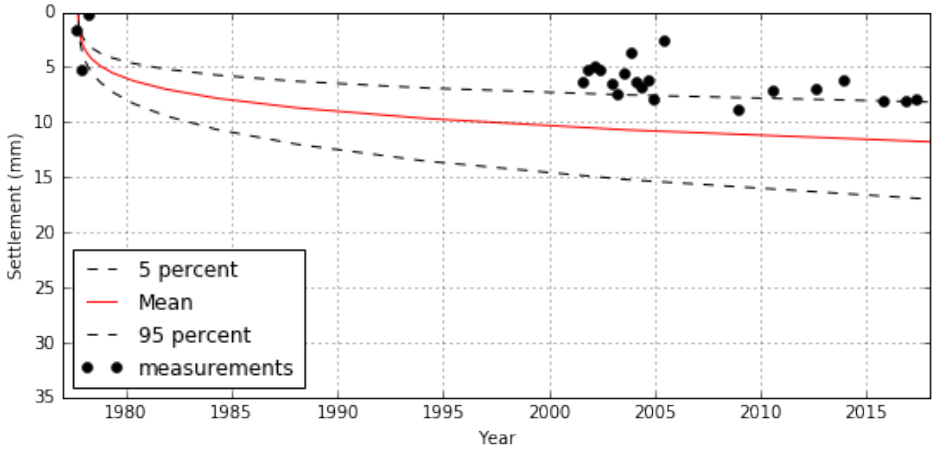

The calculated settlement of location 21 using the upper bound scenario has a 5% probability of being smaller than 8.23 mm and a 95% of being smaller than 17.23 mm in 2018. This means that the measured settlement of around 8 mm in 2018 is smaller than the calculated values of the upper bound.

D.1.3 Settlement Kiltunnel Location 23

Fig. D.6.: Probability boundaries of modelled settlement of measurement location 23 of the middle element of the Kiltunnel due to tidal loading, creep in lower bound scenario compared to the measured settlement.

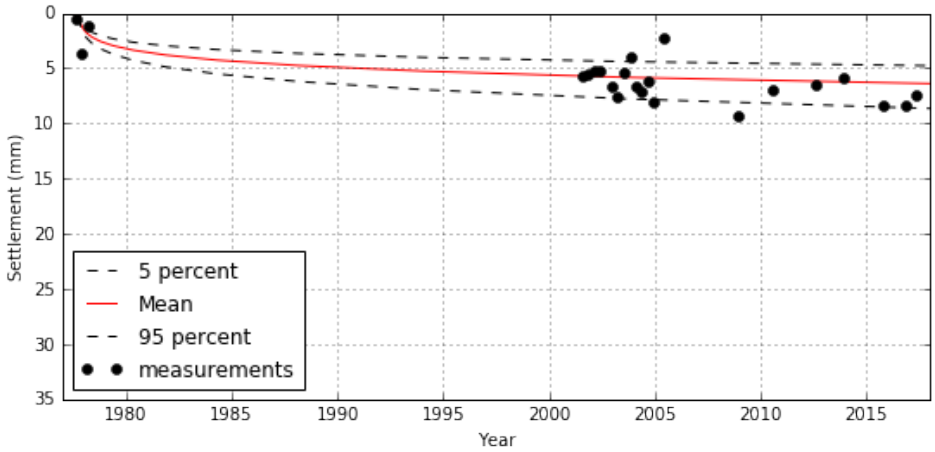

The calculated settlement of location 23 using the lower bound scenario has a 5% probability of being smaller than 4.79 mm and a 95% of being smaller than 8.69 mm in 2018. The measured settlement at location 23 of around 8 mm in 2018 is within this calculated range of the lower bound.

Fig. D.7.: Probability boundaries of modelled settlement of measurement location 23 of the middle element of the Kiltunnel due to tidal loading, creep in upper bound scenario compared to the measured settlement.

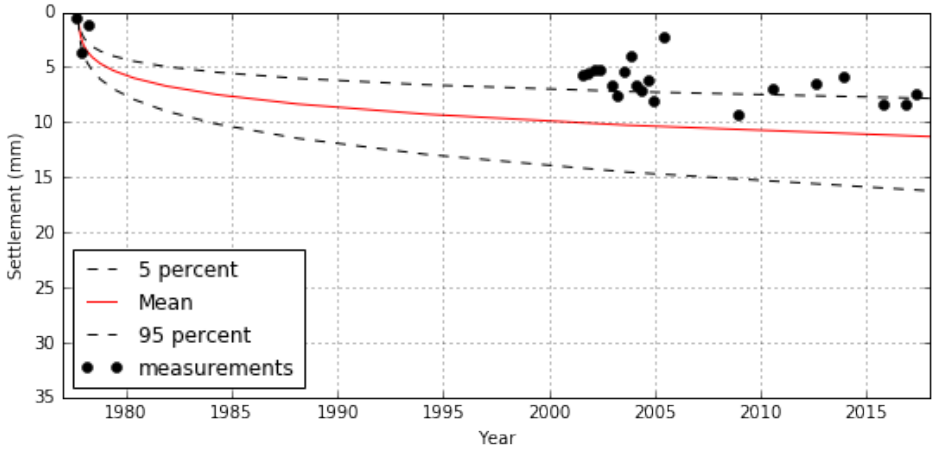

The calculated settlement of location 23 using the upper bound scenario has a 5% probability of being smaller than 7.87 mm and a 95% of being smaller than 16.33 mm in 2018. The measured settlement at location 23 of around 8 mm in 2018 is within this calculated range of the upper bound.

D.1.4 Settlement Kiltunnel Location 25

Fig. D.8.: Probability boundaries of modelled settlement of measurement location 25 of the middle element of the Kiltunnel due to tidal loading, creep in lower bound scenario compared to the measured settlement.

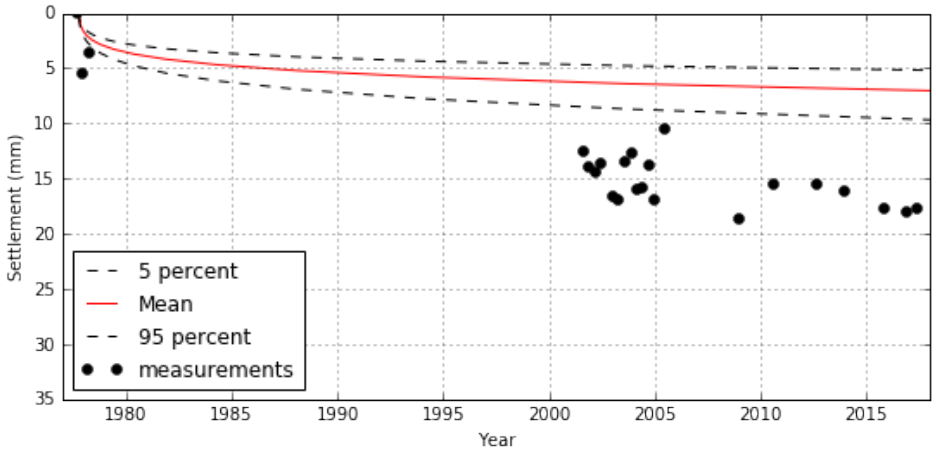

The calculated settlement of location 25 using the lower bound scenario has a 5% probability of being smaller than 5.20 mm and a 95% of being smaller than 9.72 mm in 2018. The measured settlement at location 25 of around 17 mm in 2018 is smaller than the calculated range of the lower bound.

Fig. D.9.: Probability boundaries of modelled settlement of measurement location 25 of the middle element of the Kiltunnel due to tidal loading, creep in upper bound scenario compared to the measured settlement.

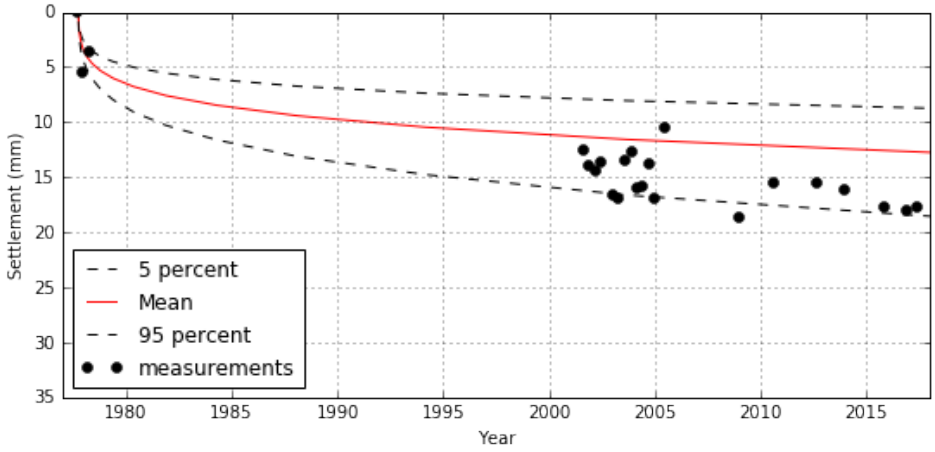

The calculated settlement of location 25 using the upper bound scenario has a 5% probability of being smaller than 8.77 mm and a 95% of being smaller than 18.65 mm in 2018. The measured settlement at location 25 of around 17 mm in 2018 is within the calculated range of the upper bound.

D.1.5 Settlement Kiltunnel Location 27

Fig. D.10.: Probability boundaries of modelled settlement of measurement location 27 of the middle element of the Kiltunnel due to tidal loading, creep in lower bound scenario compared to the measured settlement.

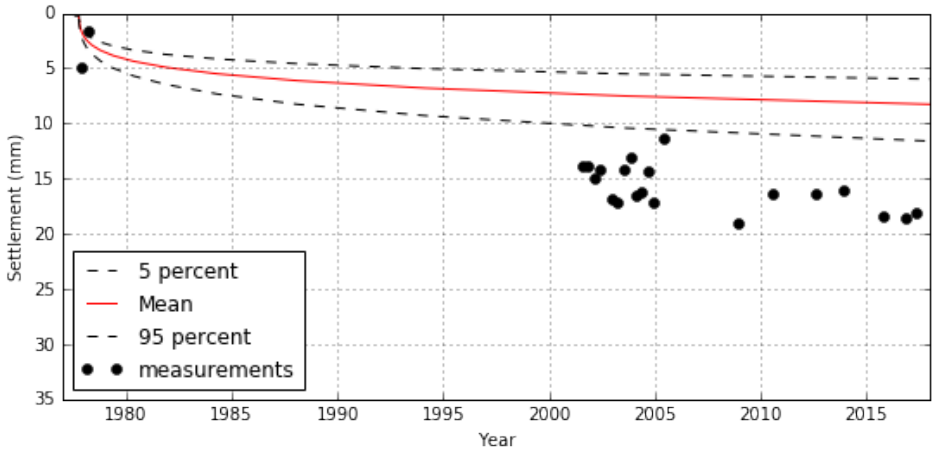

The calculated settlement of location 27 using the lower bound scenario has a 5% probability of being smaller than 6.00 mm and a 95% of being smaller than 11.66 mm in 2018. The measured settlement at location 27 of around 18 mm in 2018 is smaller than the calculated range of the lower bound.

Fig. D.11.: Probability boundaries of modelled settlement of measurement location 27 of the middle element of the Kiltunnel due to tidal loading, creep in upper bound scenario compared to the measured settlement.

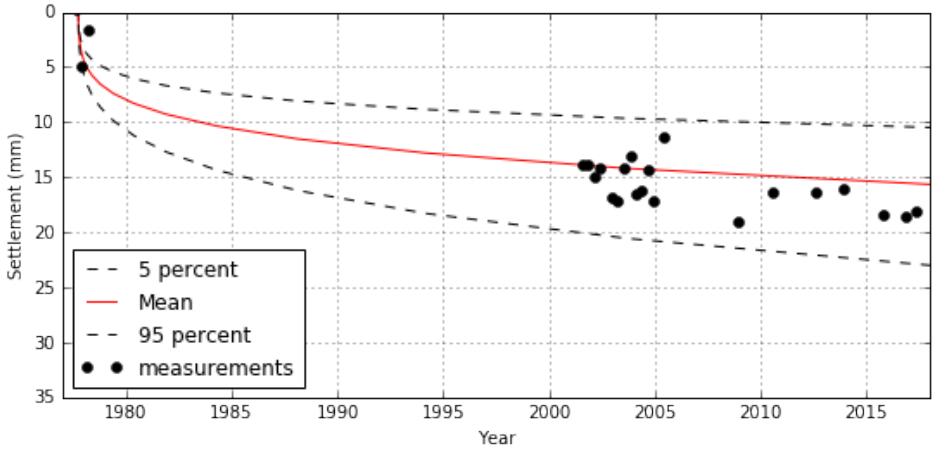

The calculated settlement of location 27 using the upper bound scenario has a 5% probability of being smaller than 10.52 mm and a 95% of being smaller than 23.13 mm in 2018. The measured settlement at location 27 of around 18 mm in 2018 is within the calculated range of the upper bound.

D.1.6 Settlement Kiltunnel Location 29

Fig. D.12.: Probability boundaries of modelled settlement of measurement location 29 of the middle element of the Kiltunnel due to tidal loading, creep and temperature effects in lower bound scenario compared to the measured settlement.

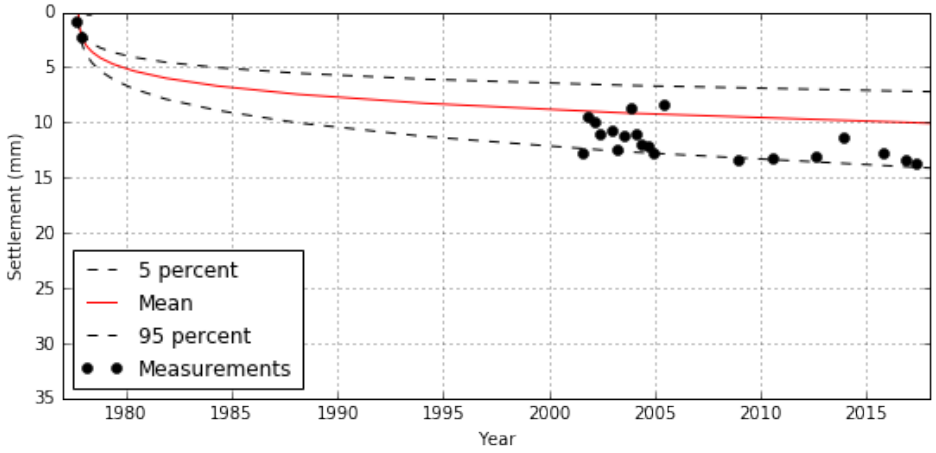

The calculated settlement of location 29 using the lower bound scenario has a 5% probability of being smaller than 7.24 mm and a 95% of being smaller than 14.20 mm in 2018. The measured settlement at location 29 of around 14 mm in 2018 is within the calculated range of the lower bound.

Fig. D.13.: Probability boundaries of modelled settlement of measurement location 29 of the middle element of the Kiltunnel due to tidal loading, creep and temperature effects in upper bound scenario compared to the measured settlement.

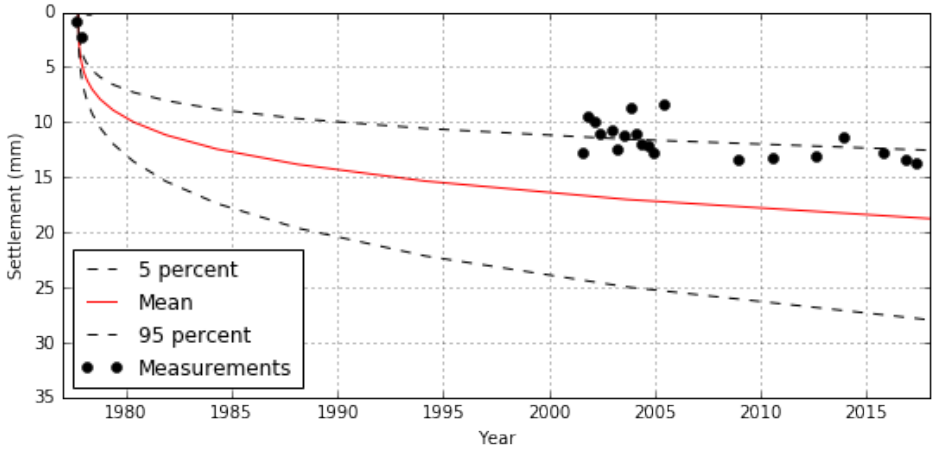

The calculated settlement of location 29 using the upper bound scenario has a 5% probability of being smaller than 12.61 mm and a 95% of being smaller than 28.11 mm in 2018. The measured settlement at location 29 of around 14 mm in 2018 is within the calculated range of the upper bound.

D.2 Summary settlement results lower and upper bound scenario Kiltunnel

The results from the settlement calculation using the lower and the upper bound loading are summarised in table D.1.

Tab. D.1.: Summary settlement results lower and upper bound scenario Kiltunnel

		5 %	95 %	Measured	Within range?
Location 19	LB	5.96	11.16	34	Too small
	UB	9.94	21.34	34	Too small
Location 21	LB	4.97	9.08	8	Yes
	UB	8.23	17.23	8	Too large
Location 23	LB	4.79	8.69	8	Yes
	UB	7.87	16.33	8	Yes
Location 25	LB	5.20	9.52	17	Too small
	UB	8.77	18.65	17	Yes
Location 27	LB	6.00	11.66	18	Yes
	UB	10.52	23.13	18	Yes
Location 29	LB	7.24	14.20	14	Yes
	UB	12.61	28.11	14	Yes

Appendix E: Python Codes used in the thesis

E

This appendix contains the python script relevant for the calculations of the thesis.

E.1 Data processing of CPT files Heinenoord

The CPT data of the Heinenoord files consisted of 65 .xml-files that contained the data of the 65 CPT's. This data was transported into .txt-files and processed using this code.

```
import xlrd
import matplotlib.pyplot as plt
import numpy as np
from pandas import read_csv
%matplotlib inline

data = dict()   #import all data from xml file (transported into txt file)

data[0] = read_csv('C:\GeoEngineering\MasterThesis\Heinenoord\BRO\CPT02522.txt',
sep=',|;',engine='python',header=None)
data[1] = read_csv('C:\GeoEngineering\MasterThesis\Heinenoord\BRO\CPT08869.txt',
sep=',|;',engine='python',header=None)
data[2] = read_csv('C:\GeoEngineering\MasterThesis\Heinenoord\BRO\CPT08870.txt',
sep=',|;',engine='python',header=None)
data[3] = read_csv('C:\GeoEngineering\MasterThesis\Heinenoord\BRO\CPT08871.txt',
sep=',|;',engine='python',header=None)

#Repeat procedure data[...] for all 65 CPT's

N = np.zeros(len(data))
z, qc,Fr = dict(), dict(), dict()

for i in range(len(data)):
    N[i] = round(len(data[i].columns)/25)
```

```
    #Number of measurements for each variable
    z[i] = np.zeros(int(N[i]))
    qc[i] = np.zeros(int(N[i]))
    Fr[i] = np.zeros(int(N[i]))

    for j in range(int(N[i])):
        z[i][j]  = data[i].iloc[0,j * 25 + 1]  #Store depth data
        qc[i][j] = data[i].iloc[0,j * 25 + 3]  #Store cone penetration resistance
        Fr[i][j] = data[i].iloc[0,j * 25 + 24] #Store Friction ratio

from scipy.stats import rankdata

z_ord, qc_ord, Fr_ord = dict(), dict(), dict()
#Data mixed up sometimes, needs to be ordered from z = z0 to z = zmax

for i in range(len(data)):
    a = (rankdata(z[i]) - 1).astype(int)
    z_ord[i] = np.zeros(int(N[i]))
    qc_ord[i] = np.zeros(int(N[i]))
    Fr_ord[i] = np.zeros(int(N[i]))

    for j in range(int(N[i])):
        b = np.where(a == j)[0]
        z_ord[i][j] = z[i][int(b)]
        qc_ord[i][j] = qc[i][int(b)]
        Fr_ord[i][j] = Fr[i][int(b)]

file = open('CPT_data.txt','w')

for i in range(len(z_ord)):
    for j in range(len(z_ord[i])):
        file.write(str(round(z_ord[i][j],3)))
        file.write(' ')
        file.write(str(round(qc_ord[i][j],3)))
        file.write(' ')
        file.write(str(round(Fr_ord[i][j],3)))
        file.write('\n')
file.close()

file = open('CPT_data_len.txt','w')
file.write(str(0))
file.write('\n')
```

```
for i in range(len(z_ord)):
    file.write(str(len(z_ord[i])))
    file.write('\n')
file.close()
```

E.2 Settlement calculations

This example is for the values of the Kiltunnel.

```
import xlrd
import matplotlib.pyplot as plt
plt.style.use('classic')
import numpy as np
import math
import numpy.random as rnd
%matplotlib inline

file_loc_S = 'C:\Geo Engineering\Master Thesis\Kiltunnel
\Statistical_data_Kiltunnel.xlsx'
#locatie van bestand van de metingen
workbook_S = xlrd.open_workbook(file_loc_S)
#Openen van bestand van de metingen
sheets_S   = workbook_S.sheet_by_index(0)
#Openen tabblad 0

file_loc_M = 'C:\Geo Engineering\Master Thesis\Kiltunnel\MASW Kil Tunnel.xlsx'
#locatie van bestand van de metingen MASW
workbook_M = xlrd.open_workbook(file_loc_M)
#Openen van bestand van de metingen MASW
sheets_M   = workbook_M.sheet_by_index(0)
#Openen tabblad 0

file_loc_K = 'C:\Geo Engineering\Master Thesis\Kiltunnel
\Measurements_middle_element.xlsx'
#Locatie bestand metingen settlement
workbook_K = xlrd.open_workbook(file_loc_K)
#Openen van bestand
sheets_K = workbook_K.sheet_by_index(0)
#Openen tablad 0
```

```
x_MASW = np.zeros(sheets_M.ncols-1)
#Measurement locations
for i in range (sheets_M.ncols-1):
    x_MASW[i] = sheets_M.cell_value(2,i+1)

Vs = np.zeros([sheets_M.nrows-7,sheets_M.ncols-1])
#Shear wave velocity in depth for each location
for i in range(sheets_M.nrows-7):
    for j in range(sheets_M.ncols-1):
        Vs[i,j] = sheets_M.cell_value(i+3,j+1)

z_MASW = np.array([0.00, 0.80, 1.60, 2.60, 3.70, 4.80, 6.00,
              7.40, 8.80, 10.30, 11.90, 13.60, 15.50, 20.50]
#Measurement location transition point
z_avg_MASW = np.zeros(len(z_MASW)-1)                                    #Average of
dz_MASW = np.zeros(len(z_MASW)-1)
for i in range (len(z_avg_MASW)):
    z_avg_MASW[i] = (z_MASW[i] + z_MASW[i+1]) / 2.0
    dz_MASW[i] = z_MASW[i+1] - z_MASW[i]

z_avg_NAP_MASW = np.zeros([sheets_M.nrows-7,sheets_M.ncols-1])
#2D array with z locations in NAP for every measurement
z_NAP = np.zeros([sheets_M.nrows-6,sheets_M.ncols-1])
#2D array with z locations in NAP for the transition points
xx_MASW = np.zeros([sheets_M.nrows-7,sheets_M.ncols-1])
#2D array with x locations for every measurement

for i in range(sheets_M.nrows-7):
    xx_MASW[i,:] = x_MASW
for i in range(sheets_M.ncols-1):
    if x_MASW[i] <= 110.0:
        z_avg_NAP_MASW[:,i] = z_avg_MASW + 14.12 + (19.19 - 14.12) / 110.0 * x_MASW[i]
        z_NAP[:,i] = z_MASW + 14.12 + (19.19 - 14.12) / 110.0 * x_MASW[i]
    if 110.0 < x_MASW[i] <= 220.0:
        z_avg_NAP_MASW[:,i] = z_avg_MASW + 19.19
        z_NAP[:,i] = z_MASW + 19.19
    if x_MASW[i] > 220.0:
        z_avg_NAP_MASW[:,i] = z_avg_MASW + 19.12 - (19.19 - 14.12) / 110.0 * (x_MASW[i] -
        z_NAP[:,i] = z_MASW + 19.12 - (19.19 - 14.12) / 110.0 * (x_MASW[i] - 220.0)

def find_nearest(array,value):
#function that finds and returns the nearest index of 'value' in 'array'
```

```
    idx = np.searchsorted(array, value, side="left")
    if idx > 0 and (idx == len(array) or math.fabs(value - array[idx-1])
    < math.fabs(value - array[idx])):
        return idx-1
    else:
        return idx

n_l = [5,4,5]
n = 0 #Number of the CPT used for simulation

z_layer = np.zeros(n_l[n]+1)
mean, sig, sig_res = np.zeros(n_l[n]), np.zeros(n_l[n]), np.zeros(n_l[n])
a_trend, b_trend = np.zeros(n_l[n]), np.zeros(n_l[n])
SOFv_M, SSE_M = np.zeros(n_l[n]), np.zeros(n_l[n])
SOFv_G, SSE_G = np.zeros(n_l[n]), np.zeros(n_l[n])

for i in range(n_l[n]+1):
    z_layer[i] = sheets_S.cell_value(i*10+1,n+1)

for i in range(n_l[n]):
    mean[i]    = sheets_S.cell_value(i*10+2,n+1)
    sig[i]     = sheets_S.cell_value(i*10+3,n+1)
    sig_res[i] = sheets_S.cell_value(i*10+4,n+1)
    a_trend[i] = sheets_S.cell_value(i*10+5,n+1)
    b_trend[i] = sheets_S.cell_value(i*10+6,n+1)
    SOFv_M[i]  = sheets_S.cell_value(i*10+7,n+1)
    SSE_M[i]   = sheets_S.cell_value(i*10+8,n+1)
    SOFv_G[i]  = sheets_S.cell_value(i*10+9,n+1)
    SSE_G[i]   = sheets_S.cell_value(i*10+10,n+1)

inter = 0.05                #Interval of z-values in simulated CPT's
n_z = np.zeros(n_l[n])
d_z,rho = dict(),dict()
L = dict()

for i in range(n_l[n]):
    n_z[i] = round((z_layer[i+1] - z_layer[i]) / inter ,0)
    #Number of qc points simulated for this layer
    d_z[i] = np.linspace(z_layer[i],z_layer[i+1]-inter,int(n_z[i])) - z_layer[i]
    #Distance from first data point of layer
    rho[i] = np.zeros([int(n_z[i]),int(n_z[i])])
    #Correlation matrix
```

```
    if SSE_M[1] > 0: #SSE_M[1] <= SSE_G[1]:
        for j in range(int(n_z[i])):
            for k in range(int(n_z[i])-j):
                rho[i][j+k,k] = round(np.exp(- 2 *(d_z[i][j]/SOFv_M[i])),4)
                rho[i][k,j+k] = round(np.exp(- 2 *(d_z[i][j]/SOFv_M[i])),4)

    L[i] = np.linalg.cholesky(rho[i])
    #Lower triangular matrix

sig_res_ln = dict()
mu_normal, mu_lognormal = dict(),dict()

for i in range(n_l[n]):
    mu_normal[i] = a_trend[i] * (d_z[i] + z_layer[i]) + b_trend[i]
    #Mean trend normal distribution
    mu_lognormal[i] = np.zeros(len(d_z[i]))
    #Mean trend lognormal distribution

    sig_res_ln[i] = np.zeros(len(d_z[i]))
    #Standard deviation lognormal distribution
    for j in range(len(d_z[i])):
        sig_res_ln[i][j] = (np.log(1+(sig_res[i]/mu_normal[i][j])**2))**0.5
        mu_lognormal[i][j] = np.log(mu_normal[i][j]) - 0.5 * sig_res_ln[i][j] ** 2

def Par_sim(D):
#Function that simulates the parameters for this single simulation
    sig_a = 0.021
    #Standard deviation of a-factor in rho-Vs correlation
    sig_b = 0.0087
    #Standard deviation of b-factor in rho-Vs correlation
    Rho_w = np.zeros(13)
    #Wet unit weight taking distribution of unit weight into account [kN/m^3]
    G0 = np.zeros(13)
    #Small strain shear stiffness taking distribution of unit weight into account [kPa]
    E0 = np.zeros(13)
    #Small strain stiffness taking distribution of unit weight into account [kPa]

    #Simulation of CPT profile
    U,G = dict(), dict()
    qc_sim_l = dict()
    m = np.zeros(n_l[n])
```

```
for j in range(n_l[n]):
    U[j] = rnd.standard_normal(int(n_z[j]))
    #Array with n_z values with normalised random numbers
    G[j] = np.dot(L[j],U[j])
    #Correlated matrix of normalised random processes

    qc_sim_l[j] = np.zeros(int(n_z[j]))
    #qc values simulated based on statistics and correlations
    for k in range(int(n_z[j])):
        qc_sim_l[j][k] = np.exp(mu_lognormal[j][k] +
        sig_res_ln[j][k] * G[j][k])

#Put CPT profile in one array
qc_sim = np.zeros(int(sum(n_z)))
d_z_all = np.zeros(int(sum(n_z)))
count1  = 0
count2 = 0

for j in range(n_l[n]):
    count2 += n_z[j]
    qc_sim[int(count1):int(count2)] = qc_sim_l[j]
    d_z_all[int(count1):int(count2)] = d_z[j] + z_layer[j]
    count1 += n_z[j]

find1 = find_nearest(d_z_all,start_MASW)
find2 = find_nearest(d_z_all,start_MASW+D)
qc_avg = np.mean(qc_sim[find1:find2])

#Simulation small shear strain profile
for l in range(13):
    random_a  = rnd.standard_normal(1)
    random_b  = rnd.standard_normal(1)
    random_Vs = rnd.standard_normal(1)
    Rho_w[l]  = (4.12 + random_a * sig_a) *
    ((1+0.07 * random_Vs) * Vs[l,loc]) ** (0.262 + random_b * sig_b)
    G0[l] = ((1+0.07 * random_Vs)*(Vs[l,loc])) ** 2.0 * Rho_w[l] / 10
    E0[l] = round(2.2 * G0[l] ,2)

E0_w = E0 * dz_MASW
find3 = max(np.where(D > z_MASW)[0])
if D < z_MASW[11]:
```

```
        E0_sum = np.sum(E0_w[0:find3]) + (D - z_MASW[find3]) * E0[find3+1]
    if D > z_MASW[11]:
        E0_sum = np.sum(E0_w[0:find3]) - (z_MASW[find3] - D) * E0[find3]
    E0_avg = E0_sum / D

    return qc_sim,d_z_all,qc_avg,E0_avg

def Set_sim(N,Qapp,alpha,E0,qc_avg):
#Function that uses the Mayne model to calculate initial settlement.
    Ihrv = 0.85                    #Shape factor [-]
    beta = alpha / (1 - (10*alpha * qc_avg * Ihrv * Lf) / ((E0) * Bf)) ** (1/0.3)
    Qult = beta * (qc_avg * Bf * Lf)
    s = (Qapp * Ihrv) / (Bf * E0 * (1 - (Qapp/Qult)**0.3  ))

    return s

s_measured = np.zeros([6,sheets_K.nrows-1]) #Measurement kiltunnel
for i in range (6):
    for j in range(sheets_K.nrows-1):
        s_measured[i,j] = sheets_K.cell_value(j+1,i+1)

t_measured = np.zeros(sheets_K.nrows-1)
for j in range(sheets_K.nrows-1):
    t_measured[j] = sheets_K.cell_value(j+1,0)

m = 29  #name of measurement location
loc = int(len(z_NAP[0,:])/15*(5 + (m - 19)/2))
#location of CPT in MASW profile
end_MASW = z_NAP[len(z_NAP[:,loc])-1,loc]
start_MASW = z_NAP[0,loc]

t = np.logspace(np.log(0.25),np.log(365*41),25,base=2.718281)
def creep(Qapp,qc_avg):
    Sc = np.zeros(len(t))
    a = alpha + 0.005 * rnd.standard_normal(1)
    Qult = a * qc_avg * Bf * Lf * 1000
    m = 0.02 * (Qapp/Qult)**2
    for i in range(len(t)):
        Sc[i] = m * (Bf*1000) * np.log(t[i]/50)

    return Sc
```

```
def Cyclic(s,s_T,t):
    s_Tc = np.zeros(len(t))
    for i in range(len(t)):
        s_Tc[i] = (s_T - s) * A ** (np.log10(t[i]*2))
    return s_Tc

N = 10000
D = 13.30  #Zone of influence (m)

E0 = np.zeros(N)
qc_avg = np.zeros(N)
s = np.zeros(N)                  #Intial settlement
s_c = np.zeros([N,len(t)])       #Creep settlement
s_T = np.zeros(N)                #Initial settlement tidal loading

s_Temp_i = np.zeros(N)           #Initial temperature loading
s_Temp_c = np.zeros([N,len(t)]) #Temperature cyclic settlement
s_T_cycl = np.zeros([N,len(t)]) #Tidal loading settlement
s_T_cr = np.zeros([N,len(t)])    #Tidal loading + creep settlement
s_all = np.zeros([N,len(t)])     #Tidal loading + creep + temperature settlement

Bf = 22.3
Lf = 31.0
alpha = 0.2

for i in range(N):
    qc_sim,d_z_all,qc_avg[i],E0[i] = Par_sim(D)
    #Parameters
    s[i] = Set_sim(N=1,Qapp=24800,alpha=0.20,E0=E0[i],qc_avg=qc_avg[i]*1000)
    * 1000
    #Initial settlement
    s_c[i,:] = creep(Qapp=24800,qc_avg=qc_avg[i])
    #Creep settlement

    Qapp_T = 24800 + 0.9 * (8 + 0.67 * rnd.standard_normal(1)) * Bf * Lf
    #Applied loading tides
    A = 1.6 + 0.1 * rnd.standard_normal(1)
    #A-value cyclic loading model

    s_T[i] = Set_sim(N=1,Qapp=Qapp_T,alpha=0.20,E0=E0[i],qc_avg=qc_avg[i]*1000)
    * 1000
    #Initial settlement tidal loading
```

```
    s_T_cycl[i,:] = Cyclic(s[i],s_T[i],t=t)
    #Tide settlement

    s_Temp_i[i] = Set_sim(N=1,Qapp=24800 + 268 * 4.29,alpha=0.20,E0=E0[i],
    qc_avg=qc_avg[i]*1000) * 1000
    s_Temp_c[i] = Cyclic(s[i],s_Temp_i[i],t=t/365)
    #Cyclic settlement temperature effects

    s_T_cr[i,:] = s_T_cycl[i,:] + s_c[i,:]
    #Tides + Creep
    s_all[i,:] = s_T_cycl[i,:] + s_c[i,:] + s_Temp_c[i]
    #Tides + Creep + Temp settlement


#Sort all calculations

s_c_sorted = np.zeros([N,len(t)])       #Creep sorted
s_T_cycl_sorted = np.zeros([N,len(t)]) #Tides sorted
s_Temp_c_sorted = np.zeros([N,len(t)]) #Temperature sorted
s_T_cr_sorted = np.zeros([N,len(t)])    #Tides + creep sorted
s_all_sorted = np.zeros([N,len(t)])     #Tides + creep + Temperature sorted

for i in range(len(t)):
    s_c_sorted[:,i] = np.sort(s_c[:,i])
    s_T_cycl_sorted[:,i] = np.sort(s_T_cycl[:,i])
    s_Temp_c_sorted[:,i] = np.sort(s_Temp_c[:,i])
    s_T_cr_sorted[:,i] = np.sort(s_T_cr[:,i])
    s_all_sorted[:,i] = np.sort(s_all[:,i])

fig, ax = plt.subplots(figsize=(9,4))
ax.ticklabel_format(useOffset=False)

ax.plot(t/365+1977.75,s_all_sorted[int(N*0.05)-1,:],'k',linestyle='--')
ax.plot(t/365+1977.75,s_all_sorted[int(N*0.50)-1,:],'r')
ax.plot(t/365+1977.75,s_all_sorted[int(N*0.95)-1,:],'k',linestyle='--')

plt.plot(t_measured,-s_measured[5,:],'ko')

#plt.gca().set_ylim(bottom=0)
ax.set_ylim(0,35)
ax.set_xlim(1977,2018)
plt.xlabel('Year')
```

```
plt.ylabel('Settlement (mm)')
plt.legend(['5 percent','Mean','95 percent','Measurements'],loc=3)
plt.gca().invert_yaxis()
plt.grid(b=None, which='major', axis='both')
plt.show()
print('All')
print(t[24]/365+1977)
print(s_all_sorted[int(N*0.05)-1,24])
print(s_all_sorted[int(N*0.50)-1,24])
print(s_all_sorted[int(N*0.95)-1,24])
```

E.3 Zone of influence

This example is for the values of the Heinenoord tunnel

```
import matplotlib.pyplot as plt
plt.style.use('classic')
import numpy as np
%matplotlib inline


x = np.linspace(-50,50,101)
#x-coordinates of the points that are calculated
z = np.linspace(0.5,40,80)
#z-coordinates of the points that are calculated

Q_total = 19500 #kN
B = 30.7 #m
L = 24.0 #m
q0 = Q_total/B/L #kPa

inter = 0.5
#Dimensions of area's in which the segment
#is divided to simulate the distributed load in meter
N_x = int(B/inter + 1)  #Number of area's in x direction
N_y = int(100/inter+1)  #Number of area's in y direction
Q = q0 * inter**2       #Total load of each area

d_Q = np.zeros([len(z),len(x)])
#Increase of stress due to all point loads
```

```
x_Q = np.linspace(-B/2,B/2,N_x)
#x-coordinates of the middle of the area's
y_Q = np.linspace(-50,50,N_y)
#y-coordinates of the middle of the area's


def Boussinesq(x,z):
    qv = 0
    for i in range(len(x_Q)):
        for j in range(len(y_Q)):
            r = ((x-x_Q[i])**2 + (0-y_Q[j])**2)**0.5
            #Horizontal distance from point load to point in subsurface
            Ab = 3/(1+(r/z)**2)**2.5 / (2*np.pi)
            qv += Q / z**2 * Ab
            #Increase in stress of point in subsurface
    return qv

for i in range(len(z)):
    for j in range(len(x)):
        d_Q[i,j] = Boussinesq(x[j],z[i])

fig, ax = plt.subplots(figsize=(12,8))
plt.ylim(0,40)
CS = ax.contour(x, z, d_Q, 10, colors='k')
ax.clabel(CS, inline=1, fontsize=10)
ax.set_xlabel('Distance from centre of the tunnel (m)')
ax.set_ylabel('Depth below bottom of the tunnel (m)')
plt.gca().invert_yaxis()

sig_v_in_situ = 8 * z
B_lin = np.linspace(-15,15,31)
a = np.zeros(len(B_lin))
Zi = np.zeros(len(B_lin))

for i in range(len(B_lin)):
    a[i] = max(np.where(0.25 * sig_v_in_situ < d_Q[:,35+i])[0])
    b = 0.25 * sig_v_in_situ[int(a[i])] - d_Q[int(a[i]),35+i]
    c = 0.25 * sig_v_in_situ[int(a[i])+1] - d_Q[int(a[i])+1,35+i]

    Zi[i] = (a[i]+1) * 0.5 + 0.5 * (-b/(c-b))

plt.figure(figsize=(6,8))
```

```
plt.plot(0.25*sig_v_in_situ,z)
plt.plot(d_Q[:,51],z)
plt.plot(0.25 * 8 * Zi[16],Zi[16],'k_',ms=12)
plt.ylim(0,20)
plt.xlim(0,60)
plt.gca().invert_yaxis()
plt.xlabel('Stress (MPa)')
plt.ylabel('Depth from bottom of the tunnel (m)')
plt.legend(['Increase in stress due to static loading tunnel',
'0.25 * effective in-situ stress','Zone of influence at this location'],loc=4)

plt.figure(figsize=(10,4))
plt.plot(B_lin,Zi)
plt.plot([-0.5*B,0.5*B],[np.mean(Zi),np.mean(Zi)],'r')
plt.ylim(0,16)
plt.gca().invert_yaxis()
plt.legend(['Zone of influence at that location','Mean zone of influence'])
plt.ylabel('Zone of influence (m)')
plt.xlabel('Distance from centre of the tunnel (m)')
print(np.mean(Zi))
```

E.4 Correlations

```
import xlrd
import xlwt
import matplotlib.pyplot as plt
plt.style.use('classic')
import numpy as np
%matplotlib inline

data = np.loadtxt('CPT_data.txt')
data_len = np.loadtxt('CPT_data_len.txt')
data_x_y_z0 = np.loadtxt('Loc_x,y,z0.txt')

x_CPT = data_x_y_z0[:,1]
y_CPT = data_x_y_z0[:,2]
z0_CPT = data_x_y_z0[:,3]

z_all = data[:,0]
qc_all = data[:,1]
```

```
Fr_all = data[:,2]

z_CPT, qc_CPT, Fr_CPT = dict(), dict(), dict()

for i in range(len(data_len)-1):
    z_CPT[i]  =  z_all[int(sum(data_len[0:i+1])):int(sum(data_len[0:i+2]))]
    z_CPT[i]  =  z_CPT[i] - z0_CPT[i] + z_CPT[i][0]
    #Express z_CPT in m below NAP
    qc_CPT[i] = qc_all[int(sum(data_len[0:i+1])):int(sum(data_len[0:i+2]))]
    Fr_CPT[i] = Fr_all[int(sum(data_len[0:i+1])):int(sum(data_len[0:i+2]))]

file_loc = 'C:\Geo Engineering\Master Thesis\Heinenoord\MASW_Heinenoord.xlsx'
#locatie van bestand van de metingen
workbook = xlrd.open_workbook(file_loc)
#Openen van bestand van de metingen
sheets   = workbook.sheet_by_index(1)
#Openen tabblad 1

x_MASW = np.zeros(sheets.ncols-1)
#Measurement locations
for i in range (sheets.ncols-1):
    x_MASW[i] = sheets.cell_value(0,i+1)

Vs_MASW = np.zeros([sheets.nrows-1,sheets.ncols-1])
#Shear wave velocity in depth for each location
for i in range(sheets.nrows-1):
    for j in range(sheets.ncols-1):
        Vs_MASW[i,j] = sheets.cell_value(i+1,j+1)

z_MASW = np.array([0.00, 0.80, 1.60, 2.60, 3.70, 4.80, 6.00,
              7.40, 8.80, 10.30, 11.90, 13.60, 15.50, 20.50]
#Measurement location transition point
z_avg_MASW = np.zeros(len(z_MASW)-1)
#Average of measurement location
for i in range (len(z_avg_MASW)):
    z_avg_MASW[i] = (z_MASW[i] + z_MASW[i+1]) / 2.0

z_avg_NAP_MASW = np.zeros([sheets.nrows-1,sheets.ncols-1])
#2D array with z locations in NAP for every measurement
z_NAP_MASW = np.zeros([sheets.nrows,sheets.ncols-1])
#2D array with z locations in NAP for the transition points
xx_MASW = np.zeros([sheets.nrows-1,sheets.ncols-1])
```

```
#2D array with x locations for every measurement

for i in range(sheets.nrows-1):
    xx_MASW[i,:] = x_MASW
for i in range(sheets.ncols-1):
    if x_MASW[i] <= 245.0:
        z_avg_NAP_MASW[:,i] = z_avg_MASW + 8.69 +
        (19.12 - 8.69) / 245.0 * x_MASW[i] + 2.00
        z_NAP_MASW[:,i] = z_MASW + 8.69 +
        (19.12 - 8.69) / 245.0 * x_MASW[i] + 2.00
    if 245.0 < x_MASW[i] <= 300.0:
        z_avg_NAP_MASW[:,i] = z_avg_MASW + 19.12 +
        (19.75 - 19.12) / 55.0 * (x_MASW[i] - 245.0) + 2.00
        z_NAP_MASW[:,i] = z_MASW + 19.12 +
        (19.75 - 19.12) / 55.0 * (x_MASW[i] - 245.0) + 2.00
    if 300.0 < x_MASW[i] <= 355.0:
        z_avg_NAP_MASW[:,i] = z_avg_MASW + 19.75 -
        (19.75 - 19.12) / 55.0 * (x_MASW[i] - 300.0) + 2.00
        z_NAP_MASW[:,i] = z_MASW + 19.75 -
        (19.75 - 19.12) / 55.0 * (x_MASW[i] - 300.0) + 2.00
    if x_MASW[i] > 355.0:
        z_avg_NAP_MASW[:,i] = z_avg_MASW + 19.12 -
        (19.12 - 8.69) / 245.0 * (x_MASW[i] - 355.0) + 2.00
        z_NAP_MASW[:,i] = z_MASW + 19.12 -
        (19.12 - 8.69) / 245.0 * (x_MASW[i] - 355.0) + 2.00

Rho_MASW = np.zeros([sheets.nrows-1,sheets.ncols-1])
#Wet density in depth for each location based on correlation with V
Rho_eff_MASW = np.zeros([sheets.nrows-1,sheets.ncols-1])
#Effective density in depth for each location based on correlation with V
G = np.zeros([sheets.nrows-1,sheets.ncols-1])
#Approximation of the G-modulus based on V and Rho

for i in range(sheets.nrows-1):
    for j in range(sheets.ncols-1):
        Rho_MASW[i,j] = 4.12 * Vs_MASW[i,j] ** 0.262
        Rho_eff_MASW[i,j] = Rho_MASW[i,j] - 10.0
        G[i,j] = Vs_MASW[i,j] ** 2.0 * Rho_MASW[i,j] / 10000
        #Check if it has to be dry or wet

# Correction Vs for vertical stress
Pa = 100.0 #kPa
```

```
delta_z_MASW = z_MASW[1:len(z_MASW)] - z_MASW[0:len(z_MASW)-1]
sig_v_MASW = np.ones([sheets.nrows-1,sheets.ncols-1]) * 26.0
Vs1_MASW = np.zeros([sheets.nrows-1,sheets.ncols-1])

for i in range(sheets.nrows-1):
    for j in range(sheets.ncols-1):
        if i == sheets.nrows-1:
            sig_v_MASW[i,j] += 0.5 * Rho_eff_MASW[i,j] * delta_z_MASW[i]
            #Vertical stress
            Vs1_MASW[i,j] = Vs_MASW[i,j] * (Pa / sig_v_MASW[i,j]) ** 0.25
            #Correction for vertical stress Vs into Vs1
        else:
            sig_v_MASW[i,j] += 0.5 * Rho_eff_MASW[i,j] * delta_z_MASW[i]
            sig_v_MASW[i+1:sheets.nrows-1,j] +=
            Rho_eff_MASW[i,j] * delta_z_MASW[i]
            Vs1_MASW[i,j] = Vs_MASW[i,j] * (Pa / sig_v_MASW[i,j]) ** 0.25

# Correction qc for vertical stress
Pa = 100.0 #kPa
Ic, qc1_CPT, sig_v_CPT = dict(), dict(), dict()

for i in range(len(z_CPT)):
    Ic[i] = np.zeros(len(z_CPT[i]))
    qc1_CPT[i] = np.zeros(len(z_CPT[i]))
    sig_v_CPT[i] = np.zeros(len(z_CPT[i]))

    for j in range(len(z_CPT[i])):
        sig_v_CPT[i][j] = (z_CPT[i][j] - z_CPT[i][0]) * 8 + 5 #kPa
        qc1_CPT[i][j] = (qc_CPT[i][j] * 1000 / 100) * (Pa / sig_v_CPT[i][j])**0.5

        if qc1_CPT[i][j] <= 0.0:
            qc1_CPT[i][j] = 0.2
            if Fr_CPT[i][j] < 0.0:
                Ic[i][j] = 3.0
            if 0.0 < Fr_CPT[i][j] < 20.0:
                Ic[i][j] =
                ( (3.47 - np.log10(qc1_CPT[i][j]))**2 + (np.log10(Fr_CPT[i][j]) + 1.22)**2
        if 0.0 < Fr_CPT[i][j] < 20.0:
            Ic[i][j] =
            ( (3.47 - np.log10(qc1_CPT[i][j]))**2 + (np.log10(Fr_CPT[i][j]) + 1.22)**2 )**
        if Fr_CPT[i][j] <= 0.0:
            Ic[i][j] = 3.0
```

```
l_int = 0.02

def avg_qc_cat_Fr(z_SWV,Vs,G,z_CPT,qc_CPT,Fr_CPT,sig_v_CPT,opt=True):
#Function that determines average qc and category of soil at a MASW measurement

    if z_SWV[len(z_SWV)-1] > z_CPT[len(z_CPT)-1]:
        n = np.amin(np.where(z_SWV > z_CPT[len(z_CPT)-1]))
        #Find location where edge of MASW measurement is below the CPT
    else:
        n = len(z_SWV)

    if n == 0:
        SWV_CPT,G_CPT,qc_avg,cat = float('nan'),float('nan'),float('nan'), [-1.0]
        return SWV_CPT,G_CPT,qc_avg,cat

    a = np.zeros(n)
    SWV_CPT = Vs[0:n-1]
    #All MASW measurements that are in range of the CPT
    G_CPT = G[0:n-1]
    #All MASW measurements that are in range of the CPT
    qc_avg = np.zeros(n-1)
    sig_v_avg = np.zeros(n-1)

    for i in range(n):
        a[i] = max(np.where(z_CPT<z_SWV[i])[0])
        #Find locations where the edges of the MASW measurements are in the CPT

    for i in range(n-1):
        qc_avg[i] = round(np.mean(qc_CPT[int(a[i]):int(a[i+1]+1)]),2)

        sig_v_avg[i] = ( sig_v_CPT[int(a[i])+2] + sig_v_CPT[int(a[i+1])+1] ) / 2

    Ic_avg = np.zeros(n-1)
    Fr_avg = np.zeros(n-1)

    for i in range(n-1):
        Fr_avg[i] = np.mean(Fr_CPT[int(a[i]):int(a[i+1])])

        if Fr_avg[i] < 0.0:
            Ic_avg[i] = -1.0
            continue
```

```
            if Fr_avg[i] > 50.0:
                Ic_avg[i] = -1.0
                continue

            Ic_avg[i] = ( (3.47 - np.log10(qc_avg[i]))**2 +
            (np.log10(Fr_avg[i]) + 1.22)**2 )**0.5

            if opt == True:
                length = len(Fr_CPT[int(a[i]):int(a[i+1])])
                Ic_all = np.zeros(length)
                for j in range(length):
                    Ic_all[j] = ( (3.47 - np.log10(qc_CPT[int(a[i])+j]))**2
                    + (np.log10(Fr_CPT[int(a[i])+j]) + 1.22)**2 )**0.5
                Ic_all_sort = np.sort(Ic_all)
                if Ic_all_sort[int(0.95*length)] > 2.05:
                    if Ic_all_sort[int(0.05*length)] > 2.05:
                        if Ic_all_sort[int(0.95*length)] < 2.65:
                            continue
                    if Ic_all_sort[int(0.05*length)] > 2.65:
                        if Ic_all_sort[int(0.95*length)] < 2.95:
                            continue
                    if Ic_all_sort[int(0.05*length)] > 2.95:
                        if Ic_all_sort[int(0.95*length)] < 3.60:
                            continue

                    Ic_avg[i] = -1.0


        return SWV_CPT,G_CPT,qc_avg,Ic_avg#,sig_v_avg

    offset_x = min(x_CPT)
    offset_y = min(y_CPT)

    x_CPT_rel = x_CPT - offset_x
    y_CPT_rel = y_CPT - offset_y

    x_MASW_rel = np.linspace(94638.0,94872.0,241) - offset_x
    y_MASW_rel = np.linspace(427185.0,427737.0,241) - offset_y

    plt.plot(x_CPT_rel,y_CPT_rel,'d')
    plt.plot(x_MASW_rel,y_MASW_rel,'r')
    plt.xlim(0,600)
```

```
plt.ylim(0,600)
plt.legend(['CPT locations','MASW measurements (every 2.5 m)'])

index_MASW_CPT = np.zeros(len(data_len)-1)
dist = np.zeros([len(data_len)-1,len(x_MASW)])
min_dist = np.zeros(len(data_len)-1)

for i in range(len(data_len)-1):
    for j in range(len(x_MASW)):
        dist[i,j] = ( (x_CPT_rel[i] - x_MASW_rel[j]) ** 2 +
        (y_CPT_rel[i] - y_MASW_rel[j]) ** 2 ) ** 0.5

    index_MASW_CPT[i] = np.where(dist[i,:] == min(dist[i,:]))[0]
    min_dist[i] = min(dist[i,:])

Vs_CPT, Vs1_CPT,G0_CPT,qc_avg,qc1_avg,Ic_avg,sig_v_avg,Ic_all_sort
= dict(),dict(), dict(), dict(), dict(), dict(), dict(), dict()

for i in range(len(data_len)-1):
    if i == 7:
        continue
    Vs_CPT[i],G0_CPT[i],qc_avg[i],Ic_avg[i] =
    avg_qc_cat_Fr(z_NAP_MASW[:,int(index_MASW_CPT[i])],
    Vs_MASW[:,int(index_MASW_CPT[i])],
    G[:,int(index_MASW_CPT[i])],
    z_CPT[i],qc_CPT[i],Fr_CPT[i],sig_v_CPT[i],opt=True)
for i in range(len(data_len)-1):
    if i == 7:
        continue
    Vs1_CPT[i],G0_CPT[i],qc1_avg[i],Ic_avg[i] =
    avg_qc_cat_Fr(z_NAP_MASW[:,int(index_MASW_CPT[i])],
    Vs1_MASW[:,int(index_MASW_CPT[i])], G
    G[:,int(index_MASW_CPT[i])],z_CPT[i],qc1_CPT[i],
    Fr_CPT[i],sig_v_CPT[i],opt=True)
#Calling the function for each CPT, comparing it to the nearest MASW measurement

plt.figure(figsize=(10,6))
plt.xlim(0,300)
plt.ylim(0,350)
plt.xlabel('qc1 [kpa]') #Vs / qc [m^3/MN*s]
plt.ylabel('Vs1/qc [m^3/MN*s]') #'qc [Mpa]
```

```
for i in range(len(data_len)-1):
    #if min_dist[i] > 15.0:
    #    continue

    if i == 62:
        continue
    if i == 7:
        continue
    if Ic_avg[i][0] == -1.0:
        continue
    if i == 64:
        continue

    for j in range(len(Ic_avg[i])):
        if Ic_avg[i][j] == -1.0:
            continue
        if Ic_avg[i][j] < 2.05:
            plt.plot((qc1_avg[i][j]),(Vs1_CPT[i][j]),'o',c='xkcd:yellow',ms=5)
        if 2.05 < Ic_avg[i][j] < 2.6:
            plt.plot((qc1_avg[i][j]),(Vs1_CPT[i][j]),'o',c='xkcd:orange',ms=5)
```

E.5 Vertical scale of fluctuation Heinenoord

This section calculates the vertical scale of fluctuation of the 13 selected CPT's at Heinenoord.

```
import xlrd
import matplotlib.pyplot as plt
plt.style.use('classic')
import numpy as np
import math
%matplotlib inline

data = np.loadtxt('CPT_data.txt')
data_len = np.loadtxt('CPT_data_len.txt')
data_x_y_z0 = np.loadtxt('Loc_x,y,z0.txt')

x_CPT = data_x_y_z0[:,1]
y_CPT = data_x_y_z0[:,2]
z0_CPT = data_x_y_z0[:,3]
```

```
z_all = data[:,0]
qc_all = data[:,1]
Fr_all = data[:,2]

z_CPT, qc_CPT, Fr_CPT = dict(), dict(), dict()

for i in range(len(data_len)-1):
    z_CPT[i]  =  z_all[int(sum(data_len[0:i+1])):int(sum(data_len[0:i+2]))]
    z_CPT[i]  =  z_CPT[i] - z0_CPT[i] + z_CPT[i][0
    #Express z_CPT in m below NAP
    qc_CPT[i] = qc_all[int(sum(data_len[0:i+1])):int(sum(data_len[0:i+2]))]
    Fr_CPT[i] = Fr_all[int(sum(data_len[0:i+1])):int(sum(data_len[0:i+2]))]

index = [35,36,37,38,39,40,41,43,44,45,46,47,53]

z_CPT_l, qc_CPT_l, Fr_CPT_l = dict(), dict(), dict()
x_CPT_l1 = np.zeros(len(index))
x_CPT_l = np.zeros(len(index))
for i in range(len(index)):
    x_CPT_l1[i] = x_CPT[index[i]] - 94638.0

rank = [1,6,12,2,3,4,5,10,11,7,0,8,9]

for i in range(len(index)):
    z_CPT_l[i] = z_CPT[index[rank[i]]]
    qc_CPT_l[i] = qc_CPT[index[rank[i]]]
    Fr_CPT_l[i] = Fr_CPT[index[rank[i]]]
    x_CPT_l[i] = x_CPT_l1[rank[i]]

# Boundaries of the layers of each CPT

l_bound = dict()

l_bound[0] = [4.0,8.4,14.0,24.6,26.4,41.0]
l_bound[1] = [0.0,5.8,14.0,21.8,23.2,40.4]
l_bound[2] = [2.0,4.0,6.2,21.0,23.4,39.0]
l_bound[3] = [6.0,8.4,22.1,23.0,38.0]
l_bound[4] = [12.0,14.0,22.0,25.8,45.4]
l_bound[5] = [12.0,14.0,21.8,25.0,43.8]
l_bound[6] = [11.0,12.4,17.6,21.75,26.6,31.4,45.6]
l_bound[7] = [12.0,15.0,26.0,28.6,31.0,42.0,46.0]
```

```
l_bound[8] = [8.0,26.2,28.2,29.6,37.0,38.8]
l_bound[9] = [10.0,26.0,32.2,34.0,42.0]
l_bound[10] = [1.0,8.0,26.0,28.0,40.0]
l_bound[11] = [1.0,8.0,27.0,29.0,37.8]
l_bound[12] = [2.0,8.0,21.4,22.8,26.8,29.4,41.8]

N_l = np.zeros(len(l_bound))
N_sum = np.zeros(len(l_bound)+1)
for i in range(len(z_CPT_l)):
    N_l[i] = len(l_bound[i]) - 1
    N_sum[i+1:len(N_sum)] += len(l_bound[i]) - 1
l_int = 0.02

N, a, b                          = dict(), dict(), dict()
for i in range(len(z_CPT_l)):
    N[i], a[i], b[i]
    = [0 for j in range(int(N_l[i]))], [0 for j in range(int(N_l[i]))], [0 for j in range(
z_int, qc_int, qc_mt, qc_mt_ms   = dict(), dict(), dict(), dict()
std_z, z_std                     = dict(), dict()
m, n
= np.zeros(int(N_sum[len(N_sum)-1])), np.zeros(int(N_sum[len(N_sum)-1]))
std, std_res
= np.zeros(int(N_sum[len(N_sum)-1])), np.zeros(int(N_sum[len(N_sum)-1]))

def find_nearest(array,value):
#function that finds and returns the nearest index of 'value' in 'array'
    idx = np.searchsorted(array, value, side="left")
    if idx > 0 and (idx == len(array) or math.fabs(value - array[idx-1])
    < math.fabs(value - array[idx])):
        return idx-1
    else:
        return idx

for i in range(len(N_l)):
    for j in range(int(N_l[i])):
        a[i][j] = find_nearest(z_CPT_l[i], l_bound[i][j])
        b[i][j] = find_nearest(z_CPT_l[i], l_bound[i][j+1])
        qc_int[int(N_sum[i])+j] = qc_CPT_l[i][int(a[i][j]):int(b[i][j]+1)]
        z_int[int(N_sum[i])+j]  =  z_CPT_l[i][int(a[i][j]):int(b[i][j]+1)]
        std[int(N_sum[i])+j] = np.std(qc_int[int(N_sum[i])+j])

        A = np.vstack([z_int[int(N_sum[i])+j]
```

```
        , np.ones(len(z_int[int(N_sum[i])+j]))]).T
        m[int(N_sum[i])+j], n[int(N_sum[i])+j]
        = np.linalg.lstsq(A,qc_int[int(N_sum[i])+j],rcond=None)[0]
        #Linear depth trend of the data

        qc_mt[int(N_sum[i])+j] = qc_int[int(N_sum[i])+j]
        - n[int(N_sum[i])+j] - z_int[int(N_sum[i])+j] * m[int(N_sum[i])+j]
        #qc minus the depth trend
        std_res[int(N_sum[i])+j] = np.std(qc_mt[int(N_sum[i])+j])

        qc_mt_ms[int(N_sum[i])+j] = qc_mt[int(N_sum[i])+j] / std_res[int(N_sum[i])+

cor = dict()

for i in range(len(N_l)):
    for j in range(int(N_l[i])):
        cor[int(N_sum[i])+j] = np.zeros([len(z_int[int(N_sum[i])+j])])

        for k in range(len(z_int[int(N_sum[i])+j])):
            for l in range(len(z_int[int(N_sum[i])+j])-k):
                cor[int(N_sum[i])+j][k] +=
                qc_mt_ms[int(N_sum[i])+j][l] * qc_mt_ms[int(N_sum[i])+j][k+l]

            cor[int(N_sum[i])+j][k] = 1.0 /
            (len(z_int[int(N_sum[i])+j])) * cor[int(N_sum[i])+j][k]

r, r_in, th, Er_M, Er_G = dict(), dict(), dict(), dict(), dict()
theta_max = 1.5

for k in range(int(N_sum[len(N_sum)-1])):
    r_in[k] = z_int[k] - z_int[k][0]
    #Correlation length
    th[k] = np.linspace(0.01,theta_max,int(theta_max/0.01))
    #Possible theta's
    Er_M[k] = np.zeros(len(th[k]))
    Er_G[k] = np.zeros(len(th[k]))

    for i in range(len(th[k])):
        a = find_nearest(r_in[k],1.0)
        r[k] = r_in[k][0:int(a)]

        for j in range(len(r[k])):
```

```
            Er_M[k][i] += abs(cor[k][j] -
            np.exp(-2 * r[k][j] / th[k][i]))**2
            Er_G[k][i] += abs(cor[k][j] -
            np.exp(-np.pi * (r[k][j] / th[k][i])**2))**2

th_M = np.zeros(int(N_sum[len(N_sum)-1]))
th_G = np.zeros(int(N_sum[len(N_sum)-1]))
for i in range(len(th_M)):
    a_M = np.where(min(Er_M[i]) == Er_M[i])[0]
    a_G = np.where(min(Er_G[i]) == Er_G[i])[0]
    th_M[i] = th[i][int(a_M)]
    th_G[i] = th[i][int(a_G)]

def plot_corfit(i,j):

    k = int(N_sum[i])+j

    y1 = np.exp(- 2 *(r_in[k]/th_M[k]))
    #fit based on Markov exp function
    y2 = np.exp(- np.pi * (r_in[k]/th_G[k])**2)
    #fit based on Gaussian function

    plt.figure(figsize=(8,4))
    plt.plot(r_in[k],cor[k],'ro',ms=3)
    plt.plot(r_in[k],y1,'k')
    plt.plot(r_in[k],y2,'b')
    plt.xlabel('Correlation distance (m)')
    plt.ylabel('Correlation (-)')
    plt.legend(['Correlation','Markov','Gaussian'])
    plt.gca().set_ylim(top=1.0)
    plt.xlim(0,2)
    return

plot_corfit(6,3)
```

E.6 Horizontal scale of fluctuation Blessington

This section calculates the horizontal scale of fluctuation at at the Blessington site.

```
import xlrd
import matplotlib.pyplot as plt
plt.style.use('classic')
import numpy as np
import math
%matplotlib inline

file_loc = 'C:\Geo Engineering\Master Thesis\Blessington\CPT_data.xlsx'
#locatie of file of measurements
workbook = xlrd.open_workbook(file_loc)
#Opening of file of measurements
sheets = dict()
for i in range(10):
    sheets[i]   = workbook.sheet_by_index(i)
    #Opening tab i

z = dict()  #Read values of z
qc = dict() #Read values of qc

for i in range(10):
    z[i] = np.zeros(sheets[i].nrows-4)
    qc[i] = np.zeros(sheets[i].nrows-4)
    for j in range(sheets[i].nrows-4):
        z[i][j]  = sheets[i].cell_value(j+4,0)
        qc[i][j] = sheets[i].cell_value(j+4,1)

layers = dict()          #Divide all CPT's in layers
layers[0] = [0,1.8,8.6]
layers[1] = [0,1.8,8.6]
layers[2] = [0,1.8,8.8]
layers[3] = [0,1.8,8.4]
layers[4] = [0,1.4,9.0]
layers[5] = [0,1.4,9.0]
layers[6] = [0,1.4,9.0]
layers[7] = [0,3.0,9.0]
layers[8] = [0,1.4,8.8]
layers[9] = [0,1.6,7.0]

x,y = dict(), dict()   #Define x and y coordinates of CPT's
x[0],y[0] = -3, -1.5
x[1],y[1] = -3, 1.5
x[2],y[2] = 0, -1.5
```

```
x[3],y[3] = 0, 1.5
x[4],y[4] = 4.68, -1.5
x[5],y[5] = 4.68, 1.5
x[6],y[6] = 9.44, -1.5
x[7],y[7] = 9.44, 1.5
x[8],y[8] = 12.34, -1.5
x[9],y[9] = 2.16, 1.5

def dist(i,j): #Calculate distance between the CPT's
    r = round(((x[i]-x[j])**2 + (y[i]-y[j])**2) ** 0.5, 2)
    return r

r_CPT = np.zeros([10,10])

for i in range(10):
    for j in range(10):
        r_CPT[i,j] = dist(i,j) #Store distance between CPT's

l_b = np.asarray([3.0,8.0])              #Interval of each CPT that is used
l_lin = np.linspace(l_b[0],l_b[1],int((l_b[1]-l_b[0])*100+1))
                                         #Linear array of z values

l_qc = np.zeros([10,len(l_lin)])
#qc values for layer
l_qc_m = np.zeros(10)
#Mean of qc for layer
l_qc_avg = np.zeros(len(l_lin))
#Average of all CPT's at a certain depth
l_qc_mt = np.zeros([10,len(l_lin)])
#qc values for layer de-trended
l_qc_mt_ms = np.zeros([10,len(l_lin)])
#qc values for layer normalised and de-trended
l_std = np.zeros(10)
#Standard deviation for qc minus horiztonal trend for each horizontal part
l_std_res = np.zeros(10)
#Standard deviation for qc de-trended

a = np.zeros([30,len(l_lin)])
m = np.zeros(10)
n = np.zeros(10)
A = np.vstack([l_lin, np.ones(len(l_lin))]).T
```

```
def find_nearest(array,value):
#function that finds and returns the nearest index of 'value' in 'array'
    idx = np.searchsorted(array, value, side="left")
    if idx > 0 and (idx == len(array) or math.fabs(value - array[idx-1])
    < math.fabs(value - array[idx])):
        return idx-1
    else:
        return idx

for i in range(10):
    if i in ex_total:
        continue

    for j in range(len(l_lin)):
        a[i,j] = find_nearest(z[i],l_lin[j])
        #Find index of z in z_CPT that is closest to a certain z

        l_qc[i,j] = qc[i][int(a[i,j])]
        #Find value of qc that belongs the value of
        z_CPT that is closest to a certain z

    m[i], n[i] = np.linalg.lstsq(A,l_qc[i,:],rcond=None)[0]
    #Linear depth trend of qc
    m[i], n[i] = round(m[i], 4), round(n[i], 4)

    l_qc_m[i] = np.mean(l_qc[i,:])
    #Mean value of the layer
    l_qc_mt[i,:] = l_qc[i,:] - l_qc_m[i]
    #De-trended CPT
    l_std[i] = np.std(l_qc[i,:])
    #Standard deviation of layer
    l_std_res[i] = np.std(l_qc_mt[i,:])
    #Standard deviation of de-trended layer
    l_qc_mt_ms[i,:] = l_qc_mt[i,:] / l_std_res[i]
    #Normalised layer

h = np.zeros(9)
link = np.zeros([55,2])
#Create an array that links each individual CPT to all other CPT's

p = 0
for i in range(9):
```

```
    h[i:9] += i
    for j in range(9-i):
        link[p,1] = int(i + j + 1)
        link[p,0] = int(i)
        p += 1

cor = np.zeros(45)

for j in range(45):
    for k in range(len(l_lin)):
        cor[j] += l_qc_mt_ms[int(link[j,0]),k] * l_qc_mt_ms[int(link[j,1]),k]
        #Correlation function
    cor[j] = cor[j] / ( len(l_lin)) #sum

n = 8

r_cor = [3,4.25,4.75,5.7,7.75,8.25,9.75,12.5]
#Distance at which correlation is averaged
r_count = np.zeros(n)

cor_tot = np.zeros(n)
cor_avg = np.zeros(n)

for i in range(45):
    if link[i,0] in ex_total:
        continue
    if link[i,1] in ex_total:
        continue
    if link[i,0] == 4:
        if link[i,1] == 5:
            continue

    b = find_nearest(r_cor,r_CPT[int(link[i,0]),int(link[i,1])])

    cor_tot[int(b)] += cor[i]
    r_count[int(b)] += 1

for i in range(n):
    cor_avg[i] = cor_tot[i] / r_count[i]  #Average correlation at that interval

theta_M = np.linspace(0.1,30,300)  #Find scale of fluctuation for Markov model
theta_G = np.linspace(0.1,30,300)  #Find scale of fluctuation for Gaussian model
```

```
Er1 = np.zeros(300)
#Error between estimated correlation and theoretical correlation Markov
Er2 = np.zeros(300)
#Error between estimated correlation and theoretical correlation Gaussian

for i in range(300):
    for j in range(45):
        if link[j,0] in ex_total:
            continue
        if link[j,1] in ex_total:
            continue
        if link[j,0] == 4:
            if link[j,1] == 5:
                continue
        Er1[i] += abs(np.exp(-(2*r_CPT[int(link[j,0]),int(link[j,1])]/theta_M[i]))
        - cor[j])**2
        Er2[i] += abs(np.exp(- np.pi *
        (r_CPT[int(link[j,0]),int(link[j,1])]/theta_G[i])**2)
        - cor[j])**2

plt.plot(theta_M,Er1)
plt.plot(theta_G,Er2)
plt.ylim(ymin=0)
plt.xlabel('Distance (m)')
plt.ylabel('Summed error (-)')
plt.legend(['Markov','Gaussian'])

c1 = np.where(Er1 == min(Er1))[0]
c2 = np.where(Er2 == min(Er2))[0]
print('SOF Markov:',round(theta_M[int(c1)],1),
'Summed error is',round(min(Er1),2))
print('SOF Gaussian:',round(theta_G[int(c2)],1),
'Summed error is',round(min(Er2),2))

plt.figure(figsize=(10,4))

x_M = np.linspace(0,14,141)
y_M = np.exp(-(2*x_M/theta_M[int(c1)]))
y_G = np.exp(-np.pi*(x_M/theta_G[int(c2)])**2)
plt.plot(x_M,y_M)
plt.plot(x_M,y_G)
```

```
plt.xlabel('Distance (m)')
plt.ylabel('Correlation (-)')
plt.title('Horizontal correlation CPTs Blessington')

plt.xlim(0,14)
plt.ylim(-0.5,1)

for i in range(45):
    if link[i,0] in ex_total:
        continue
    if link[i,1] in ex_total:
        continue
    if link[i,0] == 4:
        if link[i,1] == 5:
            continue

    plt.plot(r_CPT[int(link[i,0]),int(link[i,1])],cor[i],'ro')

plt.legend(['Markov fit','Gaussian fit','Horizontal correlation'],loc='best')
#plt.plot(r_cor,cor_avg,'bd')

plt.figure(figsize=(10,4))
plt.plot(x_M,y_M)
plt.plot(x_M,y_G)
plt.plot(r_cor,cor_avg,'kx')
plt.plot(0,1,'kx')
plt.plot([0,3],[1,cor_avg[0]],'r')
plt.plot(r_cor,cor_avg,'r')
plt.ylim(-0.5,1)

plt.xlabel('Distance (m)')
plt.ylabel('Correlation (-)')
plt.title('Average horizontal correlation CPTs Blessington')

plt.legend(['Markov fit','Gaussian fit','Average horizontal correlation'],loc=3)
```

E.7 Initial settlement verification Blessington

```
import xlrd
import matplotlib.pyplot as plt
```

```
plt.style.use('classic')
import numpy as np
import math
import numpy.random as rnd
%matplotlib inline

q_qc_Bless250 = np.linspace(0,0.2,11)
s_B_Bless250 = [0,0.3,0.7,1.1,1.6,2.1,2.7,3.3,4.2,5.2,7.2]
B = 0.25
qc = 2750/0.2

s_Bless250 = np.zeros(len(s_B_Bless250))
for i in range(len(s_B_Bless250)):
    s_Bless250[i] = s_B_Bless250[i]*B
qapp_Bless250 = q_qc_Bless250*qc

def Sett_(N,alpha,sig_alpha,G0,sig_G0,qc,B,Ihrv):
    s = np.zeros([N,251])
    L = B
    rand1 = rnd.standard_normal(N)
    rand2 = rnd.standard_normal(N)
    beta = alpha / (1 - (10*alpha * qc * Ihrv * L)
    / ((G0*2.2) * B)) ** (1/0.3)
    q_qc_app = np.linspace(0,alpha,251)
    Qapp = qc * q_qc_app * B**2
    Qult = qc * beta * B ** 2

    s_avg = (Qapp * Ihrv) / (B * (G0*2.2) *
    (1 - (Qapp / Qult)**0.3)) *1000

    for i in range(N):
        alpha_rand = alpha + sig_alpha * rand1[i]
        E0_rand = 2.2 * (G0 + rand2[i] * sig_G0)
        beta = alpha_rand / (1 - (10*alpha_rand * qc * Ihrv * L)
        / (E0_rand * B)) ** (1/0.3)
        Qult = qc * beta * B ** 2
        for j in range(251):
            s[i,j] = (Qapp[j] * Ihrv) / (B * E0_rand *
            (1 - (Qapp[j] / Qult)**0.3)) *1000

    return s,s_avg,q_qc_app,Qapp,Qult
```

```
def find_nearest(array,value):
#function that finds and returns the nearest index of 'value' in 'array'
    idx = np.searchsorted(array, value, side="left")
    if idx > 0 and (idx == len(array) or math.fabs(value - array[idx-1])
    < math.fabs(value - array[idx])):
        return idx-1
    else:
        return idx

s_sorted = np.zeros([len(q_qc_app),N])
s_CDF = np.linspace(0,1,N)
find5_s = find_nearest(s_CDF,0.05)
find50_s = find_nearest(s_CDF,0.50)
find95_s = find_nearest(s_CDF,0.95)

s_sorted_5 = np.zeros(len(q_qc_app))
s_sorted_50 = np.zeros(len(q_qc_app))
s_sorted_95 = np.zeros(len(q_qc_app))

for i in range(len(q_qc_app)):
    s_sorted[i,:] = np.sort(s[:,i])
    s_sorted_5[i] = s_sorted[i,find5_s]
    s_sorted_50[i] = s_sorted[i,find50_s]
    s_sorted_95[i] = s_sorted[i,find95_s]

plt.figure(figsize=(10,5))

plt.plot(s_B_Bless250,q_qc_Bless250,'s',color='k')
plt.plot(s_B_Bless250,q_qc_Bless250,'k')
plt.grid(b=None, which='major', axis='both')

plt.plot(s_sorted_95/B/10,q_qc_app,'k',linestyle='--')
plt.plot(s_avg/B/10,q_qc_app,'r',linewidth=2)
plt.plot(s_sorted_5/B/10,q_qc_app,'k',linestyle='--')
plt.xlim(0,10)
plt.ylim(0,0.25)
plt.xlabel('s/B [%]')
plt.ylabel('q/qc [-]')

plt.legend(['Data points load-settlement response','linear line load-settlement response'
,'95 percent','mean','5 percent'],loc=4)
```